Copyright

by

Daniel Tapia

2021

The Dissertation Committee for Daniel Tapia Certifies that this is the approved version of the following dissertation:

Evaluation of a gold nanoparticle platform as highly immunogenic and protective therapy against *Burkholderia mallei, B. pseudomallei*, and Enterohemorrhagic *Escherichia coli* O157:H7

Committee:

Alfredo G. Torres, Ph.D., Supervisor

Janice J. Endsley, Ph.D.

Gregg Milligan, Ph.D.

Matthieu Gagnon, Ph.D.

Lisa Morici, Ph.D.

Evaluation of a gold nanoparticle platform as highly immunogenic and protective therapy against *Burkholderia mallei, B. pseudomallei*, and Enterohemorrhagic *Escherichia coli* O157:H7

by

Daniel Tapia, B.S.

Dissertation

Presented to the Faculty of the Graduate School of

The University of Texas Medical Branch

in Partial Fulfillment

of the Requirements

for the Degree of

Doctor of Philosophy

The University of Texas Medical Branch

March 2021

Dedication

To my parents, Modesto and Nora, for their unconditional love and support. Thank you for instilling the idea that I could always do something great, and especially for the sacrifices you made, allowing me to make it possible.

Acknowledgements

I would like to acknowledge my mentor Dr. Alfredo Torres for his support and guidance and for believing in me since I was a PREP student. I would also like to recognize my committee members Dr. Janice Endsley, Dr. Gregg Milligan, Dr. Matthieu Gagnon, and Dr. Lisa Morici for their guidance and continued support. I would also like to thank the current and past members of the Torres' Lab: Dr. Nittaya Khakhum, Joseph Thiriot, Jacob Stockton, Shane Wilson, Sarah Ainsworth, Dr. Itziar Chapartegui-Gonzales, Dr. Brittany Ross, Dr. Christopher Hatcher, Julia Myers, Dr. Laura Muruato, Dr. Gonzalo Pradenas, and everyone who was able to put up with me and had the time to listen and support me. I would also like to acknowledge my technical and emotional support and someone I could come to for anything, Kubra Naqvi. Also, to Shayla Gomez, my accomplice and lifelong best friend who has served as a source of inspiration and guidance. Lastly, I would like to immensely thank my mentor, friend, and support system, Dr. Javier Sanchez-Villamil, for his guidance and his occasional disagreements; my PhD would have been a very different story without him. Without the support and guidance from everyone mentioned, this accomplishment would not have been a reality, and for them I am forever thankful.

Evaluation of a gold nanoparticle platform as highly immunogenic and protective therapy against *Burkholderia mallei, B. pseudomallei*, and Enterohemorrhagic *Escherichia coli* O157:H7

Publication No._____

Daniel Tapia, Ph.D.

The University of Texas Medical Branch, 2021

Supervisor: Alfredo G. Torres, M.S., Ph.D.

Burkholderia mallei (*Bm*) and *B. pseudomallei* (*Bpm*) are facultative intracellular pathogens and the causative agents of glanders and melioidosis. At present, effective vaccines for the prevention of glanders, or melioidosis in humans, are not available. However, renewed attention has been directed toward developing *Burkholderia* vaccines because of the pathogens' seemingly ideal characteristics for malicious use as a biothreat agent. Additionally, a vaccine will also have significant value for the immunization of at-risk populations in melioidosis/glanders endemic areas of the world. Therefore, the following studies' long-term goal is to develop a platform that allows for the efficient generation of a multicomponent vaccine that can protect against both glanders and melioidosis. In this study, glycoconjugates coupled to gold nanoparticles (AuNPs) were tested for their protective properties in clinically relevant infection models. The flexible NP platform allow us to incorporate novel antigens identified previously by a reverse vaccinology model. In these studies, we have established an optimal immunization procedure to test the efficacies of several protein-polysaccharide NPs when delivered alone or in a combination containing various proteins in a clinically relevant and highly

controlled aerosol murine model of infection. We have demonstrated that several glycoconjugates offer protection against lethality when delivered intranasally, with increased protection afforded by a refined formulating containing the most immunogenic proteins. Also, we have shown that antigen-specific humoral responses play a significant role in the protection induced by various AuNP-coupled glycoconjugate formulations. Similarly, we have shown a protective effect of AuNP-coupled proteins in a colonization model of Enterohemorrhagic *Escherichia coli* (EHEC). Furthermore, we showed that vaccination with AuNP-coupled to EHEC-specific antigens elicits strong systemic and mucosal response associated with protection against EHEC colonization. This work proposes to bridge the properties of subunit vaccination with those of synthetic nanomaterials to enhance immune responses to vaccines against pathogenic bacteria.

TABLE OF CONTENTS

List of Tables

List of Figures

List of Illustrations

List of Abbreviations

ABSL-3	Animal biosafety lab
AgNP	Silver nanoparticle
AIEC	Adherent-invasive *Escherichia coli*
AMP	Antimicrobial peptide
ANOVA	Analysis of variance
APC	Antigen presenting cell
ARC	Animal Research Center
ATCC	American Tissue Culture Collection
AuNP	Gold nanoparticle
BALF	Bronchioalveolar lavage fluid
BCA	Bicinchoninic assay
BCAA	Branch-chain amino acid
BCG	Bacillus Calmette-Guerin
Bm	*Burkholderia mallei*
BMDM	Bone marrow-derived macrophage
Bpm	*Burkholderia pseudomallei*
BSA	Bovine Serum Albumin
BSL3	Biosafety level 3
Bth	*Burkholderia thailandensis*
CD	Cluster of differentiation
CDC	Center for Disease Control
CFU	Colony forming units
CLR	C-Type Lectin Receptor
CNS	Central nervous system
COX-2	Cyclooxygenase-2
CpG	Cytosine-guanine dinucleotides
CPS	Capsular polysaccharide
CT	Cholera toxin
CTL	Cytotoxic T lymphocyte
DAEC	Diffusely Adhering *Escherichia coli*
DAPI	4′,6-diamidino-2-phenylindole
DC	Dendritic cell
DLS	Dynamic Light Scattering
DMEM	Dulbecco's Modified Eagle's Medium
DMTMM	4-(4,6-Dimethoxy-1,3,5-triazin-2-yl)-4-methylmorpholinium chloride
DNA	Deoxyribonucleic acid
EAEC	Enteroaggregative *Escherichia coli*
ECL	Enhanced chemiluminescence
EDC	N-(3-dimethylaminopropyl)-N′-ethyl carbodiimide hydrochloride
EDTA	Ethylenediaminetetraacetic acid
EIEC	Enteroinvasive *Escherichia coli*

ELISA	Enzyme-linked immunosorbent assay
EMCH	6-maleimidocaproic acid hydrazide
EPEC	Enterohemorrhagic *Escherichia coli*
EPEC	Enteropathogenic *Escherichia coli*
ER	Endoplasmic Reticulum
ETEC	Enterotoxigenic *Escherichia coli*
FBS	Fetal bovine serum
G-CSF	Granulocyte colony stimulate factor
Gb3	Globotriaosylceramide 3
GC	Germinal center
GI	Gastrointestinal
GSK3	Glycogen synthase kinase 3
H&E	Hematoxylin and eosin
HBSS	Hank's balanced salt solution
Hcp	Hemolysin-coregulatory protein
HLA	Human leukocyte antigen
HRP	Horseradish peroxidase
HUS	Hemolytic uremic syndrome
IACUC	Institutional Animal Care and Use Committee
IC_{50}	Inhibitory concentration 50
IEC	Intestinal epithelial cell
IFA	Immunofluorescence assay
IFN	Interferon
IG	Intragastric
Ig	Immunoglobulin
IHA	Indirect hemagglutinin assay
IL	Interleukin
IM	Intramuscular
IN	Intranasal
IP	Intraperitoneal
IPTG	Isopropyl β-D-1-thiogalactopyranoside
ISCOM	Immune stimulating complex
IV	Intravenous
kDa	Kilodalton
Km	Kanamycin
KWC	Killed whole-cell
LB	Luria Bertani
LBG	Luria Bertani with 4% glycerol
LD_{50}	Median Lethal Dose
LEE	Locus of enterocyte effacement
LN	Lymph node
Lpf	Long polar fimbriae
LPS	Lipopolysaccharide
mAb	Monoclonal antibody
MALDI-TOF	Matrix-assisted laser desorption/ionization time-of-flight
MBC	Minimum bactericidal concentration

MBEC	Minimum biofilm eradication concentration
MCP-1	Monocyte chemotactic protein-1
MES	2-(N-morpholino) ethane sulfonic acid
MHC	Major histocompatibility complex
MHDA	16-mercaptohexadecanoic acid
MIC	Minimum inhibitory concentration
MLD	Mean lethal dose
MMR	Measles-Mumps-Rubella
MNGC	Multinucleated giant cell
MOI	Multiplicity of Infection
MPLA	Monophosphoryl lipid A
mRNA	Messenger ribonucleic acid
MWCO	Molecular weight cut off
NF-kB	Nuclear factor kappa-light-chain-enhancer of activated B cells
NGS	Next-generation sequencing
NHS	N-hydroxy succinimide
NK	Natural killer
NLR	Nucleotide-binding oligomerization domain-like receptors
NO	Nitric oxide
NP	Nanoparticle
OD	Optical density
OMP	Outer membrane protein
OMV	Outer membrane vesicle
OPS	O-antigen polysaccharide
ORF	Open reading frame
PAMP	Pathogen-Associated Molecular Patterns
PBS	Phosphate buffered saline
PFA	Paraformaldehyde
PGE2	Prostaglandin E2
PI	Propidium iodide
PVDF	Polyvinylidene fluoride
RNA	Ribonucleic acid
ROS	Reactive oxygen species
rRNA	Ribosomal ribonucleic acid
SATA	S-acetylthioglycolic acid N-hydroxysuccinimide ester
SC	Subcutaneous
SDS-PAGE	Sodium dodecyl sulphate polyacrylamide gel electrophoresis
STEC	Shiga toxin-producing *Escherichia coli*
Stx	Shiga toxin
T3SS	Type 3 Secretion System
T6SS	Type 6 Secretion System
TAP	Transporter associated with antigen processing
TBS	Tris-buffered saline
TEM	Transmission Electron Microscopy
TGF	Tumor growth factor
T_H	T-helper cell

TLM	Thiolactomycin
TLR	Toll-like receptor
T_M	Memory T cell
TMB	Tetramethylbenzidine
TMP-SMX	Trimethoprim-sulfamethoxazole
TNF	Tumor necrosis factor
T_{reg}	Regulatory T cell
USDA	United States Department of Agriculture
UTI	Urinary tract infection
UTMB	University of Texas Medical Branch
UV/Vis	Ultraviolet/Visible
WB	Western blot

INTRODUCTION

Chapter 1: Vaccinology

The discovery and development of vaccines are one of humanity's greatest achievements and arguably the singular most effective medical intervention with profound impacts on public health increasing longevity and health. The fundamental concept of vaccination predates the establishment of the germ theory in Asia, where artificial induction by variolation was practiced in various regions of Asia in the 1500s (1). Nonetheless, this concept of removing pus from a smallpox vesicle and introducing it to an uninfected patient would become the foundation for Edward Jenner's groundbreaking experiment in 1798, demonstrating that large-scale inoculation with cowpox was an effective means of combating smallpox (2). Over 200 years after this original observation, vaccine development has been a great success story in modern medicine, albeit with some setbacks, missteps, and even controversies. Nonetheless, today, vaccines save individuals from several debilitating disease consequences and save approximately 2 to 3 million lives each year (1). Owing to numerous global immunization strategies and programs, vaccines allowed for eradicating smallpox and have almost eliminated many others, including diphtheria, tetanus, measles, among others (2).

While the fundamental concept and mechanism of vaccination have remained relatively unchanged since its conception, the technologies and composition of these have drastically changed. That is, the idea of introducing a biological substance, for example, an antigen, that resembles a pathogen either by whole cell-modified or a single subunit (e.g., protein) to stimulate an immunological response that will develop memory or 'trained' recognition of the pathogen and mount an appropriate immune response it should re-encounter the corresponding pathogen. Recent advances in technologies used to synthesize

vaccines, such as genetic engineering and next-generation sequencing, and the understanding of how vaccine adjuvants work have allowed the application of novel vaccine technologies to be referred as “rational” vaccine development (1). However, rather than applying the direct antonym of “irrational” to traditional vaccinology, a more appropriate term should be “empiric,” and we should build on these approaches rather than exclude them (1). Over 200 years have passed since Jenner’s first experiment, yet the field of vaccinology is still trying to decipher the underlying mechanisms of protection by immunization.

Live attenuated vaccines are among the most successful empiric methods of deriving vaccines for bacterial and viral pathogens. This approach relies on the reduction of pathogenicity for an organism while maintaining protective immune responses (3). The strength of this immunization approach relies on the use of whole microbes that mimic a natural course of infection while eliciting immune responses to a wide variety of conserved antigens. Traditional live-attenuated vaccine generation methods include serial passaging of a microbe to lose virulence characteristics while adapting to a particular host. Also, growing the organism in a surrogate host, as exemplified by the measles, mumps, and rubella (MMR) vaccine, grown in chicken fibroblasts to select for mutant viruses with enhanced virulence in a host while displaying an attenuation phenotype in humans (2, 3). Nonetheless, while this attenuation method is well suitable for RNA viruses, given their high mutation rate, this method is often not employed against bacterial pathogens (1, 2). Recombinant DNA technology is the most used method for creating attenuated bacterial mutants. One example is the *Vibrio cholerae* vaccine CVD 103-HgR which does not express the enzymatically active subunit of cholera toxin (1). Live-attenuated bacterial vaccine strains have shown great promise in protecting against infection. The notion that live-attenuated organisms help broaden the breadth of immunological protection is often attributed to the idea that priming the immune system with a live organism may reflect the natural course of infection (3). In addition, live attenuated vaccines can often induce robust

cellular and humoral responses after a single or two doses of a vaccine. However, some obstacles of these traditional vaccinology approaches include the potential for reversion and safety concerns for their use in immunocompromised individuals (1, 2). Furthermore, the wide implementation of live attenuated vaccines in low-income countries can be cumbersome, as many of these have to be maintained in refrigeration for long periods (1).

One other approach against bacterial pathogens that utilizes the whole organism involves vaccination after inactivation, for example, using heat, chemicals, or radiation (1). This method, termed killed whole-cell (KWC), consists of a wild-type organism without the need to introduce mutations and artificially used different methods to attenuate its virulence in a host. Among the first vaccines that were inactivated and that were applied included typhoid, plague, cholera bacilli (1). Unlike attenuated vaccine strains, organisms generated for KWC vaccination cannot cause disease, and vaccines do not require refrigeration. However, this mechanism of vaccine development often affects the immunogenicity of the pathogen, with some studies suggesting that irradiated antigens retain some of the antigenic structures destroyed by heat. Given that this vaccination strategy uses organisms that cannot replicate in a host organism, adjuvants have been added to their formulation to augment the weak adaptive immune responses induced by KWC (1). However, local adverse reactions in the vaccination site have been observed in KWC vaccinated individuals, but most are attributed to the type of adjuvant used (1). Another disadvantage of the KWC vaccine platform is its inability to induce robust CD8+ T cell responses, which are essential mediators of protection against intracellular pathogens (1). One common obstacle of traditional whole-organism vaccines is the lack of specificity in the immune response elicited. For example, one disadvantage of whole-cell vaccines is that antibodies may be raised against proteins involved in virulence, and pathogens may modulate this to their advantage (1). Furthermore, pathogenic organisms may contain proteins that down-regulate adaptive immune responses (4). Therefore, the selection of

immunogenic candidates is essential for vaccine development against a wide range of proteins.

Recent vaccinology strategies have focused on the identification, formulation, and delivery of microbial components, also termed ‘subunits’, as a safe alternative for stimulating a potent immune response. Given that these components can be better characterized before and after formulation, they have a high degree of safety associated with human use (1, 2). However, one obstacle has been the identification of protective components. Because genetic engineering made a revolutionary impact on the development of vaccines in the 20th century, genomics and next-generation sequencing has made a breakthrough in the of vaccines of the 21st century (1, 5). Reverse vaccinology exploits the use of computational analysis of a pathogen's genome for the prediction of epitopes in an antigen (5–8). Whereas conventional antigen identification relies on the purification of an antigen and testing the ability to induce protective immunity, this process is time-consuming, and often, immunogenic proteins are only be expressed by a pathogen under certain infection conditions. Several available algorithms capable of predicting highly immunodominant epitopes based on primary sequence data alone can be selected for further testing based on protein location or predicted T-cell epitopes (6). Together with high-throughput next-generation sequencing (NGS), which allows for the analysis of sequence variants in a population, reverse vaccinology will allow for the identification and prediction of sequence variants and immunodominant epitopes to increase vaccine efficacy.

Furthermore, once identified, their isolation and delivery can be modified to target different immune pathways. For example, they may be delivered as DNA or RNA vectors for expression in host cells or given in a formulation containing one or more adjuvants (2). In the wake of the current global coronavirus disease of 2019 (COVID-19) pandemic caused by the severe acute respiratory syndrome coronavirus 2 (SARS-CoV-2), RNA technology has been one of the most recent successful vaccination technologies that use

mRNA encoding the spike protein for endogenous expression a cell to elicit protective immunity (9, 10). However, unlike traditional whole-cell vaccines, microbial components are often associated with weak inducers of long-term immunity and require adjuvants or targeted delivery to boost their efficacy (1). These adjuvants may act directly and can be made from organic or inorganic compounds and act by encapsulating antigen for uptake by antigen-presenting cells (APCs) or acting as immunostimulants (1). While the use of microbial components for subunit vaccine formulation remains an appealing, and safe alternative to traditional vaccinology methods, there is a need to develop, understand, and employ effective vaccine-delivery platforms that can augment protective immune responses while maintaining a safe profile. Some of the ramifications of these technologies may extend beyond infectious diseases and may have prophylactic or therapeutic potential in other disease models.

PROTECTIVE IMMUNE MECHANISMS

Understanding the mechanisms of vaccine-mediated protection is at the center of vaccinology today. Identifying correlates or markers of protection is a significant asset to developing new vaccine technologies and platforms or improving existing vaccinations (2). Long-term mediated vaccine protection is conferred by the maintenance of antigen-specific immune effector and induction of memory cells that may be sufficient to be rapidly activated into immune effector cells upon pathogen exposure (2, 3). The main objective of vaccination is to activate antigen-specific B and T cell effector responses capable of controlling the natural course of a disease, to a variable degree, depending on the disease model (3). At the interface of this acquired or memory response associated with B and T cell are Antigen Presenting Cells (APCs), predominantly dendritic cells (DCs) which upon pathogen sensing undergo maturation, modulate surface receptors, and migrate towards secondary lymphoid organs for the B and T cell activation to occur (3). APCs can sense

several conserved pathogen signals or pathogen-associated molecular patterns (PAMPs) by pattern-recognition receptors, such as toll-like receptors (TLRs), which can initiate innate immune activation, leading to DC activation (3). This activation results in the modulation of surface receptors and subsequent production of inflammatory cytokines and chemokines, allowing for the recruitment of additional APCs (3). Upon antigen exposure, APCs also undergo maturation resulting in the reorganization of major histocompatibility complex (MHC) structures from intracellular compartments to the surface and undergo peptide loading, furthering their T cell activation capacity (2, 3). Therefore, the first step of a successful vaccine is to provide sufficient danger signals in the form of antigens or adjuvants to trigger an inflammatory reaction by innate immune cells to allow for efficient induction of memory responses.

Upon antigen encounter, APCs can use several engulfment mechanisms, but the decision is influenced by the particle size (3, 11, 12). Generally, but not always, the process of engulfment is dictated by the direct interaction of surface receptors binding to specific ligands, such as pathogen motifs. Endocytosis of larger particles (> 0.5 μm), such as bacteria, occurs mostly by macropinocytosis and phagocytosis, which form surface extensions capable of engulfing pathogens leading to the formation of macropinosomes or endosomes, respectively (11, 12). These endocytic vesicles can fuse with early and late endosomes as well as lysosomes to form phagolysosomes. These structures contain proteolytic enzymes and reactive oxygen species (ROS) capable of degrading bacterial proteins into peptides (13). These peptides can bind MHC class II molecules for presentation on the surface and subsequent recognition by CD4+ T-helper (T_H) cells, capable of stimulating both the humoral (antibody-mediated) as well as cellular arms of the adaptive immune system (3, 11–13). Activated CD4+ Th cells can modulate their cytokine expression and further differentiate into one of two significant subclasses of effector T cells, termed T_H1 and T_H2 (3, 11, 14). This decision is regulated by the cytokine

environment generated by APCs along with other innate immune cells, including natural killer (NK cells), basophils, and mast cells (3).

T_H1 cells are essential players in the adaptive immune defenses against intracellular pathogens by the production of interferon (IFN)-γ, a type II interferon, secretion of interleukin 2 (IL-2), and tumor necrosis factor (TNF)-α (2, 3). A fraction of these cells can persist as memory CD4+ T cells (T_M), which provide a rapid enhanced response against secondary infection. IL-12 is a critical cytokine in the induction of T_H1 biased responses, whereas IL-10 has been shown to suppress the development of this response (2, 3). On the other hand, T_H2 cells are critical components in control against extracellular pathogens, and IL-4 is one of the main drivers of their development. T_H2 cells produce anti-inflammatory cytokines such as IL-4, IL-5, and IL-13 (2, 3).

Furthermore, T_H2 cells play an essential role in the induction of humoral responses by stimulating B cells in germinal centers (GCs), leading to their differentiation into memory B cells (B_M) or plasma cells (2, 3). While naïve B cells produce low-affinity immunoglobulins (Ig) like IgM and IgD, Th activated B cells undergo clonal expansion and affinity maturation to undergo Ig class switching to produce IgG, IgE, and IgA depending on the cytokine environment (2, 3). T follicular helper cells (T_{FH}) also play a fundamental role in supporting B cell differentiation and Ig class switching by providing co-stimulation in the form of IL-10 and IL-21, allowing the production of antibodies with higher binding capacity (2). Balance of effector Th cell activity is controlled by regulatory T cells (T_{regs}), which produce IL-10 and transforming growth factor β (TGF-β) producing immune homeostasis. Also, T_{regs} play a critical role in preventing the development of autoimmune diseases and allergic reaction by dampening immune responses to both self and non-self antigens (1).

The prevailing idea in antigen presentation by MHC molecules was that APCs were capable of loading exogenous peptides onto MHC-II and that endogenous peptides were loaded onto MHC-I for presentation (15–17). However, it is well accepted that APCs can

load exogenous peptides onto MHC-I molecules for presentation by antigen cross-presentation (15–17). Cross-presentation of peptides by MHC-I molecules is critical for priming a CD8+ T response against intracellular pathogens. Although the precise mechanism by which this occurs is unknown, it involves the fusion of phagosomes with the endoplasmic reticulum (ER) before loading peptides onto MHC-I (17, 18). Given the potential to produce cytotoxic T lymphocyte (CTL) responses against intracellular pathogens by exploiting the delivery of antigens into APCs to access the cytosol, there have been various attempts to create vaccines against intracellular pathogens exploiting the cross-presentation ability of APCs by various nanoparticle delivery platforms (16, 18–26).

While a natural infection, and by an extent, live vaccines, will be able to induce a mixed B and T (CD4+ versus CD8+) response, subunit vaccines have an advantage in that their composition and delivery will have a direct impact on the quality and type of immune response elicited (1, 3). Therefore, this idea allows us to reason that tailoring an immune response to a specific pathogen may be a useful strategy when designing a vaccine. For example, bacterial polysaccharides can induce B cell responses in a T cell-independent manner, but this immune response is isotype restricted and is devoid of T cell memory (13, 27). However, upon conjugation of polysaccharides to a protein carrier, also termed glycoconjugates, peptide antigens can be displayed and recognized by either CD4+ or CD8+ T cells and elicit a B cells response in a T cell-dependent manner (13, 27). Therefore, these characteristics can be tailored to favor a particular response to an antigen or multiple antigens, preventing immune escape recognition.

Designing vaccines that favor a CD8+ CTL or T_H1 response against intracellular pathogens may be an advantageous route to provide protection. Whereas the ability to tailor an immune response to a particular antigen can be one of the most challenging concepts of vaccine development strategies, today, the field of vaccinology has made tremendous advances into how delivery systems and novel adjuvants may be the driving force breaking this paradigm.

ADJUVANTS AND IMMUNE MODULATION

To circumvent some of the challenges of subunit vaccine platforms, such as decreased duration of immune response or induction of negligible cell-mediated immunity, several compounds have been developed to help improve the immunogenicity of a vaccine. Adjuvants (from Latin, *adjuvare*, meaning "to help") offer a mechanism to enhance the magnitude and modulate the type of immune response, to induce a protective and long-lasting immune response (2). Therefore, the selection of adjuvants for subunit vaccines is a critical step in increasing and directing the immunogenicity of subunit vaccines, thereby guiding the stimulation of innate immunity and developing an appropriate adaptive immune response capable of protecting against the pathogen of interest. While the precise mechanism by which many of the current adjuvant technologies work is not entirely understood, they are generally divided as particulate formulations, immunomodulatory molecules, or a combination of these two characteristics (28–30). These properties have been utilized to modulate antibody avidity and function, subclass distribution, extending or accelerating the duration of the immune response, eliciting cell-mediated immunity, which together can lower a vaccine dose, lower the number of doses, and overall augmenting or directing the immunogenicity of subunit vaccines (2, 29). Today, there are seven clinically approved adjuvants for human use, including aluminum salts (alum), emulsions, virosomes, and particulate formulations (2, 29).

For nearly 80 years, aluminum salts (commonly referred to as 'alum') have been the only adjuvant used in human vaccines. Alum is found in several clinically-administered vaccines, including diphtheria-tetanus-pertussis, human papillomavirus, and hepatitis vaccines (30, 31). Alum is postulated to act by the creation of a depot effect that allows retention of antigen for a more extended period allowing for enhanced antigen persistence at the site of vaccination and increase recruitment and activation of APCs and is associated

with provoking a more robust T_H2-biased response that is often not effective against intracellular pathogens (31). However, while alum is more commonly found in clinically used vaccines and is generally well-tolerated, there have been some adverse effects, such as the formation of granulomas at the site of vaccination when administered subcutaneously or intradermally, over intramuscularly (1, 31). In addition, renal dysfunction can lead to aluminum accumulation, which is associated with a high degree of toxicity and amyotrophic lateral sclerosis, and Alzheimer's disease (1, 31). Emulsion adjuvants (oil-in-water or water-in-oil) such as Freund's Incomplete Adjuvant (IFA) and MF59© are also associated with creating a depot effect, which is directly associated with enhancing MHC presentation by APCs (32). IFA is associated with eliciting a more robust T_H2-biased response with some T_H1 cellular response. On the other hand, MF59© is associated with the induction of both a cellular (T_H1) and humoral (T_H2) response (32). Nonetheless, the precise adjuvant mechanism of these remains to be elucidated. One of the potential complications associated with emulsifying adjuvants is the potential development of autoimmunity. However, with increasing knowledge of adjuvanticity and immunogenicity, new technologies have been implemented that are more specific and increase vaccine safety.

One important new class of adjuvants includes stimulatory adjuvants that directly bind PRRs and act by directly activating APCs, consequently influencing the adaptive immune response. Nearly all PRR family members can be used as targets for adjuvants, including TLRs, NOD-like receptors (NLRs), and C-type lectin receptors (CLRs) (25, 29, 33, 34). Stimulation of these PRRs signals through distinct adaptor molecules that lead to the activation of different transcription factors (25, 29, 33, 34). These transcription factors trigger the production of various cytokines and chemokines that play a role in the priming, expansion, and subsequent polarization of the immune responses. Unmethylated cytosine-guanine dinucleotides (CpG), which are found in bacterial DNA, and monophosphoryl lipid A (MPLA) are characterized by their ability to bind co-stimulatory signals or

intracellular signaling pathways (32). In humans, MPLA binds TLR2, which triggers the release of pro-inflammatory cytokines through NF-kB activation (32). On the other hand, CpG is recognized by TLR9, which is found in endosomal membranes, and which in conjugation with stimulatory molecules triggers the release of TNF-α and IL-12 causing a potent T_H1-biased response (32). As traditional adjuvant technologies trigger strong T_H2 biased responses with little T_H1 response, it remains a challenge to create adjuvants that trigger more robust T_H1-based responses. However, when innate immune signaling stimulatory adjuvants have been used in conjugation with alum or traditional emulsion adjuvants, they are potent stimulants of T_H1 biased responses (32)

GOLD-NANOPARTICLES IN VACCINE DEVELOPMENT

Nanotechnology is a continuously growing field that focuses on developing technologies by manipulating matter on a nanoscale. The International Organization for Standardization (ISO) defines a nanostructure as "an object that has at least one dimension within the nanoscale"; 1 - 1000 nm (1 nm = 10^{-9} m) (35, 36). Despite our understanding of subunit vaccination and its advantages over live platforms, increasing long-term immunity remains a challenge. Adjuvants have been a preferred method for enhancing protection and skewing the immune response to favor protective mechanisms. However, few adjuvants are approved for clinical use, limiting the pool of available immune enhancers for subunit vaccination. One approach we have studied is the use of NPs as delivery and stabilizing scaffolds allowing for prolonged antigen exposure and enhanced immune responses. Both inorganic (e.g., silver, gold, silica) and organic (e.g., liposomes, saccharide-based) NPs have been of particular interest due to their low toxicity, non-immunogenicity, and ability to encapsulate antigens allowing for antigen stabilization (14, 35, 37, 38). A wide array of platforms has been utilized for antibacterial vaccines and are often classified based on their composition: polymeric, inorganic, liposomes, immunostimulatory complexes (ISCOMs),

virus-like particles, emulsions, and self-assembling materials (14, 35, 37, 38). Thus far, some of the most commonly studied include outer membrane vesicles (OMVs), protein or peptide with self-assemble properties, and metallic or organic nanoparticles (38, 39). Rationally designed and tailored nanoparticle vaccines are demonstrated to overcome the delivery barriers of soluble antigens to shape and enhance adaptive immune responses. The ability to enhance protective immune responses depends on the inherent characteristics of the NPs, such as size, shape, and surface composition, which not only dictate their interactions with biological systems, and overall properties (14, 35).

Among the advantages of metallic nanoparticles for effectively delivering of biomolecules include their rigid and controllable or tunable synthesis (39). Together with their cargo loading capacity, biocompatibility, and ease of synthesis, gold nanoparticles (AuNPs) have garnered interest for medical applications, including vaccine development. These properties make AuNPs an attractive platform for delivery of antigens given their ease of fabrication into a variety of shapes (e.g., spherical, rod, cubic, etc.), with a size range of 2 - 150 nm, can be surface modified with an array of biological molecules including proteins, lipids, nucleic acids, and carbohydrates (40–46). The ability to conjugate a wide range of molecules on the surface of AuNPs by either direct conjugation methods or absorption via chemical interactions confer various antigenic and adjuvating properties (47). Among their desirable properties, AuNPs have the benefit that they do not induce antibody responses to the vehicle itself, a potential problem for other NPs, and acute cytotoxicity at high concentrations has rarely been observed (41, 43, 44, 46). Not only can AuNPs act as vehicles to APCs, but they have also been shown to promote immune cell uptake, APC activation, and cytokine production, and as a result, subsequently influences humoral and cellular immune responses (24, 38, 48–51). AuNPs have been implicated in acting as immunostimulant in bone marrow-derived dendritic cells (BMDCs) in which, following incubation, these APCs not only exhibited an activated phenotype but also produced proinflammatory cytokines such as TNFα, IL-6, and IL-12 (52, 53).

Interestingly, this phenotype was shown to be shape and size-dependent, where 40 nm NPs showed higher antibody levels for West Nile Virus (WNV) E protein when compared to 20 nm ones (50). A different study showed that AuNP ranging from 8 – 17 nm induced higher antibody responses to a foot-and-mouth disease virus peptide, more so than larger particles ranging from 37 and 50 nm particles (54). These results suggest that AuNPs may have a complex role in immune potentiation that varies according to their shape or size, or physicochemical properties.

Previous approaches of AuNP use as vaccine platforms against bacterial diseases include *Pseudomonas aeruginosa*, *Listeria monocytogenes*, *Streptococcus pneumoniae*, and *Yersinia pestis* (55–58). Two seminal studies by Dakterzada et al. and Gregory et al. using *P. aeruginosa* and *Y. pestis* (F1) antigens demonstrated that when delivered using gold nanoparticles, vaccination elicited a strong antibody response comparable to an antigen formulated with Freund's adjuvant (55, 58). The latter study showed that F1-delivered using AuNPs, the IgG_{2a} titer was found to be enhanced, compared with F1 soluble antigen (55). These results suggested an indication that AuNPs have an intrinsic property that led to T_H1 responses. Also, mice vaccinated with AuNP-delivered listeriolysin O peptide were shown to induce moderate levels of TNFα and IFNγ in sera and partially protected mice from *Listeria* infection (57). However, when the same formulation was given with Advax as an adjuvant, the T cell response and subsequent protection were further enhanced to levels similar to peptide-loaded DC vaccines (57). Furthermore, Gao et al. showed that *Escherichia coli* OMV-coated AuNPs induced enhanced DC maturation and higher levels of IFNγ and IL-17 after vaccination, suggesting the promotion of a T_H1-T_H17 biased cellular response (48).

One clear advantage of NP-delivered vaccines over soluble antigens arises from their ability to facilitate antigen uptake and activation of APCs (Illustration 1). This enhancement of antigen uptake is due to the multiple array display of an antigen on the surface, which are co-ingested by the immune cell while protecting the antigen until it

reaches its target location. The overall physicochemical properties of NPs (e.g., size, charge, and shape) dictate the interaction with APCs, their uptake, delivery, and ultimate type of immune responses (12, 28, 59). The interaction of NPs with antigens is important but necessary for all NPs (12, 28, 59). Hard material NPs, like AuNPs, can be used to attach antigens by physical adsorption, involving charge or hydrophobic interactions, but these tend to be relatively weak, leading to rapid antigen dissociation (11, 28, 59). However, chemical conjugation onto the NP's surface is a much more stable interaction as the antigen is chemically crosslinked on the surface, allowing for simultaneous uptake by the cell before intracellular release (39, 50). It has been shown that spherical AuNPs are more readily endocytosed than rod-shaped NPs (41, 50). Furthermore, localization of NPs to Lymph nodes (LNs) is primarily affected by their size, where particles ranging from 10 - 100 nm can penetrate the extracellular matrix and travel to LNs more efficiently where they are taken up by resident DCs (41, 50). However, the route of vaccination can also play a critical role in ensuring this. Also, it has been shown that smaller particles, although they are more easily endocytosed, tend to be associated with a higher degree of toxicity, but not larger particles (38, 41, 49, 50).

Particle properties such as charge, size, and shape also have fundamental implications in particle uptake mechanisms such as phagocytosis, clathrin-dependent endocytosis, or non-endosomal pathways (60) (Illustration 1). However, the type of ligand-receptor interaction mediating phagocytosis by APCs influences the downstream processing of internalized particles and their subsequent immune response. Aside from phagocytic receptors, TLRs (e.g., TLR2 and TLR4) also influence the phagosome maturation favoring antigen presentation and induction of an immune response (Illustration 1) (39, 50, 57). The endocytic pathways can direct antigen into distinct populations of early endosomes and dictate an antigen's intracellular processing and presentation mechanism. It is this mechanism, by which the endocytic process determines the pre-early endosome sorting, that will dictate subsequent loading onto MHC class I and MHC class II

(Illustration 1). The use of NPs has been shown to increase the efficiency of uptake into APCs and subsequently induce their maturation and cross-presentation to activate robust adaptive response (21, 22, 24, 37, 41, 48, 55, 57). However, exogenous antigens can be loaded onto MHC class II molecules in different compartments of the endocytic pathway, but phagosomes may also mediate the formation of peptide-MHC class II complexes (41). Antigen-MHC II can then be transported onto the cell surface for presentation to CD4+ T cells, which can help activate B cells to plasma cells that produce antibodies, thereby inducing humoral responses (Illustration 1) (39, 41, 46, 50). On the other hand, after internalization, exogenous antigens can undergo degradation and loading of peptides onto MHC-I molecules for antigen cross-presentation. AuNPs have been shown to play a role in the induction of cellular responses by promoting antigen cross-presentation (21, 39, 51, 57, 61, 62). Although the exact mechanism by which AuNPs may allow for antigen cross-presentation remains unclear, there are several hypotheses. In the first model, antigens are degraded by proteases and loaded onto MHC class I molecules inside endosomes (21, 39, 51, 57, 61, 62). In the second model, it has been postulated that antigens gain access to MHC class I by escaping the phagosomal lumen and into the cytosol where the proteasome processes them and then, through TAP-dependent import, gain access into the ER lumen where they are loaded onto MHC class I molecules (21, 39, 51, 57, 61, 62). These antigens peptide-MHC class I complexes can be transported directly toward the cell's surface or to endosomes than then travel to the cell's surface for presentation and priming CD8+ T cells, allowing for proliferation and subsequent activation of potent effector CTLs (21, 63).

New advances in vaccine technologies, antigen selection, immunology, adjuvants, a vaccine delivery platform, rational selection of different modulators can be selected to achieve optimal protective or therapeutic immune response against infection or even other disease models. However, depending on the pathogen, antigen type, and administration route, each formulation must be tailored for each model. Thus, further studies must understand how and the best method of generating protective or even therapeutic immune

responses by tailored vaccine formulations. Nonetheless, nanoparticle delivery systems will play a central role in such future attempts.

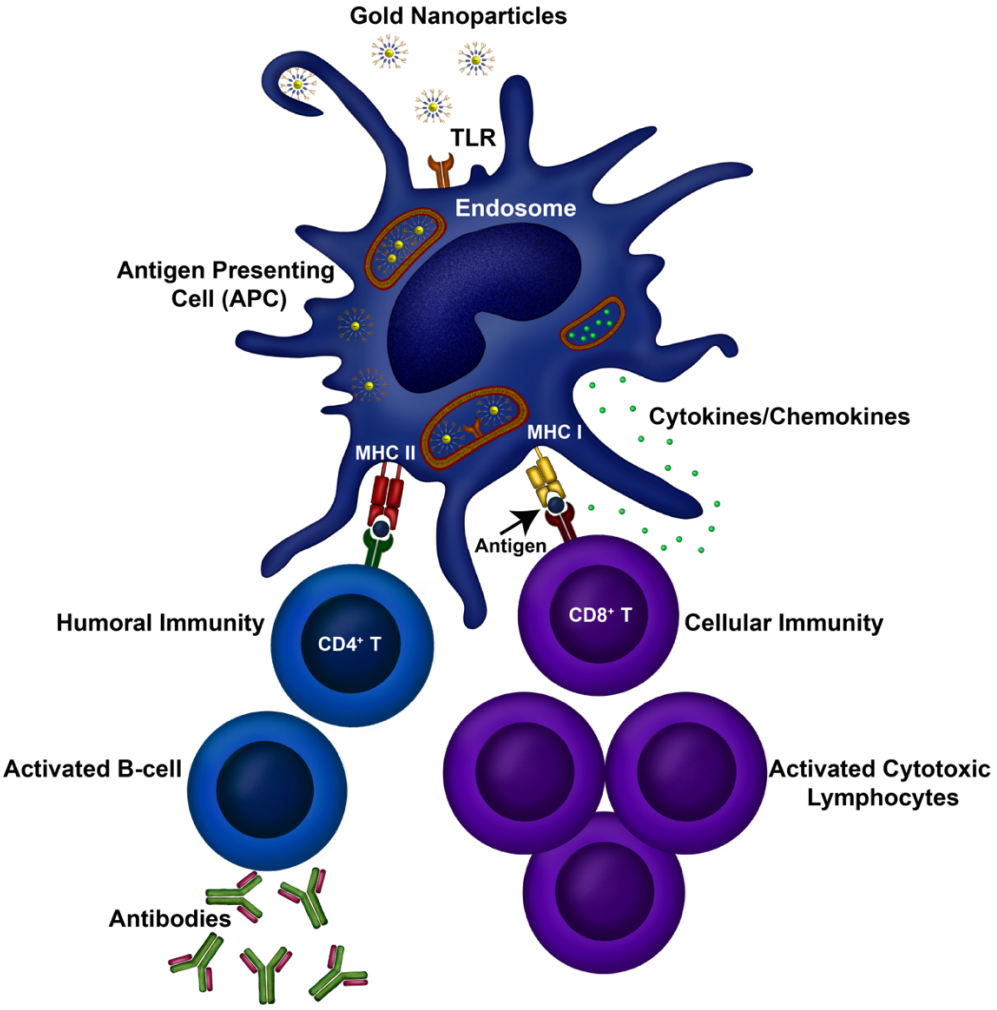

Illustration 1: Gold nanoparticle mechanisms of uptake, processing, and induction of T-helper 1 (T_H1) or T_H2 responses.

Chapter 2: Emerging Role of Biologics For the Treatment of Melioidosis and Glanders

MELIOIDOSIS AND GLANDERS

Melioidosis and glanders are two potentially life-threatening diseases caused by the Gram-negative organisms, *Burkholderia pseudomallei* (*Bpm*) and *B. mallei* (*Bm*), respectively (64–66). These genetically-related pathogens are facultative intracellular bacteria with the ability to infect both phagocytic and non-phagocytic cells, thereby effectively evading the host immune response (67). *Bpm* is a motile saprophytic bacterium capable of infecting a wide variety of mammalian, as well as non-mammalian host species and which can survive in the environment for extended periods of time (66, 68). In contrast, *Bm* is an non-motile bacterium, which requires an animal host to survive and its host tropism is limited to equines (67). The endemicity of *Bpm* is well documented in Southeast Asia and Northern Australia; however, predictive modeling has estimated the global burden of *Bpm* to be positioned in countries along the tropics with an estimate of 165,000 new cases annually of which approximately 89,000 are fatal (66, 69). Melioidosis can be contracted by inhalation, cutaneous inoculation, or ingestion of soil-contaminated food or water (68). Infections associated with *Bpm* can result in a broad spectrum of symptomology ranging from acute pneumonia, skin or organ abscesses, septicemia, or chronic infection, often depending on the route of infection (68). The estimated case fatality rate for melioidosis ranges from 10 – 50% depending on the geographical region and availability of treatment and from those that survived, approximately 5 – 28% experience reoccurring infections (66). In contrast, glanders is a zoonotic disease with high transmissibility between solipeds (horses, donkeys, and mules) (65, 70). Although glanders was eradiated from a large portion of the Western Hemisphere in the late 20th century, the disease remains endemic in Western Asia, India, Africa, and South America, with focal outbreaks still occurring (70,

71). Today, glanders is primarily an occupational disease where infections can occur when individuals come in contact with infected animals (71). Like melioidosis, both equines and humans can present a range of clinical signs depending on the route of infection (65). Disease with *Bm* can present as a pulmonary infection with nasal discharge, referred to as glanders; or cutaneous infection, known as farcy, which can develop as either acute or chronic infections (65, 70). The high mortality, common routes of transmission and the ability for aerosolization with the capability of infecting both humans and animals, has resulted in the dual classification of both *Bpm* and *Bm* as Tier 1 Select Agents by the Centers for Disease Control and Prevention (CDC) and the United States Department of Agriculture (USDA) (72). There are currently no available vaccines for humans or animals and the treatment options though limited, include a biphasic antibiotic therapy which can last up to 6 months (65, 66).

TREATMENT FOR MELIOIDOSIS AND GLANDERS

Early detection for both melioidosis and glanders is imperative for effective pathogen control and early management of disease. In regions with effective diagnosis, early implementation of proper therapy, and facilities with adequate infrastructure for managing sepsis, the mortality of septicemic melioidosis is reduced significantly to approximately ~10% (66, 73). However, such interventions are often not available or are very limited in many countries were melioidosis is endemic. Therefore, effective melioidosis treatment has the potential to reduce mortality rates against this pathogen considerably. The limited knowledge of glanders epidemiology – due in part to the limited number of cases – has resulted in the decline of studies measuring the susceptibility of *Bm* to common antibiotics and other therapies (65, 72). Given that *Bm* presents a similar antibiotic-susceptibility pattern as *Bpm*, therapeutic studies are often focused on protection against *Bpm*, and in a few cases, studies are done using both pathogens. Single drug-therapy is only partially

effective; therefore, therapy relies on the use combination of antibiotics for extended periods of time (74). An additional concern is the fact that there is a larger number of antibiotic-resistant variants of *Bm*, in comparison to *Bpm*, and proper treatment may require abscess drainage in some cases (74). Due to their genetic similarity and pathogenic life cycles, similar therapeutic approaches are recommended and routinely used to treat melioidosis, and if necessary, glanders (74). Likewise, novel vaccine candidates are often tested in cross-protective assays against both *Bpm* and *Bm*. Although not covered here, great progress has been made in the development of novel vaccine candidates and those studies are reviewed in great detail, elsewhere (75). One of the challenges for the treatment of melioidosis includes the resistance of *Bpm* to first and second-generation cephalosporins, penicillin, gentamicin, tobramycin, streptomycin, macrolide, polymyxins, and aminoglycosides (74). However, the majority of *Bpm* clinical isolates have a similar antimicrobial susceptibility pattern including, β-lactam antibiotics such as ceftazidime, meropenem, imipenem, and co-amoxiclav, and almost always present similar susceptibility patterns to bacteriostatic antibiotics like doxycycline, chloramphenicol, and trimethoprim-sulfamethoxazole (66, 74). Furthermore, concerns regarding the rise of multi-drug resistant *Bpm* by the overuse of antibiotics or by natural acquisition of resistance, combined with the limited treatment options against *Bpm* have generated the need to develop novel therapies that either enhance antibiotic therapy or that target specific mechanisms of pathogenesis (66). Although many candidates have shown variable degrees of success, none have replaced the formal guidelines for the treatment of melioidosis defined by the CDC. The treatment for melioidosis includes an intensive phase of intravenous antibiotic therapy consisting of ceftazidime or meropenem for 10 – 14 days, followed by an extensive eradication phase to prevent relapse of disease, especially in highly susceptible immunosuppressed patients (66, 68, 76). The eradication phase consists of an oral administration of trimethoprim-sulfamethoxazole that can last between 3 - 6 months, depending on clinical presentations, with more prolonged therapy recommended for neuro-

melioidosis or osteomyelitis complications (64, 66). Because of the long-term antibiotic therapy against melioidosis, adverse effects are reported in up to 40% of patients, including allergic reactions (e.g. rash, pruritus) or gastrointestinal disorders (e.g. nausea, vomiting) (76). Therefore, new therapies should address the potential side effects, specifically in the young and elder populations, or heavily immunocompromised individuals (66). In addressing the need for effective therapies, novel compounds should address the need to reduce mortality, treatment length, reduce adverse effects, and the potential for relapse.

NOVEL THERAPEUTIC APPROACHES

The natural resistance to clinically-relevant antibiotics among clinical isolates of *Bpm*, especially to oral antibiotics used during the eradication phase (e.g. 0.3%-5.1% of clinical strains are resistant to co-trimoxazole), has generated attention in the development of new therapeutic approaches against *Bpm* (66, 74, 77). As stated before, few studies assessing antibiotic sensitivity patterns of resistance have been performed but indicate a similar pattern of resistance between *Bpm* and *Bm* (65, 74). Here we provide a literature update on new targets for both the prevention and treatment of melioidosis and glanders (Illustration 2). The studies have focused mainly on the identification of novel drug targets, reappraisal or potentiation of existing treatments, or immune modulation as a means of pathogen control (Illustration 2).

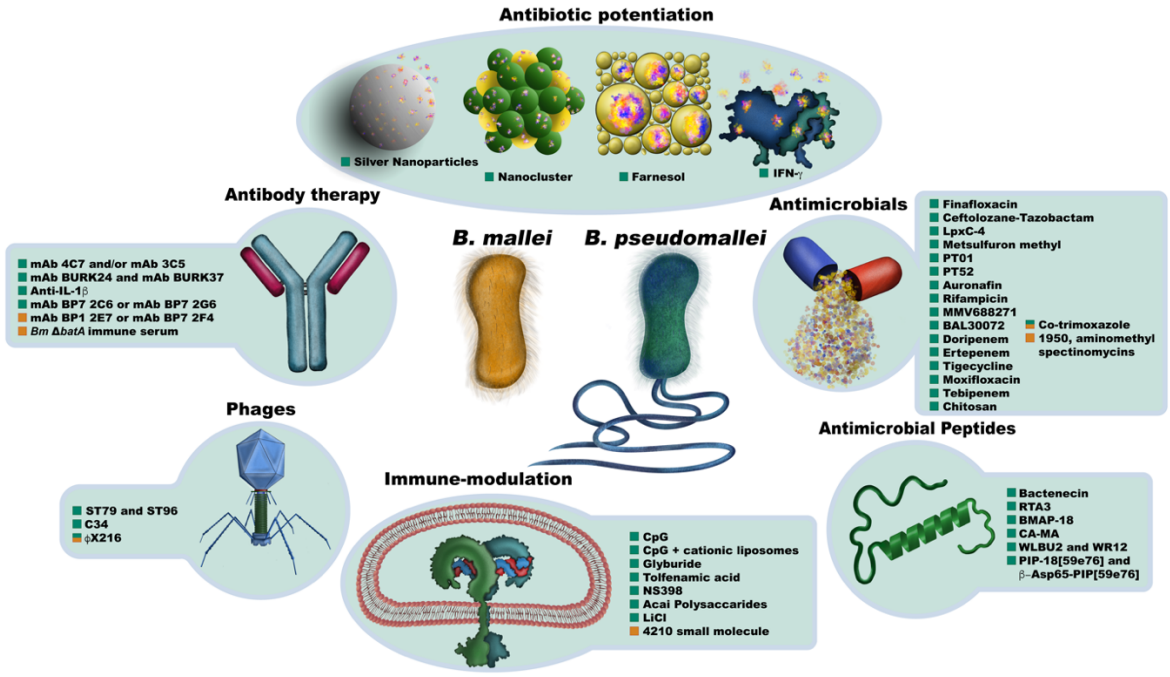

Illustration 2: Antimicrobial approaches for *B. pseudomallei* and *B. mallei*.
Summary of approaches taken for the development of preventive and therapeutic approaches against both pathogens. Green squares represent approaches taken for *B. pseudomallei*, yellow squares represent approaches taken against *B. mallei*, and combination of green/yellow squares represent approaches taken against both.

NEW ANTIBIOTICS AND NOVEL TREATMENT OPTIONS

Screening of new drugs and repurposing compounds

Ciprofloxacin is a fluoroquinolone that was routinely given as a compound during the oral eradication phase for melioidosis. However, a clinical study conducted in Thailand raised efficacy concerns while reporting a failure rate of 29%; therefore, regimens containing fluoroquinolones like ciprofloxacin are currently not recommended for treatment of melioidosis, unless no other option is available (78). A study examined the efficacy of finafloxacin, a novel fluoroquinolone with bactericidal activity at an acidic pH both *in vitro* and *in vivo* (79). Finafloxacin showed bactericidal activity against *Bpm* with a minimum inhibitory concentration (MIC) of 1-2 µg/mL (79). In addition, finafloxacin showed higher

efficacy in an inhalational murine model of infection with a 60-80% survival at 14 days post infection, and lower bacteria load in the lungs and spleens of infected animals as compared to ciprofloxacin or co-trimoxazole (79). Due to the rise in antimicrobial resistance, combinations of compounds have received attention as potential therapies against *Bpm*. Another study determined the *in vitro* efficacy of ceftolozane-tazobactam in 62 *Bpm* strains isolated from human, marine, birds, and soil samples. Of all strains tested, approximately 90% of human isolates and 100% of animal and environmental strains showed susceptibility at concentrations < 4 μg/mL (80). A separate study assessed the susceptibility of several *Bpm* clinical isolates to LpxC-4, an LpxC inhibitor, which is an enzyme involved in the biosynthesis of lipid A (81). Both bacteriostatic and bactericidal effects against *Bpm* were demonstrated at low concentrations, 2 and 4 μg/mL, respectively (81). There were no synergistic effects by combining LpxC-4 with ceftazidime; however, the minimum concentration required to inhibit 90% of both antibiotic-resistant and antibiotic-susceptible *Bpm* strains was 2 μg/mL (81). Another study focused on the inhibition of a metabolic process using 5R-thiolactomycin (TLM), a bacterial fatty acid synthesis inhibitor for β-ketoacyl-ACP synthases (KAS) (82). TLM showed anti-*Bpm* activity *in vitro* with a MIC of 8 μg/mL (82). A more recent study targeted aceto-hydroxy-acid synthase (AHAS), an enzyme important in the biosynthesis of branch chain amino acids (BCAAs) using sulfonyl-urea herbicides (SH) (83). Different SH analogs showed bacteriostatic effects against *Bpm in vitro* with chlorimuron-ethyl, and metsulfuron-methyl being the most effective with a MIC of 31.2 μM (83). Mice that received daily oral administrations of metsulfuron-methyl (50 mg/kg) exhibited 100% survival at day 10, after a lethal intranasal *Bpm* challenge (83). Another group investigated PT01, a FabI-specific enoyl-ACP reductase inhibitor, which exhibited a MIC of 1 μg/mL *in vitro* against *Bpm* (84). Animals treated with PT01 after *Bpm* infection showed lower bacterial burden in the spleen, in comparison to vehicle control, but higher than ceftazidime-treated animals (84). Later experiments assessed the efficacy of a FabI1-specific inhibitor library with

substituted diphenyl-ethers against *Bpm*, in addition to enzyme kinetics against the FabI1 enzyme (85). The most effective compound, PT52, had potent activity against FabI1 enoyl-ACP reductase, with a MIC of 1 µg/mL against *Bpm* (85). PT52 also showed activity *in vivo* against *Bpm* infection with a reduction in bacterial burden in the lung and spleen 60 h post infection, though not significantly lower than ceftazidime-treated animals (85).

The use of currently approved drugs as repurposed therapeutics has been explored *in vitro* and in small animal models for melioidosis (86). Our group recently reported the effectiveness, *in vitro*, of several drugs against a set of *Bpm* strains, the lowest MICs were established for auranofin, rifampicin and MMV688271, with doses of 150, 18-45, and 6-12 µg/mL, respectively (86). This is the first study showing the potential for these compounds to reduce the number of persister cells, a small population of bacteria closely associated with relapse and chronicity, a big obstacle in the treatment of melioidosis. Most studies concentrating in the development of new antimicrobials focus on evaluating bacterial viability, but future studies should also aim to evaluate the potential to reduce or eliminate persister cell populations as a measure of their ability to reduce disease recrudescence. Other antimicrobial compounds that have been tested *in vitro* include a new monosulfactam (BAL30072), doripenem, ertapenem, tigecycline, moxifloxacin, and tebipenem (86–88). BAL30072 showed remarkable bactericidal activity against *Bpm* with a MIC of 0.008 µg/mL (87). Given the specificity and low MIC values, a combination of BAL30072 and a FabI1 enoyl-ACP reductase, such as PT52, should be further explored for its potential potentiation in controlling *Bpm* infection *in vitro* and *in vivo*. The combination of compounds has the potential to reduce resistance and treatment length, while maintain specificity and efficacy. However, future experiments should focus in evaluating the ability to control potential relapse. Doripenem, ertapenem, tigecycline, moxifloxacin, and tebipenem have been also shown effective against *Bpm* with MICs of 1, 4, 3, 1.5, and 1-2 µg/mL (tested against 102 *Bpm* clinical isolates), respectively (88).

Most studies assessing the efficacy of novel therapeutics against *Bm* rely on the potential for cross-reactivity and test against both *Bm* and *Bpm*. For example, the antibacterial properties of N-benzyl aminomethyl spectinomycins (amSPCs), a novel class of protein synthesis inhibitors was examined *in vitro* by MIC, synergistic testing, as well as *in vivo* experiments (89). Interestingly, compound 1950 showed a potent MIC of 6.3 µg/mL against *Bm* with a dose range across 29 strains of 3.13-50 µg/mL, whereas the MIC for *Bpm* was > 200 µg/mL (89). In addition, a combination of amSPC 1950 with doxycycline or trimethoprim was tested against *Bm*, and the treatment was shown to have a synergistic effect (89). However, no synergistic effect was seen with amSPC 1950 against *Bpm*. Lastly, amSPC 1950 showed significantly increase in mice survival for up to 40 days post infection after receiving a 14 day treatment regimen, followed by an intranasal challenge with 10 lethal dose-50 (LD_{50}) of *Bm* (89). Surviving animals receiving treatment up to 6 h post infection exhibited low bacterial burden in the lungs, livers, and spleens (89). The use of amSPC 1950 with other *Bm*-specific therapies should be further evaluated in small animal models to evaluate the potential to reduce chronic infections, treatment length, and potential adverse effects. Another group tested the efficacy of co-trimoxazole (trimethoprim/sulfamethoxazole) as post-exposure prophylaxis against both pathogens (90). The MICs against *Bpm* and *Bm* were 32/16 µg/mL and 8/32 µg/mL, respectively (90). Mice that received co-trimoxazole twice for 14 days, beginning with 6 h post infection, showed 60-100% survival after a lethal challenge with *Bpm*; however, surviving animals were heavily colonized in both the lungs and spleens (90). In comparison, 67% of animals that received an equivalent treatment regimen of co-trimoxazole survived to 74 days after challenge with *Bm* (90). No differences in bacterial colonization in mice treated with co-trimoxazole from 6 h or 24 h post infection were observed (90). Single drug therapies remain an obstacle for effectively controlling *Bpm* or *Bm* infection. Therefore, we recommend that future research should focus in evaluating combination therapy options that maintain a safe profile, specifically target *Burkholderia* pathogenesis, and have the

potential to reduce bacterial latency as a gold standard for evaluating compound efficacy. Overall, development of *Burkholderia*-specific antimicrobials and the prospective use of multidrug therapies necessary for the treatment of glanders and melioidosis is feasible.

Antibiotic potentiation

The capacity to potentiate antibiotic therapy while reducing side effects is essential to improve treatment against *Bpm* and *Bm* infections. A recent study showed the antimicrobial activity and mechanism of silver nanoparticles (AgNPs) against *Bpm* (91). The determined MICs and minimum bactericidal concentration (MBC) against 9 strains of *Bpm* ranged from 32-48 and 96-128 μg/mL, respectively. In comparison, the MIC and MBC for ceftazidime against *Bpm* ranged from 128-512 and 512-1024 μg/mL, respectively (91). In addition, AgNPs were showed to have a two-phase bactericidal mechanism involving the induction of cell death by damaging the integrity of the membrane, and the production of reactive oxygen species (ROS) (91). Cytotoxicity is a concern when AgNPs are used; however, toxicity was not observed in human red blood cells at a concentration < 256 μg/mL (91). Another approach to potentiate therapeutics effectiveness includes improving their delivery. NanoCluster, a dry powder aerosol for pulmonary antibiotic delivery in humans, was shown to provide high drug doses directly into infected tissues, eliminating the need for intravenous delivery and minimizing systemic side effects (92, 93). The aerosolized NanoCluster particulates containing ceftazidime were retained in the lungs of mice for up to 6 h post exposure (92). Animals treated with nebulized ceftazidime (100 mg/kg) every 12 h after an aerosol challenge with a lethal *Bpm* dose survived up to 21 days, though animals appear symptomatic and did not recover their baseline body weight (92). Although aerosolized ceftazidime was able to control *Bpm* infection, animals had high bacterial burdens in the lungs and spleens (92). Another study evaluated the *in vitro* activity of farnesol, an oil-like substance, against *Bpm* biofilms and the potentiating effect

on the activity of several antibacterial drugs (94). The minimum biofilm eradication concentration (MBEC) had a range from 75-2400 mmol/L, and when combined with ceftazidime, amoxicillin, doxycycline, and sulfamethoxazole–trimethoprim, farnesol reduced their MBEC values by 256, 16, 4, and 4 times, respectively (94).

Targeting host immune responses by creating a balance that allows for bacterial control while preventing pathogenic immune responses in humans is an area of interest for both the prevention and treatment of melioidosis (95). To potentiate conventional antimicrobial therapy as a prophylactic treatment against *Bpm*, a group tested the combination of immunotherapy, using IFNγ, and ceftazidime to evaluate a potential synergistic effect (96). Treatment with low IFNγ doses in combination with ceftazidime showed strong synergistic correlation in the inhibition of *Bpm* replication in infected macrophages, with compound concentrations as low as 1 μg/mL. In animals treated with IFNγ and a low dose of ceftazidime and then challenged, a potentiated effect of each compound with significantly higher survivors during acute infection (day 21 post infection), lower bacterial burden, and dissemination to the spleen, was observed (96). However, no differences were seen in survival in chronically infected mice at day 60 post infection (96).

In a study to potentiate antibiotic therapy against glanders and using animals immunized with a whole-cell killed vaccine, *Bm*-challenged mice were treated with either moxifloxacin, azithromycin, or sulfamethoxazole-trimethoprim, and therapy significantly increased survival (day 21 post infection), even when antibiotic therapy was administered 5 days post challenge (97). Although this course of therapy is not realistic in a clinical setting, continuing to assess how immunotherapy works, might help potentiate the antimicrobial properties of traditional prophylactic therapies (97). Antibiotic potentiation has shown great promise, specifically in the delivery of antimicrobial compounds, an area that remains largely understudied. We recommend future studies should focus in maintaining safety while reducing treatment length.

ANTIBODY THERAPY

Recent evidence has determined the importance of antibodies for the protection against melioidosis and glanders in small animal models (75, 98, 99). Therefore, the use of monoclonal antibodies against various virulence factors of *Bpm* has gained interest. The polysaccharides of *Bpm* and *Bm* are conserved virulence factors and provide partial protection in mouse models of infection. A group recently explored the therapeutic potential of two monoclonal antibodies (mAbs) targeting the lipopolysaccharide (LPS) (4C7) and the manno-heptose domain of the capsular polysaccharide (CPS) (3C5) (100, 101). Animals challenged with a lethal inhalational dose of *Bpm* and treated with 1 mg of each antibody, or a combination 18 h post infection, exhibited increased survival compared to isotype IgG3 antibody control (101). The anti-CPS, anti-LPS, or combination formulation, had 86%, 50% and 100% survival at 21 dpi, respectively (101). In addition, animals that were immunized with the combination formulation had lower bacterial burden and no abscesses were found in the spleen, compared to single antibody immunization (101). Another study evaluated two mAbs, BURK24, and BURK37, which are reactive against outer membrane proteins and LPS, respectively, and tested their ability to limit biofilm formation, invasion, and induction of apoptosis against *Bpm* (102). Incubation of cultures in the presence of BURK24 and BURK37 mAbs resulted in a bacteriostatic effect against two strains of *Bpm* with a MIC of 30 and 62.5 μg/mL respectively (101). In addition, MBC for BURK24 and BURK37 was determined to be 125 and 500 μg/mL, respectively, and both antibodies limited the formation of biofilm and significantly reduced the invasion and apoptosis of alveolar epithelial cells (101).

A different approach has been taken by targeting the host innate system to control acute infection. IL-1β is a pro-inflammatory cytokine that produces deleterious effect when controlling infection by excessive neutrophil recruitment, thereby promoting intracellular *Bpm* growth, excessive tissue damage, and inhibition of IFNγ (103). A recent study

targeted this deleterious inflammatory response by giving a therapeutic dose of anti-IL-1β, starting at 6 h post infection, and resulting in a significant bacterial reduction in blood, lungs, and livers of animals at 24 and 72 h post infection (104). In addition, there was a significant delay in the time of death in animals treated 6 and 24 h post *Bpm* infection, although no synergistic effect was observed in the reduction in organ colonization when animals were co-treated with ceftazidime and anti-IL-1β (104). These results support the potentially protective nature of passive Abs immunization in the prevention of melioidosis.

Another study using mAbs against various surface antigens of *Bpm* and *Bm* demonstrated that antibodies targeting LPS and CPS had strong opsonophagocytic activity; however, none of them showed any bactericidal activity (105). To determine if mAbs conferred a protective effect, BALB/c mice were passively immunized with mAb BP7 2C6 (CPS reactive) and mAb BP7 2G6 (LPS reactive) showing significant increase in survival at day 21 post *Bpm* lethal challenge (105). In comparison, animals that received immunization with mAb BP1 2E7 or mAb BP7 2F4 showed a significant increase in survival, in comparison to those receiving naïve serum after challenge with a lethal dose of *Bm* (105). These mAbs had reactivity against different epitopes of CPS or LPS, supporting the importance of these antigens as targets to prevent infection. These antibodies target carbohydrates and may, as a result, prevent the initial adherence of the bacteria to the surface of the epithelium; thereby, limiting their intracellular replication (105, 106). A separate study determined the therapeutic potential of antibodies against an autotransporter protein shared by *Bpm* and *Bm*. Sera from animals immunized with a *Bm* Δ*batA* strain, and administered by passive immunization, showed protection with an increase in survival against both lethal *Bpm* and *Bm* inhalational challenges (107). Experiments also showed that the protective immunity is predominantly mediated by IgG antibodies reacting against *in vivo*-expressed antigens (107). Antibody therapy, specifically against *Burkholderia* polysaccharides has shown promising results, but the short time

window for treatment remains an obstacle for further testing, and the potential development of adverse effects should be further evaluated before initiating clinical trials.

IMMUNE MODULATION

Experimental immunotherapy has demonstrated its potential against a wide range of intracellular pathogens (74). Systemic administration of synthetic CpG oligodeoxynucleotide (ODN), a TLR9 agonist, has been shown to protect against *Bpm* and *Bm* (74). Recent work has focused on understanding the underlying immune mechanisms mediating such protection. Previously, it has been shown that CpG significantly increases the time to death and provides partial protection against *Bpm* when delivered at the time of infection, and for up to 18 h (108). In addition, administration of CpG intranasally at the time of infection delayed the onset of sepsis and reduced bacterial burden in lungs (108). The protection associated with intranasal delivery of CpG was associated with a rapid increase in the production of pro-inflammatory cytokines and chemokines such as TNFα, IL-6, and MCP-1 at days 1 and 2 post-treatment (108). However, the combination of immunization prior to challenge, along with CpG treatment at the time of challenge, provided significantly greater protection than either treatment alone and with decreased bacterial burden by > 1,000 fold (108). Besides the function of CpG as an adjuvant molecule to enhance vaccines, the potential of CpG as a therapeutic has been demonstrated when delivered at the time of or after infection (109). The prophylactic potential of CpG as a therapy for *Bpm* infection has been corroborated in our laboratory (109). Intranasal treatment with class C CpG had an increase in inflammatory monocyte and neutrophil recruitment post-treatment (109). Animals infected post CpG treatment had reduced bacterial colonization and reduced levels of pro-inflammatory cytokines and chemokines such as monocyte chemoattractant protein-1 (MCP-1), IL-1α, IL-1β, and granulocyte colony-stimulating factor (G-CSF) (109). The protective effect of CpG against *Bpm* can be

maintained when given up to 10 days prior to infection (110). Another study has extended this narrow window of protection by incorporating CpG to cationic liposomes (DOTAP) (110). Intramuscular delivery of DOTAP-CpG significantly increased survival of mice challenged with *Bpm* up to day 30 with 100% survival (110). Co-delivery of CpG with DOTAP increased the window of protection of CpG in animals receive treatment up to 30 days prior to infection (110). Delivery of DOTAP plus CpG was associated with lower IFNγ levels following intranasal infection, although macrophages from stimulated mice showed higher antimicrobial activity with lower bacterial replication, and higher nitric oxide production (110). Other studies aimed at increasing the protective effect of CpG by combining immunotherapy with vaccination (108, 111). In a recent study, animals were immunized intranasally with a live-attenuated vaccine (2D2) prior to an intranasal challenge a lethal dose of *Bpm*, then treated with CpG 18 h post infection (108). The combination of pre-exposure vaccination with 2D2 and CpG treatment up to 18 h post-infection significantly increased survival, lowered bacterial load, and delayed the onset of sepsis than either treatment alone (108).

Diabetes mellitus is among the most common risk factors associated with *Bpm* infection and its association with melioidosis includes impaired host responses like those of cytokines and macrophage killing (66). A recent study found that melioidosis patients with diagnosed diabetes prior to *Bpm* infection had a lower risk of mortality than patients without diabetes [50]. The authors found that this reduction in mortality rates was associated with the use of glyburide, rather than the diabetes disease. In addition, they found that the use of glyburide-prior to admission was associated with lower mortality and an attenuated inflammatory response [50]. Glyburide is a KATP-channel blocker, and a broad-spectrum ABC-binding cassette used to treat type 2 diabetes. In addition, there is evidence that glyburide also has a wide range of anti-inflammatory effects (114). An animal model of diabetes was used to assess the effect of glyburide in controlling *Bpm* infection (112). Although glyburide treatment did not affect glucose levels in the blood or

Bpm growth, animals treated with glyburide prior to infection showed reduced pulmonary cellular influx, reduced bacterial dissemination to both the liver and spleen, and reduced IL-1β secretion in comparison to untreated controls (112).

Another approach to modulate the inflammatory responses after *Bpm* infection is the inhibition of prostaglandin E2 (PGE2) production by blocking the enzyme cyclooxygenase-2 (COX-2) using tolfenamic acid (TA), an approved COX-2 inhibitor for migraines (115). Using an intranasal animal model of melioidosis, co-treatment with orally administered TA (MIC > 489 μM) and a sub-therapeutic dose of ceftazidime, it significantly increased survival of mice and reduced bacterial burden in the lungs of infected mice, and to some extent, a delay in the time of death in TA-only treated mice (115). Another study also wanted to exploit the inhibition of pro-inflammatory secretion of PGE2 by testing a commercially-available COX-2 inhibitor, (N-[2-(cyclohexyloxy)-4-nitrophenyl] methane sulfonamide) (NS398), as a post-exposure therapeutic agent against *Bpm* (116). Animals treated with three intraperitoneal doses of 15 mg/kg of COX-2 inhibitor (NS398) had a significant increase in survival for up to 10 days after infection, and had reduced bacterial replication in macrophages (116). Another approach screened various polysaccharides derived from the Acai berry (Acai PS), which are natural immune agonists and have immunotherapeutic potential due to their ability to enhance host resistance to infection (117). Animals treated with intranasally-delivered Acai PS prior or during infection had a significant increase in protection against intranasal infection with *Bpm* (117). Acai PS treatment reduced significantly the lung bacterial burden and subsequent dissemination to the liver and spleens of infected mice, which was associated with elevated levels of IFNγ responses produced by NK and γδ T cells in the lungs (117). Another group exploited the regulation of the inflammatory response by blocking the activity of glycogen synthase kinase-3, a well-recognized molecular switch controlling inflammatory responses during infection (118). In particular, glycogen synthase kinase 3 (GSK3β) has been shown to play a role in regulating the balance between the production

of pro- and anti-inflammatory cytokines (118–120). In a recent study, animals were given LiCl, a GSK3 inhibitor, and showed that treatment post infection significantly increased survival and reduced organ bacterial load in the lungs as well as in the spleens and livers after challenge with *Bpm* (119). Due to GSK3 inhibition, pro-inflammatory cytokines such as TNFα, IL-1β, and IFNγ were decreased in several organs whilst levels of anti-inflammatory cytokines such as IL-10 and IL-1Rα were further elevated (118). These results indicate that control of immune responses could be a potential therapy against *Bpm*, especially in immunocompromised individuals.

Few studies have assessed the importance of targeting immune mechanisms as a form of therapy against glanders. One study evaluated a dimeric structure compound, 4210, which contains a small molecule mimicking the BB-loop of MyD88 and acts inhibiting the *Bm* LPS-mediated production of pro-inflammatory cytokines in human primary cell lines, with an inhibitory concentration 50 (IC_{50}) of 10-200 μM (121). Although the experiments assess the protective ability of 4210 against endotoxemia, they suggest that controlling inflammatory responses might be effective therapeutic targets to control *Burkholderia* infection. Immunotherapy options for *Burkholderia* have shown promising results in treating these infections, but the ability of CpG to prevent *Burkholderia* infection remains an important target. Although the time window of opportunity for treatment and potential adverse effects in humans remain an obstacle, future therapeutics or preventive vaccines should aim at exploiting this compound for its antimicrobial and adjuvant properties.

ANTIMICROBIAL PEPTIDES

Antimicrobial peptides (AMPs) are important protective components of the innate immune system which help protect against invading organisms (122, 123). Although the precise mechanism by which AMPs act in their targets is non-specific, they are potent inhibitors of pathogen growth, acting directly by disrupting membrane integrity (123). Unlike

antibiotics, AMPs often have a broad spectrum of antimicrobial activity, interacting with both Gram-negative or Gram-positive outer membrane components, making them ideal candidates for use against antibiotic-resistant pathogens (123). A study evaluated the antimicrobial properties of four AMPs: bactenecin, RTA3, BMAP-18, and CA-MA. All peptides demonstrated strong bactericidal activity > 97% against *Bpm*, with bactenecin having the highest activity, at a concentration of 20 μM (124). In addition, all peptides showed potent inhibition on *Bpm* biofilm formation, and bactenecin and CA-MA showed complete inhibition of bacterial growth at 50 μM (124). Bactenecin was found to have a strong binding ability to LPS and induced perturbation of the inner membrane by changing the membrane fluidity and permeability (124). In addition, bactenecin was shown to insert into the membrane, forming dimers in the membrane, causing permeabilization and leading to leakage of the cytosol and death (124). To increase the activity of antimicrobial peptides, a phenomena sometimes dependent on the cellular environment in which it is acting, a novel approach was used by engineering de novo-synthesized cationic antimicrobial peptides (eCAPs) and tested two peptides, WLBU2 and WR12, against several pathogens including *Bpm* (125). When compared to the human CAP cathelicidin (LL-37), WLBU2 showed robust bactericidal activity against *Bpm* with a concentration of 25 μM, while all three peptides were shown to have bacteriostatic activity against *Bpm* by inhibiting bacterial growth (125). Another study screened the antimicrobial properties of naturally derived peptides synthesized from *Python reticulatus* serum proteins against *Bpm* (126). Among the different peptides tested, phospholipase A2 inhibitor peptide (PIP)-18[59e76], β-Asp65-PIP[59e67], D-Ala66- PNT.II, and D60,65E-PIP[59e67] had the strongest bactericidal activity, with PIP-18[59e76] and β-Asp65-PIP[59e67] having the lowest MIC of 3.125 μg/mL against *Bpm* (126). In addition, it was shown that both of these peptides helped promoting wound healing by enhancing specific cell activities such as cell growth, migration, and angiogenesis while displaying minor cytotoxic effects on cultured cells (126). The potential of CAPs as therapeutic agents, for their broad-spectrum activity

against multidrug-resistant organisms like *Bpm*, needs to be further investigated. Antimicrobial peptides show moderate results *in vitro* against *Bpm*, but further *in vivo* testing should be performed to evaluate their potential as therapy in combination with other antimicrobials.

OTHER APPROACHES

Some recent therapeutic approaches used to combat *Burkholderia* infections include the evaluation of phage therapy. The use of phages and their lytic proteins has regained interest due to their antimicrobial potential, especially against multidrug-resistant organisms, and has the potential to be used as an alternative to, or in combination with conventional antimicrobials (127, 128). Two lysogenic phages isolated from the soil in endemic regions showed *Bpm*-specific bactericidal activity (129). Phages ST79 and ST96 lysed 71% and 67% of all *Bpm* strains tested, respectively, and were also able to induce the formation of plaques against *Bm* (129). When tested using a multiplicity of infection (MOI) of 0.1, both ST79 and ST96 were able to lyse a mid-log phase culture within 6 h (129). In a later study with 6 phages, including ST79, they examined their bactericidal activity and ST79 had the highest lytic capability. ST79 was able to reduce the bacterial number by 4-logs after 4 hours of incubation (130). In addition, ST79 treatment using an MOI of 10 significantly reduced *Bpm* biofilm formation (130). Three derivates of ST79 were generated by serial passage in phage-resistant *Bpm* strains, allowing an increase in lytic activity from 62% to 80% (130). Another study identified the lysis gene cassette required for the induction of *Bpm* lysis and found a 1.5 kb gene cluster containing holin, peptidase M15A (endolysin), *lysB* and *lysC* genes (131). When tested individually or in combination for their ability to induce membrane lysis, co-expression of holin and peptidase M15A showed the highest lytic activity against *E. coli*, but no information was provided for *Bpm* (131). Another group identified ϕX216, a phage capable of infecting up to 78% of different *Bpm* isolates and *Bm*

but was not able to infect other *Burkholderia* species, including *B. thailandensis*, an environmental bacterium (132). Although no antimicrobial effects were described, the broad strain infectivity, combined with the specificity for both *Bpm* and *Bm* indicate that ϕX216 would be a viable candidate for therapy. A more recent study investigated the potential of C34, a phage isolated from seawater, for treatment of *Bpm*-infected cells (133). C34 was able to lyse 39.5% of clinical *Bpm* strains and treatment of human lung epithelial cells with an MOI of 100 of C34 prior to infection increase cell survivability by approximately 20% (133). In addition, treatment of mice with C34 prior to infection, had a significant increase in survival to 33% at day 14 post infection (133). Although still in very early stages of clinical development, advances in the understanding of phage biology have made this therapy a promising approach and preventive biological measure against *Burkholderia* infections.

Another antibacterial agent recently tested against *Bpm* is chitosan, a natural biopolymer derived from chitin which has been shown to have antimicrobial activity against many drug-resistant bacteria and acts by compromising the bacterial cell wall (134). Chitosan at 5 mg/mL had complete bactericidal activity against four environmental strains of *Bpm* within 24 h, while 2 mg/mL lowered the viability of *Bpm* by 20% within the same time span (134). It was determined that the mechanism of action of chitosan against *Bpm* was the disruption of the bacterial membrane, releasing intracellular contents, and with subsequent bacterial death (134). Although phage therapy as antimicrobial therapy is still a developing field, the potential to control persistent infections has shown great success with other pathogens (135), and continuous progress has been made in the last ten years. Future studies should focus in evaluating *Bpm*-specific phages alone or in combination with other forms of therapy to reduce treatment length and chronic infections.

COMMENTARY OF FUTURE *BURKHOLDERIA* THERAPEUTICS

Although melioidosis and glanders are bacterial infections that have affected humans and animals since the 18th century, efforts to develop effective therapeutic approaches have not gained significant attention and treatment was solely dependent on the use of antibiotics. Reinvigoration in the therapeutic field was dependent on the inclusion of these two pathogens in the Select Agent registration list. As a result, multiple research groups have developed a wide variety of approaches as standalone treatment or as co-treatment options associated with either antibiotic or vaccine therapy. The area of vaccine development has been extensively reviewed elsewhere (75) and in further detail in the next sections of this dissertation. However, vaccines are a field that have made enormous advances in a short period of time in developing, testing, and advancing to pre-clinical evaluation, particularly in the case of a melioidosis vaccine. In contrast, other therapeutic approaches have made steady-state advances, but further testing, optimization and eventually implementation are needed. One strong justification to develop alternative approaches is the fact that implementation of a melioidosis and/or glanders vaccine might be limited to some endemic regions or only used for military personnel deployed to areas of endemicity. As these pathogens have been demonstrated to be present in all tropical areas around the world, it is necessary to have other treatment options available. In addition to antibiotics, it is desirable to have supportive therapy that can specifically target the disease in patients that accidentally encountered these pathogens in nature or upon contact with infected animals.

The advancements in treatments designed for military personnel that might be intentionally or accidentally exposed to these pathogens require that such therapeutic agents act quickly and specifically and that can prevent recurrence or recrudescence of the disease. If such supportive treatment is implemented in addition to the conventional antibiotic therapy, it will provide the community at large with more options to reduce the time for treatment and will potentially support areas where antibiotics are not available, or patients might not be able to financially afford a long treatment. More exciting is the fact

that developing alternative options to treat these devastating diseases has opened the door for novel therapeutic approaches that can be directed to treat a wide variety of pathogens, many of them that do not have an effective vaccine, or which current treatment is not effective.

Chapter 3: Pathogenic *Escherichia coli*

PATHOTYPES AND ENTEROHEMORRHAGIC *E. COLI* O157:H7

Escherichia coli is an innocuous member of the intestinal microbiota in the gastrointestinal tract of humans and other mammals; however, it also can cause severe diarrheal and extraintestinal disease using a wide range of virulence factors affecting several cellular processes (136, 137). These virulence factors, which are often encoded on mobile genetic elements, can move into different strains creating novel combinations of virulence factors allowing for adaptation and survival in new niches in a wide range of environments (137). This remarkable ability of *E. coli* species to adapt to a wide range of environments also contributes to the broad spectrum of disease. These fixed combinations of virulence factors have been used to define specific "pathotypes" of *E. coli*, each with a unique lifestyle and capable of causing disease in healthy individuals with three general syndromes: enteric/diarrheal disease, urinary tract infections (UTIs), and sepsis or meningitis (137). Many of the *E. coli* pathotypes are a significant public health concern and are associated with outbreaks common in developing and developed nations, often associated with fatal consequences (136, 137).

Among the pathotypes, diarrheagenic pathotypes are a significant contributor to the mortality associated with diarrhea, particularly in children under five years of age (136). While various pathotypes can contribute to diarrhea, the clinical outcomes and mechanism of the disease can differ. The different traits associated with the different pathotypes come from the genome plasticity and evolutionary adaptability through the acquisition of different combinations of virulence traits or virulence islands (136, 137). Therefore, the description of different pathotypes has conventionally relied on a signature of characteristics including clinical manifestations, epidemiological, and genotypic or phenotypic traits (137). The major diarrheagenic *E. coli* pathotypes include

enteropathogenic *E. coli* (EPEC), Shiga toxin-producing *E. coli* (STEC) (which encompass enterohemorrhagic *E. coli* [EHEC]), *Shigella*/enteroinvasive *E. coli* (EIEC), enteroaggregative *E. coli* (EAEC), diffusely adherent *E. coli* (DAEC), and enterotoxigenic *E. coli* (ETEC), as well as a more recently recognized pathotype, adherent invasive *E. coli* (AIEC) (136, 137). However, while many pathotypes can contribute to diarrhea, STEC is one of the pathotypes associated with the highest mortality in healthy individuals.

Members belonging to the STEC pathotype are predominantly foodborne pathogens transmitted orally mainly by consuming contaminated products that posing a significant public health concern in both high and low-to-middle income countries (136). The presence of Shiga toxins 1 and 2 (Stx_1 and Stx_2, respectively) in an *E. coli* isolate constitutes a characteristic of STEC (136, 137). However, while there are over 400 different STEC serotypes, only a small subset of them has been demonstrated to cause illness in humans. STEC infections in humans can range from mild to bloody diarrhea to hemolytic uremic syndrome (HUS). Enterohemorrhagic *E. coli* (EHEC) is a subset group within the STEC pathotype that was described by the association with hemorrhagic colitis (HC), which is clinically distinct from shigellosis as well as genotypic and phenotypic differences from EPEC (136, 138, 139). Members of the EHEC subgroup of STEC isolates contain a chromosomal pathogenicity island known as the Locus of Enterocyte Effacement (LEE), essential for the formation of Attaching and Effacing lesions (A/E), a phenotype fundamental for bacterial virulence (136, 138). The formation of A/E lesions is caused by the injectosome known as the type 3 secretion system (T3SS), encoded by the LEE, which translocates several virulence factors into the host cell (136, 138, 140). This PAI encodes the products or virulence factors that contribute to the survival in a wide range of environmental conditions and commensal competition in the host (136, 138, 140). One of the large contributors to this genomic plasticity and virulence traits are lambdoid bacteriophages integrated into the chromosome and encode both Stx_1 and Stx_2 (138). Shiga toxins are the main virulence characteristic defining STEC isolates and a key virulence

factor associated with HUS. These Stx-carrying phages have the potential of becoming lysogenic upon bacterial stress, causing the release of toxins from lysed bacterial cells during the lytic cycle of these phages (138).

The most common EHEC serogroup in outbreaks is O157:H7 and has been classified by the U.S. Department of Agriculture (USDA) as an adulterant in beef since 1994 (136). As a member of the STEC pathogroup and LEE-positive pathogen, the repertoire of effector molecules for pathogenesis is broad, of which 62 possible effector genes have been identified in its genome (136, 140). Several adhesins encoded in LEE-positive STECs likely contribute to the colonization of the intestinal epithelium upon ingestion, including fimbriae, pili, autotransporters, etc. Long polar fimbriae (Lpf) have been shown to attach to the extracellular matrix of protein laminin (136, 137). Following attachment, the formation of A/E lesion occurs by subversion of the actin cytoskeleton machinery of the host cell-mediated by the interaction between intimin and the bacterial translocated intimin receptor, Tir (138). In culture, this intimin-mediated attachment with the epithelium creates a unique morphological feature resembling a pedestal (137, 138). Intimin-mediated attachment of EPEC to intestinal epithelial cells (IECs) requires the subversion of diverse signaling pathways within the host, and many of these are found in the LEE PAI. Using the type 3 secretion system (T3SS), intimate attachment is mediated by the interaction of intimin and Tir, which uses an effector to recruit the host cell cytoskeleton to mediate actin assembly (137, 138).

EHEC O157:H7 AND DISEASE

Transmission of STEC, including EHEC O157:H7, is through the fecal-oral route (138). Ruminants, such as cattle, are reservoirs for pathogenic STEC, and exposure to fecal matter in meat and dairy presents an important source of human illness worldwide (136). In addition, direct exposure by contact with animals or their feces is also an important route

of exposure to STEC (138). Contaminated food and water are important contributors to the sporadic, but often in large numbers, of outbreak-related illnesses due to STEC (136). In the US alone, ~68% of STEC-related illnesses are related to the consumption of contaminated meat and produce, while in a recent outbreak, only approximately 19% of cases were associated with the person-to-person transmission (141). EHEC-related outbreaks remain a significant cause of disease in the US, with an annual cost that exceeds $500 million (136).

Infections with STEC can range from mild watery diarrhea to hemorrhagic colitis (HC) and the risk of developing severe HUS complications. In the United States, there were approximately 463 STEC O157:H7 (0.97 per 100,000 population) cases in 2011 (136). Hospitalizations associated with STEC O157:H7 were two-fold higher for O157:H7 (43.3%) over non-O157 STEC (18%) (136). Likewise, the mortality rate associated with O157:H7 related strains is two-fold higher than non-O157 EHEC. EHEC O157:H7 is prevalent in developed and developing countries such as Argentina, which has the highest incidence worldwide of HUS in children under the age of five (136, 138). Although disease manifestation and severity depend on a wide range of factors, including serotype, dose, virulence factors, incubation period, and the first symptoms include diarrhea, which may be accompanied by fever, abdominal pain, or vomiting (136). Following diarrhea, patients may experience HC in the following days, where O157-related infections result in a significantly higher rate of bloody diarrhea than non-O157 EHEC infections (136). Reports have shown that diarrhea caused by O157:H7 can generally resolve after a week following the initial onset of symptoms; however, reports have shown that non-O157 EHEC infections may persist longer (136).

Despite the resolution of diarrheal episodes in many cases, EHEC-associated illnesses are of particular concern due to the association with HUS. A key contributor to the induction of HUS are the Stx toxins, which belong to the AB class of toxins, and its mechanism of action involves renal cells (globotriaosylceramide positive on their cell

surface (Gb3+)), the intestinal epithelium, and the vascular epithelium (136, 137). Shiga toxins can be classified into two main types, Stx_1 and Stx_2, with three (a, b, and d) and seven subtypes (a-g), respectively (136). STEC, including EHEC, can carry a single variant of either *stx*$_1$ or *stx*$_2$, both *stx*$_1$/*stx*$_2$, or a combination of *stx*$_2$ subtypes (136, 138). Both Stx_1 and Stx_2 are associated with the induction of HUS; however, *stx*$_2$ is associated with severe disease (142). Stx trafficking and enzymatic activity mechanisms involve an initial binding to Gb3 on the surface of endothelial cells, followed by its internalization and trafficking from the Golgi apparatus to the endoplasmic reticulum (ER) and eventual release into the host cell cytoplasm (136). The A subunit of Stx has RNA-glycosidase activity, which removes an adenine from 28S rRNA, thereby inhibiting protein synthesis is causing cell death (136). HUS involves thrombocytopenia, hemolytic anemia, and acute renal failure with a mortality rate that can reach 4% in children under ten years of age (136). Additionally, 20-40% of children have long-term sequelae from HUS, including GI complications, cardiac complications, and neurological disorders (136).

The use of antibiotics to treat EHEC-associated infections can be contentious due to the stimulation of an SOS response in the bacteria resulting in the stimulation of the lytic cycle and exacerbated release (143). Furthermore, one study found that the use of fluoroquinolones also had the ability to increase the production of Stx_2 in EHEC O157:H7 (144).

TREATMENT AND VACCINES FOR EHEC O157:H7

With the alarming consequences of HUS, especially in children, combined with no precise treatment, there have been several studies on potential therapeutics to protect against a potentially fatal outcome. Experimental treatment in both pre-clinical and clinical trials has focused mainly targeting the Stx activity (136, 145). Monoclonal antibodies (mAbs) studies blocking both Stx_1 and Stx_2 have been shown to reduce cytotoxicity *in vitro* and

have shown to be well tolerated in a single dose phase I clinical trial (146–148). While the effects of toxin neutralization by these mAbs have been demonstrated in mice, the effectiveness in humans in preventing HUS after the onset of diarrhea remains to be established (146). Short, cell-permeable peptides blocking Stx transport through epithelial cells have also been shown to reduce renal injury upon delivery in a baboon model of infection (149, 150). Furthermore, a conjugate of globotriose with chitosan was found to neutralize Stx_1 and Stx_2 cytotoxicity in a mouse model of STEC O157:H7 by directly neutralizing toxin activity (151). Other therapeutic strategies include using secreted molecules by *Lactobacillus acidophilus* as probiotics; these were shown to inhibit STEC adherence to epithelial cells *in vitro* and reduce bacterial shedding *in vivo* (151). The inadvisable use of antibiotics for the treatment of EHEC-related infections, the emergence of antibiotic-resistant strains, and the rise of HUS episodes have prompted the development of effective preventive countermeasures.

Given the role of Stx toxin during EHEC infection, restriction to antibiotic therapy use, and complexity of disease symptomology, one of the main strategies targeting vaccine development is the neutralization to reduce its effect (136, 145). An attenuated EHEC O157:H7 strain lacking the *ler* and *stx*$_2$ (*ler*/*stx*$_2$) genes and carrying a plasmid-encoded detoxified Stx_{A1} and Stx_{2A} subunit was generated as a vaccine candidate and shown to be safe with reduced toxicity after intraperitoneal (IP) administration (152). Animals immunized and with the *ler*/*stx*$_2$ vaccine strain were shown to reduce wild-type bacterial shedding 6 days after challenge. Another model using an attenuated *Salmonella* strain expressing heterologous recombinant EspA, Intimin, and the B subunit of the Stx_1 (EIS) induced strong serum IgG and fecal IgA titers against each protein after oral or oral/subcutaneous immunization (152). Another attenuated *Salmonella enterica* serovar Typhimurium expressing the EHEC γ-intimin (*eae*) significantly increased serum IgG and fecal IgA humoral responses, associated with reduced EHEC O157:H7 shedding post-challenged (153). However, attenuated *Salmonella* bacteria were recovered from Peyer's

patches and spleen. Another approach exploited for mucosal antigen delivery was based on Bacillus Calmette-Guerin (BCG), due to its mucosal immunoreactivity and ability to boost humoral responses. A recombinant BCG expressing the B subunit of the Stx_2 (rBCG-Stx_{2B}) induced increased levels of Stx_2-specific IgG antibody titers in the serum directly correlated with a reduction in colony-forming units (CFUs) and a significant increase in survival rate (63%) after challenge with EHEC O157:H7 (153). Another platform exploited against EHEC was based on bacterial ghost (GC) as an attenuated bacterial antigen delivery strategy. Although GC of EHEC O157:H7 have been generated and immunization results in an increased survival rate and reduced bacterial shedding post-challenge, immunized animals showed disease symptoms after challenge, including weight loss and reduced activity (154). More recently, another approach using BG expressing a chimeric protein of Stx_{2A} and Stx_{1B} was engineered (Stx_{2A}m-Stx1B) (154). Vaccination with this BG cell producing a recombinant chimeric Stx protein induced higher antigen-specific IgG and IgA antibody titers and increased survival (52%) after intragastric challenge with a high dose of O157:H7 (154).

In recent studies, chimeric proteins using the Stx toxin have been approved to be an attractive approach for protein-based vaccination. A chimeric protein containing the A1 subunit of Stx_2 and the N-terminus of EspA was generated and shown to induce higher antigen-specific IgG titers after subcutaneous immunization (155). This Stx_{2A1} / EspA chimeric protein significantly increased survival (95% survival) after challenge with Stx_2 (155). However, while serum against the Stx_{2A1}/EspA could neutralize toxin activity *in vitro*, it did not prevent bacterial adherence onto HeLa cells (155). A chimeric protein constructed with the subunit B from Stx_1 and Stx_2 along with a truncated intimin protein (Stx_1/Stx_2/Int) induced higher IgG antibody titers in mice associated with a significant increase in survival (100%) after challenge with EHEC O157:H7 strain 88321 (156). While serum from immunized animals with the Stx_1/Stx_2/Intimin chimera showed anti-toxin and anti-adhesion activity, an effect absent in sera of vaccines using single proteins, the fusion

protein was unable to block wild type bacterial adhesion *in vitro*. A more recent study, a chimera containing the Stx_{1B} subunit and an inactive Stx_{2A} subunit (Stx_{2A}m-Stx_{1B}, SAmB) was shown to induce a T_H2-biased immune response associated with the induction of humoral responses (157). Animals challenged with lysed EHEC 88321 showed increased survival with up to 93%, and even higher survival rates against Stx_1, Stx_2, or $Stx_{1/2}$ challenge (157). One approach in vaccine development to reduce the risk of developing adverse reactions while helping protect the antigen from degradation is using plant microencapsulation system using plant-based expression systems. Using this vaccine platform, a chimeric gene composed of *espA*, *eae*, and *tir* (EIT) was cloned in a codon-optimized plant-expression vector under the control of FAE promoters for tobacco and canola plants (158–160). Animals immunized with the recombinant EIT protein was associated with a significant reduction in bacterial colonization and increased antigen-specific IgG and IgA titers after subcutaneous or oral immunization (159). A polysaccharide-based glycoconjugate vaccine containing O-specific polysaccharide conjugated to recombinant exotoxin A of *Pseudomonas aeruginosa* (O157-rEPA) was shown to induce strong serum IgG titers in children with 20-fold higher levels by 26-weeks post-vaccination (161). Vaccinated children showed mild to no-collateral reactivity to the vaccine, and anti-bacterial activity in serum correlated with anti-LPS IgG titers (161).

Although several novel vaccine candidate platforms are available, no vaccine is available for human use. The complexity of *E. coli* pathogenesis and antigenic differences between different pathotypes has hindered the development of broadly protective vaccines. Therefore, future EHEC vaccine targets and technologies should target different EHEC serotypes and antigens that may provide cross-reactivity against multiple pathotypes. Whole-genome approaches such as reverse vaccinology, based on the bioinformatic prediction of antigens, will enable the prediction of protective immunogenic candidates that can serve as the basis for the development of broadly protective vaccines against pathogenic *E.coli*.

OBJECTIVES OF THIS STUDY

The long-term objective of this study is to develop a safe and effective vaccine against the intracellular pathogens, *B. mallei* and *B. pseudomallei* that provides sterilizing immunity. Another objective of this study is to identify a subunit vaccination platform capable of eliciting protective immunity against the extracellular pathogen, enterohemorrhagic *E. coli* (EHEC) O157:H7. To develop an appropriate non-replicative vaccination platform that is safe and works against intra- and extracellular pathogens, the research focus on identifying broad mechanisms of vaccine delivery to amplify cell- and humoral responses. It was also critical to understand the protective responses for each infection model, especially for *Burkholderia* infection, which are relatively uncharacterized. Therefore, a more immediate objective of this study was to evaluate the multivalent delivery of antigens using a gold nanoparticle (AuNP) platform to elicits cross-protection against *B. mallei* and *B. pseudomallei*. AuNPs have gained interest in vaccine development because of their biocompatibility and ability for functionalization for different applications. Nanoparticles (NPs), including gold (Au), are well established inert molecules with a large surface/volume ratio capable of being exploited for a wide range of applications (29, 50, 162, 163). Some of these applications include drug delivery, diagnostics, and recently, in vaccine design as platforms for antigen delivery. Recent studies have exploited the cargo-loading capacity of AuNPs to deliver biomolecules targeted to antigen presenting cells (APCs) allowing enhanced humoral and cellular immunity (11, 38, 164).

Thus, I hypothesized that gold nanoparticle delivery glycoconjugates using immunogenic proteins would generate protective immunity against *B. mallei* and *B. pseudomallei* in a C57BL/6 mouse model. I have tested my hypothesis by completing the following three aims: 1) To assess the protective effects of AuNP-delivered glycoconjugates against *B. mallei*, 2) Determining the cross-protective effects against *B. pseudomallei* using AuNP-delivered glycoconjugates, 3) Evaluating the important humoral

or cellular mediated protective markers elicited by AuNP-glycoconjugate as they relate to protection. To evaluate this work, I chose a C57BL/6 model of infection for both *B. mallei* and *B. pseudomallei* using previously identified *B. mallei*-specific antigens by reverse vaccinology. I evaluated the induction of humoral and cellular responses and assessed protection *in vivo*. In addition to this work, I wanted to evaluate the ability of AuNP-delivered antigens to protect against an extracellular pathogen, EHEC O157:H7 using a similar vaccination strategy. For this, I chose two predicted antigens by reverse vaccinology using a BALB/c model of colonization. I evaluated protection *in vivo* and *in vitro*.

Chapter 4: *B. mallei* Vaccine Study Materials and Methods

BACTERIAL STRAINS AND GROWTH CONDITIONS

Burkholderia thailandensis (*Bth*) E264 and *B. mallei* (*Bm*) ATCC 23344 (China 7) were routinely grown aerobically at 37°C in Luria-Bertani (LB) medium containing 1% NaCl or LB medium supplemented with 4% glycerol (LBG), respectively. All chemical reagents, unless otherwise noted, were purchased from Sigma-Aldrich.

PROTEIN PURIFICATION

Open reading frames (ORFs) from each candidate amplified from genomic DNA from *Bm* 23344: *hcp1* (BMAA0742), *ompW* (BMA2010), *opcP* (BMAA1353), *opcP1* (BMAA1122), *flgL* (BMA3336), and Hemagglutinin-family protein (HA; BMAA1324) were cloned in pET30a(+) expression vector with a 6× histidine (His) tag positioned in the C-terminus (165). Briefly, in-frame genes of each candidate were amplified from purified *Bm* 23344 genomic DNA using the restriction enzymes NdeI and XhoI and the plasmids were transformed into competent *E. coli* BL21 (DE3) (New England BioLabs). To induce protein expression, overnight cultures were diluted 1:20 in 1 L of Luria Bertani (LB) broth containing 50 μg/mL of kanamycin, grown to an optical density at 600 nm (OD_{600}) between 0.6 and 0.8, and induced with 1 mM (final concentration) of isopropyl-D-1-thiogalactopyranoside (IPTG). Cultures were centrifuged (4,000 × *g* for 15 min) after 3 h post-induction, and each resulting bacterial pellet was frozen at –20°C. The bacterial pellets were then resuspended in 40 mL of 1× Dulbecco's phosphate- buffered saline (DPBS) containing 10% glycerol and 25 mM sucrose with a 1 mg/mL final concentration of lysozyme and 0.2% sodium deoxycholate and a tablet of Complete EDTA-free protease

inhibitor cocktail (Roche, Germany). This lysate was then sonicated, centrifuged, and the pellet was used for subsequent washes to maximize soluble protein extraction. After spinning down at 20,000 × *g* for 40 min, the supernatant was subjected to sterilization using a 0.2-μm pore size filter (Millipore). Soluble protein extracts were then bound to Talon® cobalt (Co^{2+}) columns (GE Healthcare, USA) and washed with PBS buffer–50 mM imidazole. Proteins were eluted from affinity columns by applying a 1× PBS buffer with 10% glycerol, 25 mM sucrose and 250 mM imidazole. Fractions containing soluble protein were collected and pooled before dialysis into PBS containing 10% glycerol and 25 mM sucrose overnight at 4°C. Endotoxin levels were tested using a Pierce LAL chromogenic endotoxin quantification kit (ThermoFisher Scientific, USA) following manufacturer's specifications. The limit of detection for endotoxin is approximately 0.1 EU/mL of solution. The purified proteins and protein standards were subjected to a colorimetric bicinchoninic acid assay (BCA) in accordance with the manufacturer's protocol and were then stored at -80°C until use (Pierce™ Protein Assay Kit, ThermoFisher Scientific). For protein visualization, 0.25 μg of each protein was run on SDS-PAGE gel by electrophoresis. Gels were transferred to a nitrocellulose membrane for Western blot analysis. A mouse anti-histidine antibody (Invitrogen™ Catalog No. R930-25) was used (1:5,000) and the reaction mixture incubated overnight at 4°C, followed by horseradish peroxidase (HRP)-conjugated rabbit anti-mouse IgG (Southern Biotech™ Catalog No. OB1030-05) was used (1:10,000) as a secondary antibody. Protein bands were visualized by adding ECL substrate (ThermoFisher Scientific), and the results were imaged on film. Molecular weight markers were visualized using Precision Plus Protein™ WesternCTM Blotting Standards (Bio-Rad) with StrepTactin-HRP conjugate (Supplemental Fig. 1). WB and Coomassie-stained gel were generated from the same experiment and processed in parallel.

LIPOPOLYSACCHARIDE EXTRACTION

The LPS from *Bth* E264 was isolated by the hot phenol-extraction method (165, 166). Briefly, a pellet of 4 L of LB-grown *Bth* to stationary phase (24 h at 37°C and 200 RPM) was collected (6,000 × *g* for 15 min) and lysed in the presence of a mixture of 1:1 phenol in water (ThermoFisher Scientific). After lysis at 80°C, phenol was removed by dialysis 4× into ultra-pure water and centrifuged (15 min at 6,000 × *g*) to clarify the solution, and the supernatant was lyophilized. The lyophilized solution was resuspended in an aqueous solution containing 10 mM Tris-HCl (pH 7.5), 1 mM $MgCl_2$, 1 mM $CaCl_2$ and digested with RNase, DNase I and Proteinase K (50 µg/mL each). After clarification (100,000 × *g* for 3 h), the resulting supernatant containing LPS was lyophilized. The sample containing the LPS was washed 5× times with 90% ethanol and lyophilized. After lyophilization, the pellet was weighed, resuspended in PBS, and stored at -80°C until use. The purity of LPS was assessed by SDS-PAGE electrophoresis, followed by Silver Staining following manufacturers protocol (PierceTM Color Silver Stain Kit).

GOLD NANOPARTICLE SYNTHESIS AND COUPLING

Spherical 15 nm gold nanoparticles (AuNPs) were synthesized by the Turkevich method (167). Briefly, 1 mM gold (III) chloride trihydrate underwent a reduction reaction with 90 mM sodium citrate dihydrate. Particle size and shape was analyzed by transmission electron microscopy (TEM). To stabilize the conjugation of soluble antigens onto the AuNP surface, 0.1 mM 16-mercaptohexadecanoic acid (16-MHDA) and 0.1% Triton X-100 were added to AuNPs. After 2 h of incubation, this solution was filtered by centrifugation (EMB Millipore Amicon^{TM} Ultra-15, 30 kDa molecular weight cutoff [MWCO]), and the procedure was repeated for 2 h to ensure complete coverage. Covalent protein conjugation by carbodiimide synthesis (165) was achieved by the addition of 20 µg of protein per mL for maximum coating of nanoparticles in the presence of 1 mM DMTMM

[4-(4,6-dimethoxy-1,3,5-triazin-2-yl)-4-methyl-morpholinium chloride]. The AuNP-protein conjugation reactions were carried out in 100 mM borate buffer for 12 h. Attachment of 16-MHDA and protein was confirmed by measuring plasmon resonance via UV-Vis spectroscopy, TEM, as well as by SDS-PAGE. To conjugate LPS onto the AuNP-protein conjugates, we employed the thiol-maleimide synthesis mechanism. To achieve this, LPS was activated by the addition of 80 mM EMCH (N-(ε-maleimidocaproic acid hydrazide) cross-linker in the presence of 40 mM EDC (*N*-(3-Dimethylaminopropyl)-*N*′-ethylcarbodiimide hydrochloride) and 10 mM NHS (*N*-hydroxysuccinimide) in 50 mM MES buffer (pH 7.0). After 1 h at room temperature, LPS was concentrated to desired concentration using AmiconTM Ultra-15, 30 kDa MWCO. After desalting the LPS in 5 mM EDTA, 20 μg of activated LPS were added per mL of protein-coupled AuNPs previously activated in the presence of 250 μM SATA (S-acetyl thioglycolic acid *N*-hydroxysuccinimide ester) for 1 h at room temperature. After 4 h of incubation, the reaction was quenched with 5 mM N-ethylmaleimide. The AuNP-protein-LPS conjugates were washed 2× with PBS containing 10% glycerol and 25 mM sucrose and concentrated to desired volume containing a concentration of ~ 0.23 μg/μL of both protein and LPS using an Amicon® Stirred Cell containing a 100 kDa MWCO filter.

ANIMAL STUDIES

Female 6-to-8-week-old C57BL/6 mice were purchased from Jackson Laboratories (Bar Harbor, ME, USA). Animals were housed in microisolator cages under pathogen-free conditions with food and water available *ad libitum* and maintained on a 12 h light cycle. To allow adequate acclimation, mice were housed within the animal facility for 1 week prior to experimentation. C57BL/6 mice (n=9 per group) were inoculated intranasally (i.n.) three times in 2-week intervals with 50 μL formulations. Animals received each of the AuNP-protein-LPS conjugate. Two combination AuNP formulations were synthesized:

AuNP-Combo1-LPS (containing Hcp1, OmpW, OpcP, OpcP1, FlgL, and HA) or AuNP-Combo2-LPS (containing HA, OmpW, and OpcP). Each vaccine formulation contained a total of approximately 10 μg of protein, 10 μg LPS, along with 20 μg of CpG ODN 2395 (InvivoGen, USA). Control groups received 20 μg of adjuvant alone. To evaluate antibody titers, blood was drawn retro-orbitally 2-weeks following the last boost (n=5). To isolate sera, blood was incubated for 30 min at room temperature (RT) to allow clotting and centrifuged (10,000 × *g* for 10 min). Sera was removed and stored at –80°C until use. For assays requiring serum, the samples from immunized animals (n=5) were pooled and stored. Three-weeks after administering the last immunization, animals were i.n. challenged with a low- or high-dose challenge of *Bm* 23344 in 50 μL formulations. The low dose challenge animals received 2 LD_{50} (2.8×10^4 CFU per mouse), while the high-dose challenge received 50 LD_{50} (7×10^5 CFU per mouse). To enumerate bacterial colonization, the lung/spleen (low-dose challenge) or lung, liver, and spleen (high-dose challenge) of mice were collected. Organs were homogenized in 1 mL of 1× PBS, serially diluted, and plated on LBG agar and incubated at 37°C for 48 h. The bacterial limit of detection (LOD) was determined to be 1 CFU/organ.

DETECTION OF ANTIGEN-SPECIFIC ANTIBODIES

Baseline and post-vaccinated sera were collected from animals administered with adjuvant only, individual AuNP-protein-LPS conjugates, and from AuNP-Combo-LPS formulation two-weeks after the second boost. Whole blood was collected via retro-orbital bleeding and stored in Microvette tubes without anticoagulant. The sera were separated by centrifugation and stored at –80°C. The protein-specific total IgG, IgG_1, and IgG_{2c} titers were determined by indirect enzyme-linked immunosorbent assay (ELISA) (168). Briefly, a microplate (Costar, Cambridge, MA) was coated with each protein or LPS antigen (1 μg/well) in a mixture with 1× PBS (Corning, USA) and maintained overnight at 4°C. Wells

were washed twice with washing buffer (0.05% Tween 20 – DPBS) and then blocking buffer (0.05% Tween 20, 2% bovine serum albumin [BSA], 1×DPBS) was added at RT for 2 h. The blocked wells were washed twice before the addition of sample diluent (1% BSA – 0.05% Tween 20 – 1× DPBS). The sera were added to each top dilution well in triplicate, and 2-fold dilutions were performed following incubation at RT for 2 h. Diluted goat anti-mouse IgG-HRP (Southern Biotech™ Catalog No. OB1030-05), IgG_1-HRP (Southern Biotech™ Catalog No. 1070-05) or IgG_{2c}-HRP (Southern Biotech™ Catalog No. 1077-05) (1:5,000) was added into each well and then incubated for 3 h after washing. Plates were washed four times prior to addition of tetramethylbenzidine substrate solution (Invitrogen, USA). Stop solution (2N H_2SO_4) was added, and the samples were immediately read at 450 and 570 nm using a microplate reader (BioTek, USA). The results were reported as the reciprocal of the highest titer, giving an optical density (OD) reading of at least the mean ≥ 2 standard deviations compared to the baseline sera. All assays were performed in triplicate, and results were reported as mean reciprocal endpoint titers.

SERUM ADHERENCE INHIBITION ASSAY

Murine respiratory alveolar epithelial cells LA-4 (American Type Culture Collection (ATCC®) CCL-196™) were maintained at 37°C with 5% CO_2 in complete F-12-Kaigh's (F12-K) medium (Gibco, USA). Complete F12-K minimum was supplemented with penicillin and streptomycin (100 U/mL and 100 µg/mL, respectively), and 10% fetal bovine serum. For adhesion assays, 12-well plates were seeded with 5×10^5 cells/per well. At approximately 1 h prior to infection, the monolayer was washed twice with 1 mL PBS prior to addition of 1 mL of medium containing no supplements. Bacterial inoculum (input) was prepared from 16 h cultures of *Bm* 23344 and adjusted to an MOI of 10 (5×10^6 CFU) and incubated in the presence or absence of immune serum from individual AuNP-protein-LPS, AuNP-Combo2-LPS, adjuvant-only serum, or naive sera (final concentration of 10%) for

1 h at 37°C with slight agitation. After incubation in the presence of sera, bacteria were collected in 1 mL of fresh media and used to infect cell culture plates containing 5×10^5 cells. Monolayers were incubated for 1 h at 37°C with 5% CO_2. After incubation, cells were washed three times with PBS prior to the addition of 100 µL of 0.1% Triton X-100 in PBS. After detachment, the cells were serially diluted in PBS and plated on LBG agar plates for 48 h to enumerate the number of adhered bacteria (output). The percentage of adhered bacteria was determined as the output/input × 100. Data represent results of two independent experiments performed using pooled sera from (n=5) mice.

MACROPHAGE SURVIVAL AND FLUORESCENCE MICROSCOPY

C57BL/6 murine bone marrow-derived primary macrophages (BMDM) (Cat No. C57-6030, Cell Biologics Inc., Chicago) were routinely grown in complete primary cell culture medium following manufacturer's instructions (Cat No. M3368, Cell Biologics, Chicago). Cells were incubated at 37°C and 5% CO_2. For infection and microscopic analysis, 5×10^5 cells were grown in 12-well cell-culture grade plates (Corning) or round cover slips and incubated overnight, prior to treatment. Bacterial inoculum used at an MOI of 10 (5×10^6 CFU) was incubated in the presence or absence of (56° for 30 min) immune serum from AuNP-protein-LPS, AuNP-Combo2-LPS, or naive sera (final concentration of 10%) for 1 h at 37°C with slight agitation. After incubation in the presence or absence of sera, bacteria were collected in 1 mL of fresh media and used to infect cell culture plates containing 5×10^5 cells. For cell infection, monolayers were incubated for an additional 2 h at 37°C with 5% CO_2. After infection, cells were either washed, lysed with 0.1% Triton X-100 in PBS, and plated in LBG agar for 48 h, or fixed with 4% paraformaldehyde in PBS for 30 min. Cells were permeabilized with 0.1% Triton X-100 for 5 min and polymerized actin and DNA were visualized using rhodamine isothiocyanate-phalloidin (Molecular Probes-Invitrogen, USA) or DAPI (Molecular Probes-Invitrogen, USA), respectively. *Bm* 23344

cells were detected with serum from *Bth* LPS-immunized mice (1:500), followed by a goat anti-mouse IgG, IgM (H+L) secondary antibody conjugated to Alexa 488 (ThermoFisher Scientific™ Catalog No. A-10667) (1:10,000). Cells were mounted using ProLong Gold Antifade (Molecular Probes-Invitrogen, USA) prior to visualization. Images were examined using an Olympus BX51 upright fluorescence microscope and analyzed using ImageJ software, National Institutes of Health (169).

VISUALIZATION OF LIVE AND DEAD INTRACELLULAR BACTERIA

Primary murine macrophages (5×10^5) were infected as described above with a MOI of 10, for 1 h, in the presence of inactivated serum from immunized animals. Prior to infection, bacteria were incubated in the presence of sera for 1 h and input bacteria was quantified. After infection, cells were slightly permeabilized with 0.1% saponin in PBS for 10 min at room temperature. Cells were then stained with LIVE/DEAD™ *Bac*Light™ Kit (Molecular Probes, Life Technologies) containing propidium iodide (PI) or SYTO 9, following the manufacturer's instructions. Following staining, cells were washed three times with PBS and fixed with 4% PFA for 20 min. Cells were directly mounted using ProLong gold antifade (Molecular Probes, Life Technologies) and visualized using an Olympus BX51 upright fluorescence microscope and analyzed using ImageJ software, National Institutes of Health (169).

STATISTICAL ANALYSIS

All statistical analysis was done using GraphPad Prism software (v 8.0). *P* values of <0.05 were considered statistically significant. Quantitative data are expressed as means ± standard errors. All data were analyzed for normality before the corresponding test was run. Results of colonization, antibody, serum adherence inhibition, and

opsonophagocytosis assays were analyzed by one-way analysis of variance (ANOVA) using Tukey's *post hoc* test or the Kruskal-Wallis *post hoc* test when data were not normally distributed. Significant differences between IgG_1 and IgG_{2c} titers were determined via Student´s *t* test. Statistical differences in survival were determined by the Kaplan-Meier method, followed by log-rank test. Levels of significance compared to the adjuvant-only group: * $p < 0.05$, ** $p < 0.005$, *** $p<0.0005$, **** $p <0.0001$.

Chapter 5: *B. pseudomallei* Vaccine Study Materials and Methods

BACTERIAL STRAINS AND GROWTH CONDITIONS

Burkholderia thailandensis (*Bth*) E264 and *B. pseudomallei* (*Bpm*) K96243 were routinely grown aerobically at 37°C in Luria-Bertani (LB) medium containing 1% NaCl or LB medium supplemented with 4% glycerol (LBG), respectively. All chemical reagents, unless otherwise noted, were purchased from Sigma-Aldrich.

ANIMAL STUDIES

Female 6-to-8-week-old C57BL/6 mice were purchased from Jackson Laboratories (Bar Harbor, ME, USA) and maintained in an animal biosafety level 3 (ABSL3) facility. Animals were housed in microisolator cages under pathogen-free conditions with food and water available *ad libitum* and maintained on a 12 h light cycle. All animal protocols were reviewed and approved by the Institutional Animal Care and Use Committee (IACUC) of the University of Texas Medical Branch (protocol no. 0503014D). To allow adequate acclimation, mice were housed within the animal facility for 1 week prior to experimentation.

IMMUNIZATION AND CHALLENGE STUDIES

C57BL/6 mice (n=9 per group) were inoculated intranasally (i.n.) three times in 2-week intervals with 50 μL formulations. Animals received each of the AuNP-protein-LPS conjugate. Two combination AuNP formulations were synthesized: AuNP-Combo1-LPS (containing Hcp1, OmpW, OpcP, OpcP1, FlgL, and HA) or AuNP-Combo2-LPS (containing HA, OmpW, and OpcP). Each vaccine formulation contained a total of 10 μg of protein, 10 μg LPS, along with 20 μg of CpG ODN 2395 (InvivoGen, USA). Control

groups received 20 μg of adjuvant alone. To evaluate antibody titers, blood was drawn retro-orbitally 2-weeks following the last boost (n=5). To isolate sera, blood was incubated for 30 min at room temperature (RT) to allow clotting and centrifuged (10,000 × *g* for 10 min). Sera was removed and stored at –80°C until use. For assays requiring serum, the sera from immunized animals (n=5) were pooled and stored. Three-weeks after administering the last immunization, animals were challenged with a low- or high-dose challenge of *Bpm* K96243 in 50 μL samples. The low dose challenge animals received a dose of 5 LD_{50} (~7.5×10^4 CFU per mouse), while the high-dose challenge received 6 LD_{50} (9×10^4 CFU per mouse). To enumerate bacterial colonization the lung/spleen (low-dose challenge) or lung, liver, and spleen (high-dose challenge) were collected. Organs were homogenized in 1 mL of 1× PBS, serially diluted, and plated on LBG agar to quantify bacterial colonization at 37°C for 48 h. The bacterial limit of detection (LOD) was determined to be 1 CFU/organ.

HISTOPATHOLOGY EVALUATION

At 15 days post-vaccination or 35 days post-challenge, three representative animals from each group were euthanized and their lungs, livers, and spleens were fixed with 10% normal buffered formalin. For histopathological analysis, fixed tissues were embedded in paraffin and sectioned prior to staining with hematoxylin and eosin (H&E). Representative images from each organ from one mouse per group were taken and analyzed. Pathology scoring was performed blindly by a certified pathologist from UTMB, not directly associated with the design of any experiment.

DETECTION OF ANTIGEN-SPECIFIC ANTIBODIES

Baseline and post-vaccinated sera were collected from animals administered adjuvant only, individual AuNP-protein-LPS conjugates, and from AuNP-Combo2-LPS formulation two-

weeks after the second boost. Whole blood was collected via retro-orbital bleeding and stored in Microvette tubes without anticoagulant. The sera were separated by centrifugation and stored at –80°C. The protein-specific total IgG, IgG_1, and IgG_{2c} titers were determined by indirect enzyme-linked immunosorbent assay (ELISA). Bronchioalveolar lavage fluid (BALF) from AuNP-protein-LPS or AuNP-Combo2-LPS immunized mice were collected three-weeks after receiving the last immunization and stored at -80°C (day 0). A microplate (Costar, Cambridge, MA) was coated with each protein or LPS antigen (1 μg/well) in a mixture with 1×PBS (Corning, USA) and maintained at 4°C overnight. Wells were washed twice with washing buffer (0.05% Tween 20 – DPBS) and then treated with blocking buffer (0.05% Tween 20, 2% bovine serum albumin [BSA], 1×DPBS) at RT for 2 h. The blocked wells were washed twice before the addition of sample diluent (1% BSA – 0.05% Tween 20 – 1× DPBS). Baseline sera, or adjuvant-only BALF, sera from immunized animals or BALF samples were added to each top dilution well in triplicate, and 2-fold dilutions were performed following incubation at RT for 2 h. Diluted goat anti-mouse IgG, IgG_1 or IgG_{2c}, IgA (Southern Biotech, USA) (1:5,000) was added into each well and then incubated for 3 h after washing. Plates were washed four times prior to addition of tetramethylbenzidine (TMB) substrate solution (Invitrogen, USA). Stop solution (2N H_2SO_4) was added, and the samples were immediately read at 450 and 570 nm using a microplate reader (BioTek, USA). The results were reported as the reciprocal of the highest titer, giving an optical density (OD) reading of at least the mean ≤ 2 standard deviations compared to the baseline sera or adjuvant only BALF (for lung IgA or IgG). All assays were performed in triplicate, and results were reported as mean reciprocal endpoint titers.

MACROPHAGE SURVIVAL ASSAY AND FLUORESCENCE MICROSCOPY

C57BL/6 murine bone marrow-derived primary macrophages (BMDM) (Cat No. C57-6030, Cell Biologics Inc., Chicago) were routinely grown in complete primary cell culture medium following manufacturer's instructions (Cat No. M3368, Cell Biologics, Chicago). Cells were incubated at 37°C and 5% CO_2. For infection and microscopic analysis, 5×10^5 cells/well were grown in 12-well cell-culture grade plates in round cover slips and incubated overnight, prior to treatment. Bacterial inoculum used at an MOI of 10 (5×10^6 CFU) were incubated in the presence or absence of inactivated (56° for 30 min) immune serum from AuNP-protein-LPS, AuNP-Combo2-LPS, or naive sera (final concentration of 10%) for 1 h at 37°C with slight agitation. After incubation in the presence or absence of sera, bacteria were collected in 1 mL of fresh media and used to infect cell culture plates containing 5×10^5 cells. After 2 h of infection at 37°C with 5% CO_2, cells were washed and fixed with 4% paraformaldehyde–PBS for 30 min. Following that step, cells were slightly permeabilized with 0.1% saponin in PBS for 10 min at room temperature. Cells were then stained with LIVE/DEAD™ BacLight™ Kit (Molecular Probes, Life Technologies) containing propidium iodide (PI) or SYTO 9, following the manufacturer's instructions. Cells were washed three times with PBS, fixed with 4% PFA for 20min, and then directly mounted using ProLong gold antifade (Molecular Probes, Life Technologies). Cells were visualized using an Olympus BX51 upright fluorescence microscope and analyzed using ImageJ software, National Institutes of Health (169).

CELLULAR IMMUNE RESPONSE ANALYSIS

Spleen cells from AuNP-Combo2-LPS immunized mice were obtained three-weeks after the last immunization (170). Single cell suspensions of spleen cells from immunized and control mice (Adjuvant-only) were cultured in 48-well cell-culture grade plates (Corning, USA) in duplicate at 1×10^6 cells/mL in RPMI 1640 (Gibco, Life Technologies) supplemented with 10% fetal calf serum (Invitrogen Life Technologies), 1 mM sodium

pyruvate, 2 mM L-glutamine, 100 U of penicillin/mL, 100 mg of streptomycin/ml (complete medium) with stimuli. Splenocyte cell suspensions were stimulated with different stimuli for 5 days, including: OpcP (10 μg/ml), OpcP1 (10 μg/ml), LPS (10 μg/ml), protein + LPS, αCD3/αCD28 magnetic antibody-coupled beads with 30 U/mL of mouse recombinant IL-2, or complete medium alone. After 5 days of incubation at 37°C in a humidified atmosphere (5% CO_2 and 95% air), cell culture supernatants were collected and immediately stored at -80°C until further analysis. Cytokine production was analyzed using a BioPlex kit (BioRad, USA), according to the manufacturer's instructions.

STATISTICAL ANALYSIS

All statistical analysis was done using GraphPad Prism software (v8.0). *P* values of <0.05 were considered statistically significant. Quantitative data are expressed as means ± standard errors. All data were analyzed for normality before the corresponding test was run. Results of colonization, antibody, and cytokine levels were analyzed by one-way or two-way analysis of variance (ANOVA) using Tukey's *post hoc* test or the Kruskal-Wallis *post hoc* test when data were not normally distributed. Statistical differences in survival were determined by the Kaplan-Meier method, followed by log-rank test. Levels of significance compared to the adjuvant-only group: * $p < 0.05$, ** $p < 0.005$, *** $p<0.0005$, **** $p <0.0001$.

Chapter 6: EHEC Vaccine Study Materials and Methods

BACTERIAL STRAIN AND GROWTH CONDITIONS

Diarrheagenic *Escherichia coli* used in this study, EHEC (O157:H7), EPEC (O127:H6) or EAEC (O104:H4) were routinely grown aerobically at 37°C in Luria-Bertani (LB) broth. Before cell infection, the overnight cultures were activated in DMEM medium without fetal bovine serum (FBS) and without antibiotics. Bacterial cultures were incubated for 2 h at 37°C under static growth.

CLONING

EHEC (EDL933) DNA was isolated via QIAGEN® DNeasy® Blood and Tissue Kit, according to manufacturer's directions. Sequences encoding LomW (GI: 12514345) and EscC (GI: 12518466) were amplified via Phusion® polymerase (New England BioLabs) and cloned into a pET30a(+) expression vector using NdeI and XhoI or HindIII-HF® (New England BioLabs) restriction sites. The open reading frame for each protein was inserted in-frame with a 6x-histidine (His) tag on the C- terminus. Ligation, transformation, and expression were performed according to manufacturer's directions (pET System, Novagen) with some modifications. Upon confirmation of successful gene insertion via gel electrophoresis and directional sequencing (UTMB 335 Genomics Core), plasmids were transformed into BL21 (DE3) competent *E. coli* (New England 336 BioLabs) via heat shock treatment.

PROTEIN PURIFICATION

To induce protein expression, overnight cultures were diluted 1:20 in 1 L of Luria Bertani (LB) broth, grown to OD_{600} between 0.6 and 0.8, and induced with 1 mM final

concentration of Isopropyl β-D-1-thiogalactopyranoside (IPTG). At 3 h post-induction, cultures were centrifuged (4000 x g for 15 min), and the resulting bacterial pellet frozen at -20°C. The bacterial pellets were then resuspended in phosphate buffer saline containing 10% glycerol and 25 mM of sucrose with 1 mg/mL final concentration of lysozyme, 0.2% of sodium deoxycholate and a tablet of cOmplete™ EDTA-free protease inhibitor cocktail (Roche, Germany). This lysate was then sonicated, centrifuged, and the pellet used for subsequent washes to maximize soluble protein extraction. After spin down, the supernatant was filtered sterilized (0.2 μm). Soluble protein extracts were then bound to TALON Nickel columns (GE Healthcare, USA) and washed with PBS buffer with 50 mM imidazole. Proteins were eluted from affinity columns by applying a PBS buffer with 10% glycerol and 25 mM sucrose and 250 mM imidazole. Fractions were collected and pooled before dialyzing overnight at 4°C. The purified proteins and protein standards were subjected to a colorimetric bicinchoninic acid assay (BCA) according to manufacturer's protocol, then stored at -80°C until use. For protein visualization, 2 μg of protein was run on SDS-PAGE gel by electrophoresis. Protein bands were visualized by staining with Coomassie blue stain (Bio-Rad), or gels were transferred to a nitrocellulose membrane for western blot analysis. A mouse anti-histidine antibody (1:5000) was used and incubated overnight at 4°C, and an HRP conjugated rabbit anti-mouse IgG was used as a secondary antibody. Protein bands were visualized by adding ECL substrate (ThermoFisher Scientific, USA) and imaged on a film.

COUPLING OF PROTEIN CANDIDATES ONTO AUNPS

Gold nanoparticles (AuNPs), 15 nm in diameter, were synthesized by the Turkevich method (167). One mM gold (III) chloride trihydrate underwent a reduction reaction with 90 mM sodium citrate dihydrate. Particle size and shape was established by transmission electron microscopy (TEM). To stabilize the conjugation of soluble antigens onto the

AuNP surface, 0.1 mM 16-mercaptohexadecanoic acid (16-MHDA) and 0.1% Triton X-100 were added to AuNPs. After 2 h of incubation, this solution was filtered with centrifugation (EMB Millipore AmiconTM Ultra-15, 30 kDa MWCO) and repeated to ensure coverage. To covalently link soluble protein, 20 μg per mL of nanoparticles was added in the presence of DMTMM. The reactions were carried out in 100 mM borate buffer to allow for conjugation. Attachment of 16-MHDA and protein was confirmed by measuring plasmon resonance via UV-Vis spectroscopy as well as by SDS-PAGE electrophoresis.

ANIMAL STUDIES

Female, 6 to 8-week-old BALB/c mice were purchased from Jackson Laboratories (Bar Harbor, ME, USA) and maintained in Animal Biosafety Level 2 (ABSL2). Animals were housed in microisolator cages under pathogen-free conditions with food and water *ad libitum* and maintained on a 12 h light cycle. All animal protocols were reviewed and approved by Institutional Animal Care and Use Committee of the University of Texas Medical Branch (protocol no. 1007037B). To allow adequate acclimation, mice were housed within the animal facility for 1 week prior to experimentation.

IMMUNIZATION AND CHALLENGE STUDY

To evaluate the protective immunogenicity of LomW and EscC coupled onto AuNPs (AuNP-LomW or AuNP-EscC), anesthetized BALB/c mice (n=6 per group) were inoculated subcutaneously (s.c.) three times in two-week intervals. Animals received either AuNP-LomW, AuNP-EscC, or a combination vaccine (AuNP-Combination). Each vaccine formulation contained 10 μg of protein (LomW or EscC) along with 500 μg Alhydrogel (InvivoGen, USA) and 10 μg of detoxified cholera toxin (CT) (Sigma). For the

combination group (AuNP-Combination), mice received equal parts AuNP-LomW and AuNP-EscC (5 μg each for 10 μg total protein concentration). Control groups received adjuvant alone. To evaluate antibody titers, blood was drawn retro-orbitally 2 weeks following the last boost. To isolate sera, blood was incubated for 30 min at room temperature to allow for clotting and centrifuged (10,000 x g for 10 min). Sera was removed and stored at -80°C until use. Fecal samples were taken prior to vaccination (baseline) and two weeks after the last immunization. For assays requiring serum, the sera from all immunized animals (n=8) were pooled and stored.

INFECTION AND BACTERIAL COLONIZATION

Two weeks after administering the last immunization, all mice were challenged with a dose of ~3×10^9 CFU of *E. coli* O157:H7 strain 86-24 via gavage (200 μL). Food was restricted 12 h before infection but was administered *ad libitum* throughout the remainder of the study. Two hours prior to challenge, mice were injected intraperitoneally with cimetidine (50 mg/kg, Sigma) to reduce stomach acidity. Fecal samples were collected daily for 7 days to assess bacterial shedding. Fecal pellets were homogenized in PBS, serially diluted, and plated on MacConkey agar plates and incubated at 37°C. To enumerate bacterial colonization in gastrointestinal tract, mice were euthanized, and ceca and large intestines were removed. Organs were homogenized in 1 mL PBS, serially diluted and plated on MacConkey agar to enumerate bacterial colonization.

DETECTION OF PROTEIN-SPECIFIC ANTIBODIES

Baseline serum and fecal samples from adjuvant-only, AuNP-LomW, AuNP-EscC, and AuNP-combination formulation mice were collected 7 days before prime and 14 days after the second boost. Whole blood was collected via retro-orbital bleeding and stored in

microvette tubes without anti-coagulant. The serum was separated by centrifugation and stored at -80°C. Fecal pellets were suspended in 1 mL of PBS, centrifuged to remove fecal debris, and the supernatants were stored at -80°C until use. The protein-specific total IgG and IgA titers were determined by indirect ELISA. The microplate (Costar, Cambridge, MA) was coated at 4°C overnight with 1 μg/well of LomW or EscC in 1x Dulbecco's Phosphate-Buffered Saline (DPBS) (Corning, USA). Wells were washed twice with washing buffer (0.05% Tween-20 in 1× DPBS) and then blocked with blocking buffer (0.05% Tween-20, 2% BSA, 1× DPBS) at RT for 2 h. The blocked wells were washed twice before adding sample diluent (1% BSA, 0.05% Tween-20 in 1× DPBS. The sera were added to each top dilution well in triplicate and two-fold dilutions were performed following incubation at RT for 2 h. The diluted goat anti-mouse IgG, (1:5000) (Southern Biotech, USA) was added into each well and then incubated for 3 h after washing. Plates were washed four times prior to adding tetramethylbenzidine (TMB) substrate solution (Invitrogen, USA). The stop solution (2N H_2SO_4) was added, and the samples were immediately read at 450 and 570 nm using a microplate reader (Biotek, USA). The results were reported as the reciprocal of the highest titer giving an optical density (O.D.) reading of at least mean + 2 standard deviation of baseline sera. All assays were performed in triplicate, and results were shown as the mean reciprocal endpoint titer.

ADHERENCE INHIBITION BY SERUM ASSAY

Caco-2 cells (ATCC® HTB-37™) were maintained at 37°C with 5% CO_2 in complete HTB-37 medium. Complete Dulbecco's Minimum Essential Medium (DMEM, GIBCO, USA) supplemented with 2 mM glutamine, 1mM sodium pyruvate, 1× non-essential amino acids, penicillin-streptomycin (100 U/mL, 100 μg/mL), and 10% fetal bovine serum. For adhesion assays, 12-well plates were seeded with 1 x 10^6 cells/per well. Approximately 1 h prior to infection, the monolayer was washed twice with 1 mL PBS prior to addition of

1 mL medium containing no supplements. Overnight culture of EHEC O157:H7 strain 86-24 were diluted in DMEM (1:20) without supplements and incubated at 37°C under static growth conditions for 2 h. Bacterial inoculum was adjusted to a MOI of 10 (1×10^7 CFU) and incubated in the presence of AuNP-LomW, AuNP-EscC, AuNP-Combination immune serum, adjuvant-only serum, or naïve sera (10%) for 1 h at 37°C with slight agitation. After incubation in the presence of sera, bacteria were collected in 1 mL of fresh media and used to infect cell culture plates containing 1×10^6 cells. Monolayers were incubated for 2 h at 37°C with 5% CO_2. After incubation, cells were washed three times with PBS prior to addition of 100 µl of 0.1% Triton X-100 in PBS. After detachment, the cells were serially diluted in PBS and plated on LB agar plates to enumerate adhered bacteria (output). The percentage of adhered bacteria was determined as the output/input × 100. Data was representative of two independent experiments using pooled sera from (n=8) mice.

SERUM BACTERICIDAL ASSAY

Serum bactericidal assay were done as previously described with modifications (171, 172). Sera from immunized animals (n=8) were pooled and, either stored at -80°C or heat inactivated (56°C for 30 min). Serum from naïve BALB/c mice was added to inactivated serum as an active source of complement. Bacterial cultures were done as described above. Overnight EHEC 86-24 cultures were diluted 1:20 in DMEM without supplements and activated under static growth conditions for 2 h. Once the bacteria reached an OD_{600} of 0.5, 50 µL reactions containing 1 x 10^6 CFU were prepared with 10% of active, inactive, or inactive serum along an exogenous source of complement. Bacteria were incubated in the presence of serum for 1 h at 37°C with slight agitation. Viable CFU counts were determined by plating on LB agar plates 1 h post incubation in mouse serum. The negative control contained bacteria with serum from adjuvant-only immunized mice. The serum bactericidal percentage of serum was determined using the following equation (Bacterial

CFU in adjuvant only sera – bacterial CFU in treatment group sera) / bacterial CFU in adjuvant only sera × 100. The results are obtained from two independent experiments using pooled sera from (n=8) mice.

FLUORESCENCE MICROSCOPY

For microscopy fluorescence analysis, Caco-2 cells were cultured in round cover slips placed at the bottom of 12-well plates and incubated for 24 h at 37°C with 5% CO_2. Bacterial inoculum using a MOI of 10 (1×10^6 CFU) was incubated in the presence of AuNP-LomW, AuNP-EscC, or naïve sera (10%) for 1 h at 37°C with slight agitation. After incubation in the presence or absence of sera, bacteria were collected in 1 mL of fresh media and used to infect cell culture plates containing 1×10^5 cells. Additionally, evaluation of bacterial viability was performed by using the LIVE/DEAD staining (LIVE/DEAD® *Bac*Light™ Bacterial Viability Kit, Invitrogen, USA), using manufacturer's instructions. For cell infection, monolayers were incubated for additional 2 h at 37°C with 5% CO_2. After infection, cells were washed and fixed with 4% paraformaldehyde-PBS. Polymerized actin was detected by staining with tetramethyl rhodamine isothiocyanate-phalloidin (Molecular Probes-Invitrogen, USA). DNA from cell nuclei and bacteria were mounted using Fluoroshield™ and detected with DAPI. EHEC (86-24) was detected by immunofluorescence with anti-*E. coli* O + *E. coli* K antibody coupled to FITC (Abcam, USA). Images were taken using an Olympus BX51 upright fluorescence microscope and analyzed by Image J software (University of Wisconsin-Medicine).

STATISTICAL ANALYSIS

All statistical analysis was done using GraphPad Prism software (v8.0). P-values of <0.05 will be considered statistically significant. Quantitative data is expressed as the mean ± standard error. All data was analyzed for normality before running the corresponding test. Colonization, antibody results, serum adherence inhibition, and bactericidal assays were analyzed by one-way ANOVA (Tukey post-test) or Kruskal-Wallis when data was not normally distributed.

Chapter 7: A Nano-glycoconjugate Vaccine Against *B. mallei*

INTRODUCTION

Glanders is a zoonotic disease with a high degree of transmissibility to humans and mortality in solipeds (e.g. horses, mules, and donkeys) (67, 71, 173). The infection is caused by the Gram-negative pathogen *B. mallei* (*Bm*). This historic pathogen has been intentionally used as a biothreat agent a number of times because of its high transmissibility, mortality, and amenability for aerosolization (71, 72, 74). In addition, *Bm* is a non-motile intracellular pathogen with a complex intracellular lifestyle that uses a myriad of secreted effectors to allow survival and evasion of host immune responses (72, 74). Due to the pathogen's inability to survive for long periods of time outside its mammalian host, *Bm* is thought to have evolved by reductive evolution from its genetically related counterpart, *B. pseudomallei* (*Bpm*), the causative agent of melioidosis (65, 66). Both of these pathogens are capable of infecting and surviving inside phagocytic and non-phagocytic cells, including lung epithelial cells (66, 67). Depending on the route of infection, by either percutaneous inoculation (also known as farcy) or inhalation (glanders), humans and equines can present a wide range of clinical signs and symptoms (65). Pulmonary infection with *Bm* can be developed as either acute or chronic infections (65, 70). Its aerosolization properties together with the ability of infecting both humans and animals, has resulted in the dual classification of *Bm* as a Tier 1 Select Agent by the Centers for Disease Control and Prevention (CDC) and the United States Department of Agriculture (USDA) (72).

Bm and *Bpm* are naturally resistant to a wide range of antibiotics, and the available ones are limited or require extensive treatment regimens (67, 74). Furthermore, *Bm*-

specific therapeutic interventions have not gained much interest in the last ten years and fewer vaccine candidates have been reported for *Bm,* in comparison to *Bpm* (173, 174). Therefore, there is a need to identify and develop specific preventive measures for each of these pathogens for which no vaccine is currently available. Although glanders was eradicated from the Western Hemisphere in the late 20th century; today, glanders remains largely an occupational hazard for individuals that come in close contact with infected animals, including endemic areas in Western Asia, India, Africa, and South America (65, 70). Although a variety of vaccine candidates have been tested, live attenuated vaccines have provided the best evidence of complete protection and near-sterilizing immunity (99, 170). One outstanding concern associated with the live-attenuated vaccine approaches is their safety, especially if an effective vaccine will be used in immunocompromised individuals. Further, many other vaccines have failed to define the biomarkers of protection or the vaccine-mediated immune protective mechanisms. Therefore, alternative vaccination strategies, such as subunit vaccines, have to overcome the obstacles of conventional vaccine platforms to surmount the challenges of inducing robust humoral immune responses and engaging cellular immune responses (12).

Nanoparticle formulations offer attractive features that dictate and direct the immune response, including protection of the antigen from degradation, facilitating antigen movement across the epithelia, uptake and processing by antigen-presenting cells (APCs), depot formation, and co-delivery of antigens (12, 59). Given that the processes that govern antigen uptake and presentation by antigen presenting cells (APCs) are dependent on particle characteristics, nanovaccines offer a mean of augmenting the immunogenicity of subunit candidates that could result in increased protection. Gold nanoparticles (AuNPs) represent a platform with documented evidence of safety in a number of models, including infectious disease and cancer, as well as their use as effective nano-delivery systems which utilizes a number of mechanisms, including increased antigen uptake and processing, resulting in robust protective immune responses (38, 62, 168, 175). The goal of the current

study was to exploit the use of the AuNP platform to augment the protective ability of *Burkholderia* antigens that were identified using bio- and immuno-informatic analysis and testing those vaccines in a murine model of glanders. We conjugated each antigen along with lipopolysaccharide (LPS) of *B. thailandensis* (*Bth*), a tested immunogen, to elicit robust humoral responses to all these multiple antigenic molecules and test their protective properties either alone (AuNP-protein-LPS), or as a combination antigenic formulation (AuNP-Combo-LPS) after intranasal delivery. We tested whether single AuNP-protein-LPS formulations afford variable degrees of protection, and if a combination AuNP-glycoconjugate formulation improved the degree of protection against a lethal *Bm* challenge. Further, we also tested if serum from the AuNP-protein-LPS formulations showed antigen-specific responses against protein and LPS and whether this immune response was associated with a profile of anti-*Bm* activity including adherence inhibition to lung epithelial cells and opsonophagocytic activity in macrophages. We identified three protective antigenic vaccine candidates against *Bm* and reinforced the use of AuNPs as attractive antigen-delivery vehicle to augment protective immune responses.

RESULTS

Design and synthesis of gold (AuNP) nanoglycoconjugate vaccine platform

Using a previously published immuno- and bio-informatic prediction model for the identification of predicted antigens conserved between *B. pseudomallei* and *B. mallei*, we selected candidates based on their desirable physicochemical properties and predicted antigenicity and narrowed it to six candidates based on their amenability for purification (165). These candidates were recombinantly expressed in *E. coli* BL21 and purified by affinity chromatography where all proteins showed undetectable endotoxin levels. All six histidine (His)-tagged proteins were visualized on an SDS-PAGE gel followed by Coomassie staining (Fig. 1a) and by western blot (Fig. 1b, Supplementary Fig. 1). To

synthesize the glycoconjugate moiety on the surface of AuNPs, we purified the lipopolysaccharide (LPS) of *B. thailandensis* (*Bth*) and showed a high purity yield by SDS-PAGE gel electrophoresis followed by silver stain (Fig. 1c). Consistently spherical 15-nm-diameter AuNPs were synthesized using the Turkevich method, and visualized by transmission electron microscopy, before and after conjugation to proteins (Fig. 1d). The protein candidates were immobilized on the AuNP surface by the addition of 16-mercaptohexaundecanoic acid (MHDA), which is a small linker with a thiol group that readily binds AuNPs and possesses a carboxylic acid on the distal end involved in conjugation by carbodiimide synthesis. We covalently coupled *Bth* LPS on protein-decorated AuNPs by thiol-maleimide synthesis (Fig. 1d and e). To confirm the conjugation, we used UV-visible light (UV-Vis) spectroscopy to measure the difference in wavelength displacement indicating a red-shift, as seen after the addition of every protein and subsequent addition of LPS (Fig. 1e). This red shift (2 nm difference on average) after the addition of proteins onto the AuNPs allowed us to characterize the stable coupling of protein (amide bond) and LPS (thioether bond) complex onto the surface of the AuNP platform for subsequent *in vivo* studies (Fig. 1f).

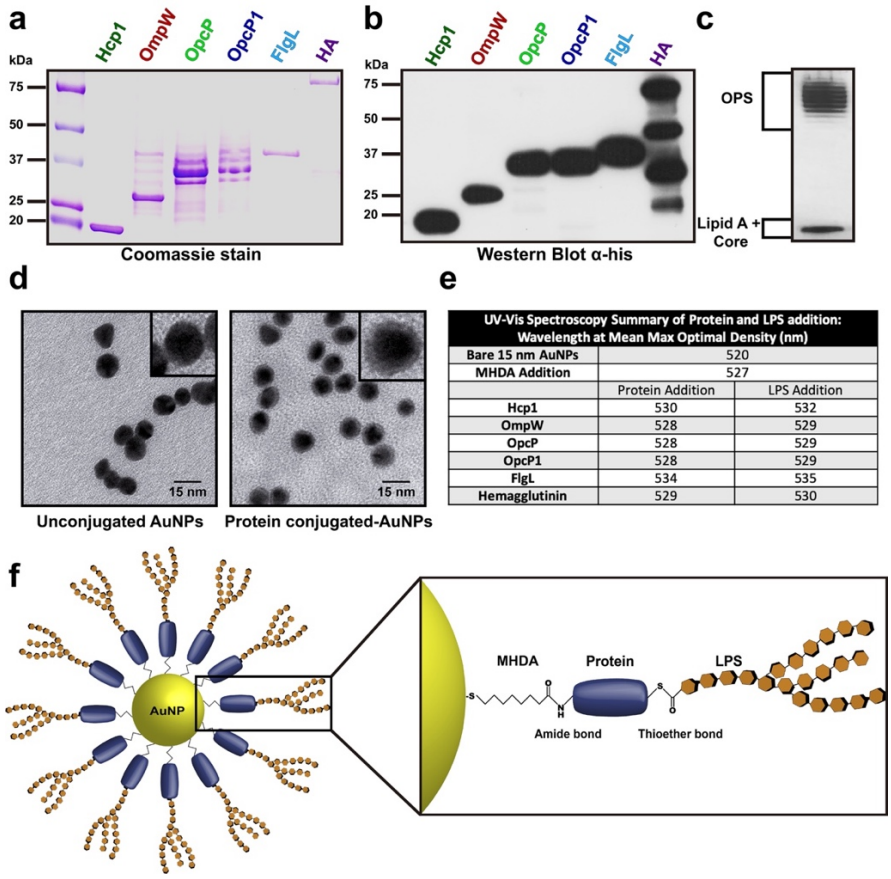

UV-Vis Spectroscopy Summary of Protein and LPS addition: Wavelength at Mean Max Optimal Density (nm)		
Bare 15 nm AuNPs	520	
MHDA Addition	527	
	Protein Addition	LPS Addition
Hcp1	530	532
OmpW	528	529
OpcP	528	529
OpcP1	528	529
FlgL	534	535
Hemagglutinin	529	530

Figure 1. Design and synthesis of gold nanoparticles (AuNP)-coupled as glycoconjugates to bio-and immuno-informatically identified candidates. (a) Coomassie-stained SDS-PAGE gel and (b) Western blot (WB) of recombinantly expressed protein antigens after purification. WB and Coomassie-stained gel were generated from the same experiment and processed in parallel. (c) Silver-stained gel of *B. thailandensis* LPS. (d) TEM of bare spherical 15 nm AuNPs prior to conjugation and representative particles after conjugation to OmpW. Scale bar 15 nm. (e) UV-Vis spectroscopy showing the Mean Maximum Wavelength (nm) of bare AuNPs, after the addition of 16-mercaptohexadecanoic acid (MHDA) linker, the addition of each protein, and after conjugation to LPS. (f) Graphical scheme of AuNP-linked glycoconjugate showing the amide bond between protein and MHDA linker after carbodiimide synthesis, and the thioether bond between LPS and protein after thiol maleimide synthesis.

Intranasal delivery of gold-nanoglycoconjugates protect against lethal inhalational glanders.

To test the protective properties of the different candidates when delivered as vaccines, we used AuNPs alone (AuNP-protein-LPS), or in combination (AuNP-Combo1-LPS), and

immunized C57BL/6 mice intranasally using a prime and two-boost vaccination strategy during two-week intervals (Fig. 2a). Each formulation contained a final concentration of 10 μg of protein and 10 μg of LPS coupled to AuNPs and 20 μg of CpG, (TLR9 agonist, as adjuvant) in a final volume of 50 μL. A group of animals also received a combination formulation containing equivalent amounts of each individually conjugated antigen [~1.67 μg/protein (Hcp1, OmpW, OpcP, OpcP1, FlgL, and HA)] along with LPS (AuNP-Combo1-LPS) and CpG. Two weeks after receiving the last immunization, animals were bled to evaluate antibody responses to individual antigens (Fig. 2a). Using a low-dose challenge model, animals were challenged with 2 Lethal Dose-50 (LD_{50}) of wild type (WT) *Bm* 23344 three-weeks after receiving the last immunization and to evaluate protective differences between the antigens (Fig. 2a). Animals immunized with AuNP-OmpW-LPS or AuNP-OpcP-LPS had a significant increase (100% survival) in survival at 35 days post infection (dpi), compared with animals that received an adjuvant-only formulation (Fig. 2b). In addition, animals immunized with AuNP-Hemagglutinin (HA)-LPS or AuNP-Hcp1-LPS displayed a significant increase (90% survival) in survival compared to adjuvant-only treated mice (Fig. 2b). In contrast, only partial protection was provided by the AuNP-OpcP1-LPS (70%), AuNP-Combo1-LPS (80%), or AuNP-FlgL-LPS (40%) formulations (Fig. 2b). After 35 days post infection, surviving animals were euthanized and the lungs and spleens were analyzed for bacterial load. We observed that most animals immunized with single AuNP-protein-LPS formulations had significant colonization in the lung with approximately 10^3 CFU/gram of tissue (Fig. 2c). However, we also found that most animals immunized with the AuNP-Combo1-LPS formulation (6 of 7) had no recoverable bacteria in the lung, except for one mouse (no significant differences) (Fig. 2c). In addition, most animals that survived to 35 days post infection had bacterial colonization in the spleen (no significant difference); however, 60% of animals immunized with the AuNP-Combo1-LPS formulation had no recoverable bacteria (Fig 2d).

To further increase the protection afforded by the candidates with the highest percent survival in the low dose-challenge, we conducted an *in vivo* protection study focusing on antigens OmpW, OpcP, HA, and a combination of these three (AuNP-Combo2-LPS). Using a similar vaccination strategy as depicted in Fig. 2a, animals were immunized with single protein-LPS formulations, and a formulation containing equivalent amounts of OmpW, OpcP, or HA (~3.33 μg/protein) (AuNP-Combo2-LPS). Three-weeks after receiving the last vaccination, animals were challenged intranasally with 50 LD_{50} of *Bm* 23344 (Fig. 3a). Animals immunized with AuNP-Combo2-LPS displayed 100% survival compared with the adjuvant-only control after 35 dpi, while animals immunized with AuNP-OpcP-LPS, AuNP-OmpW-LPS, or AuNP-HA-LPS, showed 80%, and 50% survival, respectively (Fig 3a). Surviving animals from each group were evaluated for bacterial infection in the lung, liver, and spleen (Fig. 3b-d). Animals immunized with AuNP-HA-LPS had no recoverable bacteria in either the lung or liver (Fig. 3b-c). Furthermore, 60% of animals immunized with this candidate vaccine did not show any recoverable bacteria in the spleen (Fig. 3d). In addition, 80% and 44% of animals vaccinated with the AuNP-Combo2-LPS did not show any recoverable bacteria in the lung and liver, respectively (Fig. 3b-c). Nonetheless, the highest colonization was found in the spleen of those surviving animals receiving the AuNP-OmpW-LPS formulation (Fig. 3d). These results indicate that the different AuNP-glycoconjugate formulations protect mice against a lethal inhalational challenge with *Bm*, being the highest protection the one provided by the optimized nanovaccine combination (AuNP-Combo2-LPS).

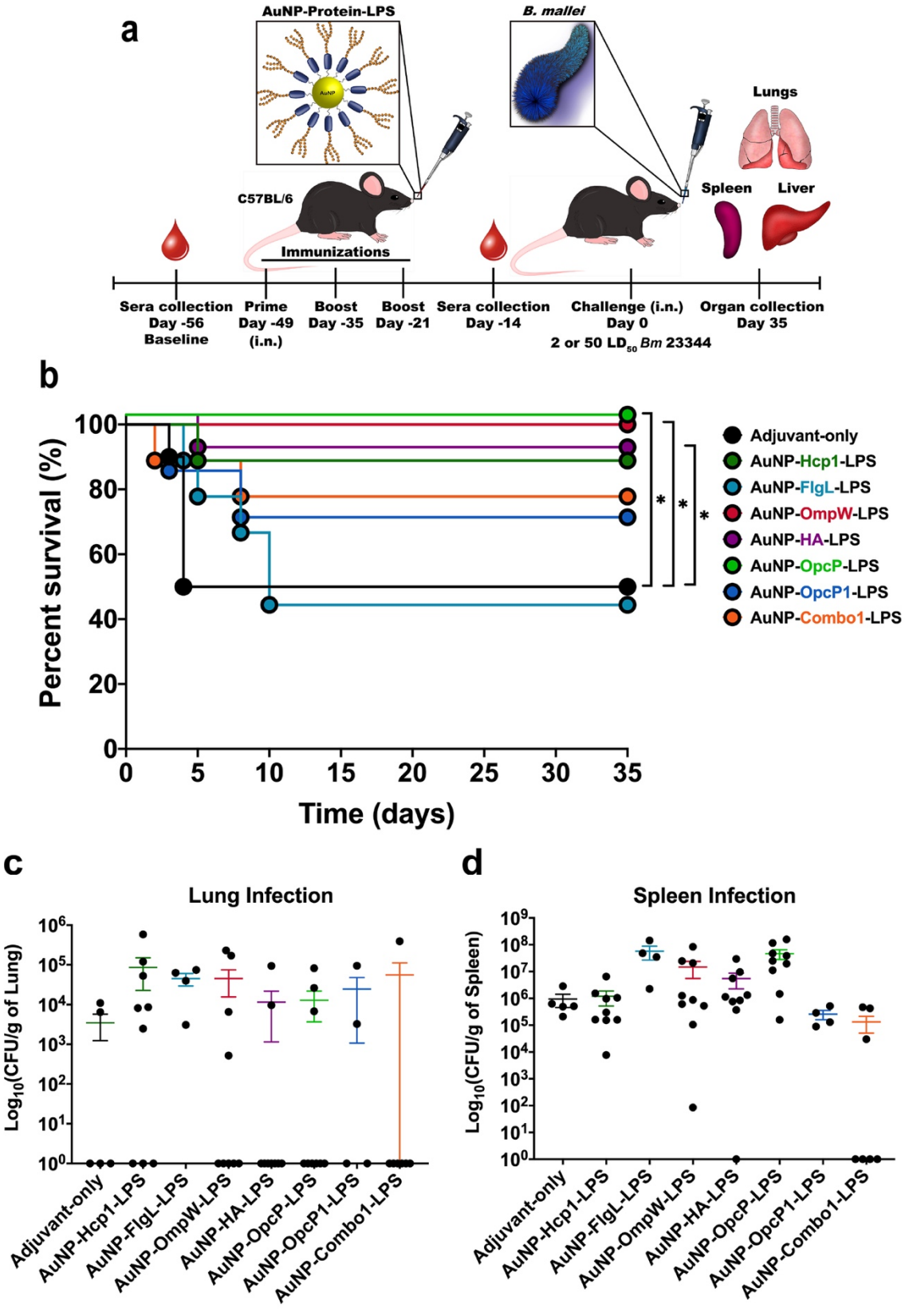
a
AuNP-Protein-LPS
B. mallei
Lungs
Spleen
Liver
C57BL/6
Immunizations
Sera collection Day -56 Baseline
Prime Day -49 (i.n.)
Boost Day -35
Boost Day -21
Sera collection Day -14
Challenge (i.n.) Day 0
2 or 50 LD50 Bm 23344
Organ collection Day 35
b
Percent survival (%)
Time (days)
Adjuvant-only
AuNP-Hcp1-LPS
AuNP-FlgL-LPS
AuNP-OmpW-LPS
AuNP-HA-LPS
AuNP-OpcP-LPS
AuNP-OpcP1-LPS
AuNP-Combo1-LPS
c
Lung Infection
Log10(CFU/g of Lung)
d
Spleen Infection
Log10(CFU/g of Spleen)

Figure 2. Increased survival from AuNP-OmpW-LPS, -HA-LPS, and OpcP-LPS after low-dose challenge with *Bm* 23344.
(a) Graphical illustration of the vaccination timeline. C57BL/6 mice (n=9) were immunized intranasally with formulations containing 10 μg of protein, 10 μg of LPS, and 20 μg of CpG ODN 2395, 3× in two-week intervals. Combination formulation included equivalent amounts of protein (Hcp1, FlgL, OmpW, HA, OpcP, and OpcP1) from each candidate for a total of 10 μg of protein. (b) After intranasal challenge with 2 LD_{50} (2.8×10^4 CFU per mouse) of *Bm* 23344, the (c) lungs and (d) spleens of surviving animals were collected at 35 days post-infection to perform bacterial enumeration. Bacterial load was determined per gram of tissue, and representative panels for colonization are shown in log scale. All colonization data are shown as means ± standard errors of the means (SEM) of results determined per group. Statistical analyses were determined by the Kaplan-Meier method, followed by log-rank test. Levels of significance compared to the adjuvant-only group: * $p < 0.05$.

To evaluate the immunogenicity of the different AuNP-coupled glycoconjugates and assess the protection differences afforded by different antigens, we evaluated the antigen-specific humoral responses associated with the highest protection against *Bm* lethality. Animals immunized with each individual formulation containing OpcP, OmpW, or HA had total IgG of $\geq 10^7$ endpoint titers against each antigen (Fig. 4a-c). In addition, animals that received the AuNP-Combo2-LPS formulation, containing equivalent amounts of OpcP, OmpW, and HA, showing robust responses against each antigen, which were equivalent to single protein-LPS formulations (Fig. 4a-c). Further, animals immunized with either AuNP-OmpW-LPS, AuNP-HA-LPS, AuNP-OpcP-LPS, as well as with AuNP-Combo2-LPS, maintained robust humoral responses against LPS with the highest titers of 10^6, and AuNP-OmpW-LPS associated with the lowest 10^5 endpoint titers (Fig 4d). To evaluate the differences in immune polarization or functionality, we measured the isotype changes in single-protein formulation after vaccination (Fig. 4e-g). We observed robust T_H1-biased immune response with statistically higher levels of IgG_{2c} in animals immunized with OpcP- and OmpW-formulations (Fig. 4e-f). These results indicate the ability of intranasally immunization with AuNP-delivered glycoconjugates to induce robust antigen-specific antibody titers and a T_H1-biased immune response that correlated with protection.

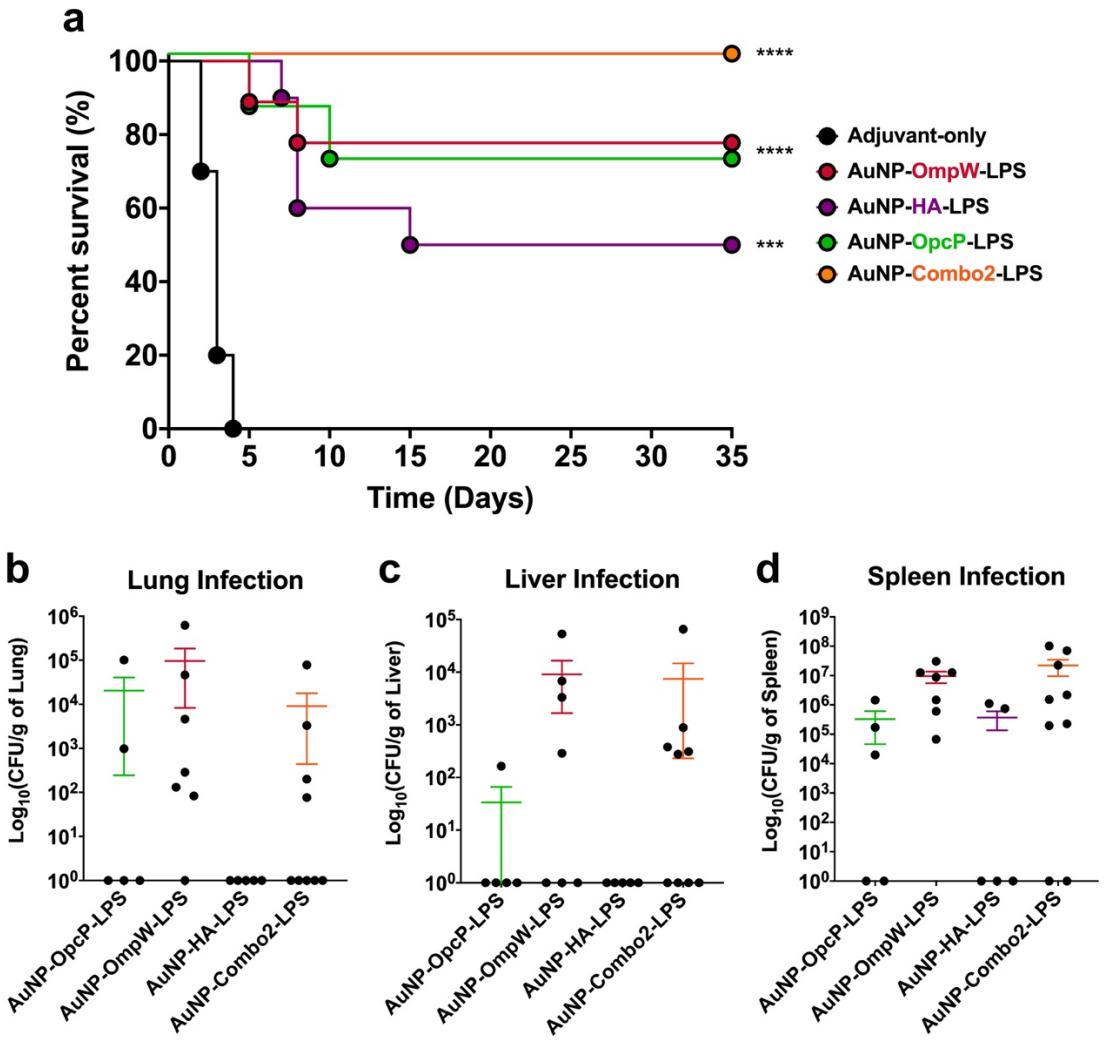

Figure 3. Increased protection by AuNP-Combo-LPS, -OmpW-LPS, -HA-LPS, and OpcP-LPS against high-dose challenge with *Bm* 23344.
C57BL/6 mice (n=9) were immunized as described. The AuNP-Combo-LPS vaccinated group contained equivalent amounts of protein (OmpW, HA, and OpcP) from each candidate for a total of 10 µg of protein. (a) After intranasal challenge with 50 LD_{50} (7×10^5 CFU per mouse) of *Bm* 23344, the (b) lungs, (c) livers, and (d) spleens of surviving animals were collected at 35 days post-infection and bacterial enumeration performed. Bacterial load was determined per gram of tissue, and representative panels for colonization are shown in log scale. All colonization data are shown as means ± standard errors of the means (SEM) of results determined per group. Statistical analyses were determined by the Kaplan-Meier method, followed by log-rank test. Levels of significance compared to the adjuvant-only group: *** $p<0.0005$, **** $p<0.0001$.

Serum from AuNP-glycoconjugate vaccination is associated with a reduction in bacterial adherence and increased opsonophagocytosis linked to bacterial death.

The differences in functionality between the vaccine groups were analyzed by evaluating the ability of serum from immunized mice to block bacterial adherence onto epithelial cells or to increase macrophage-mediated phagocytosis. Bacteria in the presence of sera from AuNP-OpcP-LPS or AuNP-Combo2-LPS had a significant reduction in adherence to murine lung epithelial cells, compared to bacterial infection without sera (Fig. 5a). The other sera did not significantly interfere with the bacterial adherence properties. In contrast, by 2 h post infection, bacteria in the presence of sera from AuNP-OpcP-LPS, AuNP-HA-LPS, and AuNP-Combo2-LPS immunized groups were associated with significantly lower levels of surviving *Bm* in primary mouse macrophages in comparison to bacteria in the presence of naïve sera (adjuvant-only group) (Fig. 5b). In the presence of serum from AuNP-OpcP-LPS, AuNP-HA-LPS, and AuNP-Combo2-LPS, we observed an increase in the number of internalized bacteria by primary murine macrophages by 1 h post infection, comparing to bacteria in the presence of serum from naïve animals (Fig. 5c). In addition, using a live/dead bacterial stain, we were able to visualize the viability of intracellular bacteria in primary macrophages by assessing the loss of membrane integrity via the incorporation of propidium iodide (Fig. 5d). In the presence of sera from the immunization groups AuNP-OpcP-LPS, AuNP-HA-LPS, and AuNP-Combo2-LPS, we noticed a larger proportion of internalized bacteria by macrophages had compromised membranes, as visualized in red within the bacterial cytoplasm (Fig. 5d). These results confirm that the antibodies in the serum from AuNP-protein-LPS-immunized animals block bacterial adherence to lung epithelial cells and enhance antibody-mediated phagocytosis by macrophages. More importantly, we showed that both effects are present in serum from animals immunized with AuNP-Combo2-LPS formulation.

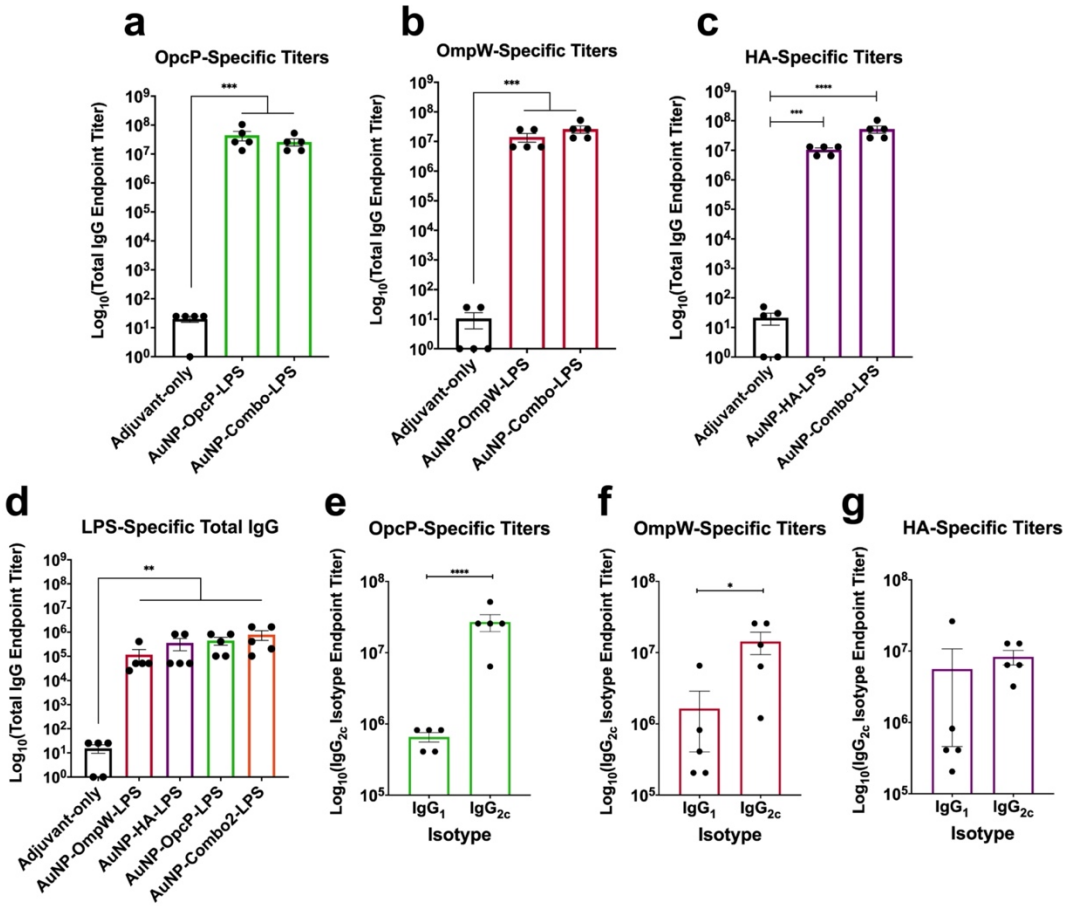

Figure 4. Sustained antibody responses after intranasal delivery of AuNP-nano-glycoconjugate immunization.
(a-c) protein- and (d) LPS-specific total IgG titers were assessed by ELISA, with endpoint titers defined as twice the standard deviation (SD) of the levels measured for naive sera. Sera samples taken from the mice immunized with the combination formulation (OpcP, OmpW, and HA) were used to assay protein-specific total IgG antibody titers. (e-g) IgG_1 and IgG_{2c} isotype titers were determined by reciprocal endpoint titers against each antigen using anti-mouse IgG_1 or IgG_{2c} antibodies, respectively. All antibody data are expressed as mean ± SEM of results from at least 5 mice per group and analyzed in triplicate. Significant differences between IgG_1 and IgG_{2c} titers were determined via a one-way ANOVA followed by Tukey's test or Student′s *t* test. *$p < 0.05$, ** $p < 0.01$, *** $p < 0.001$ **** $p<0.0001$.

DISCUSSION

Efficient delivery of antigens by AuNPs requires a stable association with the AuNPs interface (47). This nanovaccine platform has been used for the delivery of a variety of

biomolecules and in vaccine delivery, and it has been shown to help deliver protein antigens and enhance protection. Although the exact mechanism by which this may occur is not entirely understood, it is believe that nanoparticles may act as adjuvants to enhance antigen stability, improve the ability to cross mucosal barriers, and for antigen presentation upon antigen-presenting cell internalization (11, 12, 59).

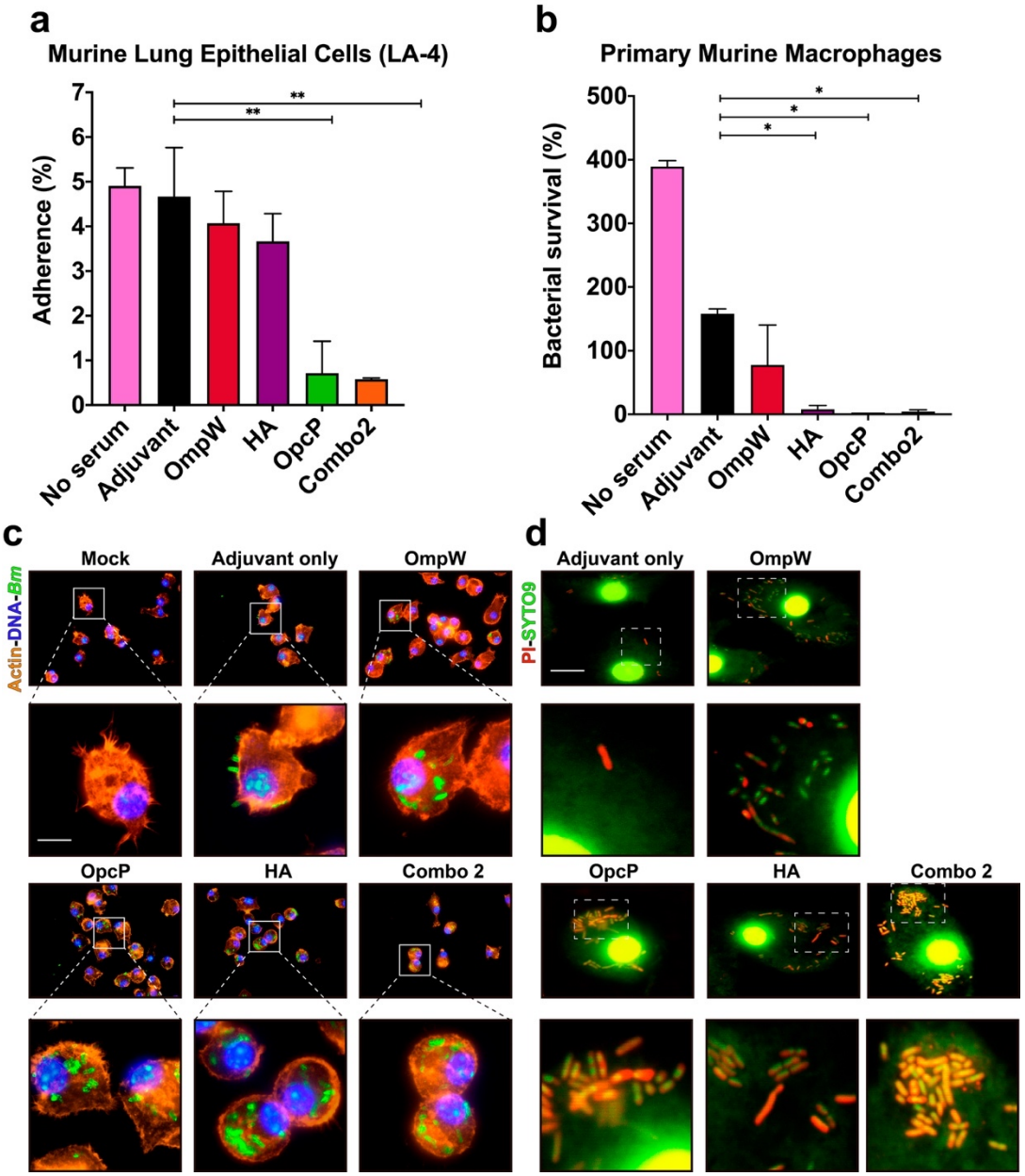

Figure 5. Sera from surviving animals reduce adherence to mouse lung epithelial cells and promote bacterial opsonophagocytosis by primary murine macrophages, leading to bacterial death.

Bm 23344 bacterial cells (5×10^6 CFU) were incubated in the presence or absence of immunized serum (10% of final volume) from animals immunized with each vaccine group (pooled from at least 5 animals) for 1 h at 37°C. Serum from naive mice (adjuvant-only) served as controls. After incubation, bacteria were used to infect (a) LA-4 cells or (b) primary murine macrophages for 2 h and 1 h, respectively. After infection, LA-4 cell monolayers or primary macrophages were processed to enumerate adhered or surviving bacteria, respectively. All data are expressed as mean ± SEM of results from two independent experiments using sera from n=5 mice per group. Significant differences were determined via one-way ANOVA followed by Tukey's post hoc test compared to the Adjuvant-only group (*$p < 0.05$, **$p < 0.001$). (c) Fluorescence microscopy analysis of primary murine macrophages after *Bm* 23344 infection in the presence of immune serum (from vaccinated groups). After infection, cells were fixed, permeabilized, and stained with phalloidin-rhodamine (actin), DAPI (bacteria and cell nuclei), and examined by IFA (sera anti-LPS followed by a rabbit anti-mouse Alexa Fluor-488). (d) LIVE/DEAD™ *Bac*Light™-stained primary murine macrophages infected with *Bm* 23344 in the presence of sera from each immunization group as described above. Panels below each group represent magnifications (10×) of the images on top. Images were taken using an Olympus BX51 upright fluorescence microscope (60×) and processed using Image J software. Scale bars 25 μm.

A recent study showed that upon antigen delivery and dendritic cell internalization, OVA-conjugated AuNPs showed enhanced OVA-specific polyfunctional T cells responses, including the induction of CD8+ cytotoxic T cells (62). In addition, the mechanism of nanoparticle uptake to draining lymphatic organs is more efficient compared to soluble antigens-alone, an effect dependent on the NP's physicochemical characteristics, such as their size, shape, or charge (11, 51, 62, 175). Based on these premises, we covalently linked each recombinant predicted antigen to the surface of AuNPs by a covalent modification via a small hydrophobic linker (16-MHDA). To exploit the stability, loading efficiency of AuNPs, and the multivalent display of antigens, we conjugated the LPS of *Bth* containing both the O-antigen molecule (OAg) as well as the lipid A moiety onto the protein-decorated NPs, to expand the protective response against *Bm*. The LPS of *Bth* has been demonstrated to have immune and adjuvant stimulatory activity (176). To

induce antibody responses against the LPS moiety of *Bth*, a well-known T cell-independent antigen, we covalently coupled LPS to proteins on the surface of AuNPs to engage T cell help and allowing for memory B cell development, and long-lived T cell memory (177). In addition, the final vaccine formulation contained 20 μg of CpG ODN 2395, a toll-like receptor 9 (TLR9) agonist shown to help induce a T_H1-biased response and a therapeutic molecule in helping control *Bm*-infection during early times post infection (178, 179). Together, the function of AuNPs as antigen delivery vehicles along with a T_H1-biased adjuvant could help augment and divert the immunogenicity of the protein and LPS antigens. As predicted, we were able to show the synthesis, by covalent coupling of both the protein and LPS antigens, to the surface of a single AuNP by using UV-Vis and TEM.

Given that inhalation of *Bm* is a potential exposure route, a vaccine that elicits robust mucosal responses is expected to provide the most efficient protection against aerosol infection. Most vaccines platforms that are delivered by the parenteral route fail to induce strong mucosal responses (59). Therefore, intranasal vaccination is an efficient and appealing strategy for the induction of mucosal-specific immunity (59). Among the multiple challenges hindering the development of nasal vaccination are the inefficient antigen uptake, rapid antigen clearance, size-restriction across epithelial barriers, and safe use of adjuvant for intranasal delivery (59). Nanoparticle-based vaccines offer a mucosal-adjuvant strategy that is safe and efficient for antigen delivery, uptake, and processing (12, 38, 62). Using a murine model of glanders, we evaluated six bio- and immuno-informatically predicted antigens for their protective ability against a low-dose challenge. We found that three new antigens provide significant protection against such inhalational challenge. OpcP and OmpW are two predicted porins that are among the most abundant proteins in the outer membrane of *Bpm* and *Bm* (180). Hemagglutinin is a predicted member of the autotransporter family of proteins with an unknown active function in the pathogenesis or life cycle of *Bm*. Our results indicated that these antigens alone provided significant protection against a low-dose *Bm* intranasal challenge. In addition, these

candidates provided a high degree of protection against a high-dose challenge of *Bm*, with the highest protection afforded by OpcP and OmpW, two proteins present in a wide range of growth conditions in both *Bpm* and *Bm* (180). In addition, a combination vaccine formulation of the three most-protective antigens (AuNP-Combo2-LPS) provided 100% survival against a high-dose *Bm* challenge, although no observable difference was seen when delivered in combination with three other proteins (FlgL, Hcp1, and OpcP1). Plausible justifications for this observation might be that the protective antigens in a formulation containing all six candidates are diluted, not reaching the appropriate concentration, in comparison to the formulation containing only three antigens. Another option is that the protective responses to those antigens are out-competed in the combination formulation containing all six antigens (AuNP-Combo1-LPS). Future studies should focus on determining the optimal antigen dose and combination that provide the most effective protection against *Bm* colonization in the lungs, liver, and spleen, while maintaining establishment of an acute infection.

Our results also demonstrated that AuNP-conjugated glycoconjugates induce strong antigen-specific humoral responses when delivered intranasally. Interestingly, in vaccine groups with the highest survival rate, the total IgG titers remained equivalent when the antigen was delivered alone or in combination with another two antigens. In addition, we also observed elevated LPS-specific humoral responses, with the highest levels seen in the AuNP-Combo2-LPS formulation. We have shown that AuNP-protein-LPS delivery is able to maintain elevated LPS-specific titers without affecting the induction of strong protein-specific responses. Studies have shown high degree of structural similarity of the LPS in *Bth*, *Bpm*, and *Bm* as well as their function as potent innate immune stimulator (166, 176). Although the role of LPS-specific humoral responses in human glanders patients is unknown, in the case of melioidosis patients, the O-polysaccharide (OPS)-specific titers correlate to higher degree of survival in convalescent patients (181). Importantly, convalescent human melioidosis patients appear to have higher LPS-specific IgA titers,

compared with non-survivors (181). Our results further strengthen this hypothesis by demonstrating the importance of serum IgG against both protein and LPS antigens at providing protection against inhalational *Bm* infection. In addition, we previously showed a similar observation with two known protective *Bm* antigens, Hcp1 and FliC, when delivered in a AuNP-glycoconjugate model showing the best protection afforded upon conjugation of the LPS structure to a protein carrier (182).

Given the complex role of serum antibodies in mediating antibacterial responses, we also analyze the differences in antibody function in the different vaccine groups. While the C57BL/6 mouse genetic background does not express the locus for the IgG_{2a} antibody subtype, rather IgG_{2c}, we measured this antibody isotype to prevent an incorrect interpretation of murine humoral immune responses (183, 184). Our results suggest that the higher IgG_{2c} levels correspond to a T_H1-biased immune response, potentially implicating cellular-mediated immune responses as mediators of vaccine protection. However, future studies should focus in the different AuNP-glycoconjugates and assess how cellular-mediated immunity is elicited. To further analyze the potential effector function associated with the humoral responses, we decided to measure *in vitro* two other important antibody functions. We evaluated the bacterial adherence to murine lung epithelial cells in the presence or absence of serum from each vaccine group and found a significant decrease in bacterial adherence with sera from the OpcP-LPS and Combo-LPS vaccine groups. The data suggest that serum inhibition of bacteria adherence is due to the antibodies against OpcP, an such inhibitory effect is retained in the combination vaccine formulation. This bacterial protein is highly expressed on the surface of *Bm* and across a wide range of conditions and represents an efficient mechanism of blocking adherence to prevent internalization and to prevent full *Bm* pathogenesis. We also used primary mouse macrophages to define whether serum enhanced bacterial uptake and found that this phenotype was maintained in most vaccine groups, including the combination vaccine formulation (Combo2). The decrease in bacterial viability, as seen by reduced bacterial

survival, and visualization of compromised bacterial membranes within macrophages treated with the AuNP-OpcP-LPS, AuNP-HA-LPS, and AuNP-Combo2-LPS sera indicates that serum acted during bacterial uptake but also during bacterial killing. Lastly, these results indicate that antibodies against different proteins have a variety of anti-*Bm* properties and the combination vaccine formulation retained these different effector functions. Our results offer a possible explanation for the observed enhanced protection *in vivo* against inhalational glanders. Furthermore, these results indicate that a multivalent vaccine against *Bm* may provide enhance and complete protection against infection and colonization. Overall, the work highlights the identification of three new protective subunit vaccine candidates against *Bm* which warrant further investigation into the most effective formulation dose and/or combination that can be advance to human trails.

Chapter 8: A Nano-glycoconjugate Vaccine Against *B. pseudomallei*

INTRODUCTION

B. pseudomallei (*Bpm*) is an intracellular pathogen with a complex life cycle and the causative agent of melioidosis, a complex human disease associated with a high fatality rate (66). Melioidosis can be acquired by several routes including, inhalational, ingestion, or percutaneous inoculation (66, 71). A broad spectrum of complications can result from inoculation by any infection route and the predicted mortality ranges, with mortality rates exceeding 50% in some regions (66, 185). Prediction modeling highlighted the global burden of melioidosis to comprise 165,000 new cases each year, of which half of those are fatal (185). Together with the intrinsic resistance of *Bpm* to first-line antibiotics and prolonged treatment regimen for melioidosis, prompt antimicrobial therapy optimal for *Bpm* is crucial to control the infection (66, 68). However, melioidosis in endemic regions is associated with the highest mortality rates attributed to failure of early detection and limited healthcare infrastructures, reinforcing the need for effective preventive countermeasures.

The intricate host-pathogen interplay complicates the development of vaccines that are safe for use in susceptible individuals while inducing protective immune responses. Individuals who survive *Bpm* infection develop strong *Bpm*-specific humoral, and cell-mediated responses, particularly evoking an immune response skewed towards the activation of T_H1 cells, which is associated with IFNγ production (72, 186–190). In particular, human convalescent patients have higher antibody levels against LPS and increased levels of CD4+ and CD8+ T cells (186, 190–192). Individuals who succumb to infection have a decrease in the levels of T cells, and reduced IFNγ and IL-17 expression (186, 190, 192–195). Further, the pool of protective antigens, together with the dearth in vaccine delivery platforms, which can be associated with the induction of robust antibody

and cell-mediated immunity, has hindered the development of fully protective *Bpm* subunit vaccines (72). Another challenge is that sterilizing protection against inhalational exposure, which is associated with the highest mortality, remains a challenge in small animal models. The induction of mucosal-specific immunity through nasal vaccination, though appealing, has been hindered by factors such as inefficient antigen uptake, size-restricted permeability, antigen stability through epithelial barriers, and absence of effective adjuvants that help stimulate cell-mediated immunity (11, 12, 59). However, mucosal delivery of vaccine antigens is necessary to induce protective immunity (12, 59).

Nanoparticle-based vaccines are attractive as molecule carriers as they have been shown to protect the antigen from degradation, facilitating its uptake by antigen-presenting cells (APCs), depot formation, and co-delivery of antigens (11, 12, 37, 59). In particular, gold nanoparticles (AuNPs) have been exploited to deliver several biomolecules, including co-delivery of multiple proteins or DNA antigens, given their intrinsic physicochemical properties and rigid surface (39, 57, 196–199). These particles offer a means to overcome the hurdle of increasing immunogenicity without compromising the safety and tolerability of one or multiple antigens (39, 57, 196, 199). AuNPs have garnered interest in antigen delivery given their high biocompatibility, tunable physicochemical characteristics like size or shape, ability to carry multiple antigens on a rigid surface (14, 37, 39, 50, 51, 53, 56, 196, 199). Therefore, nanoparticle-based vaccine platforms represent a promising characteristic to surmount some of the challenges of classical vaccine development to elicit strong humoral and cell-mediated immunity (39, 50).

The objective of the studies described in this chapter was to exploit the use of an AuNP-based platform to deliver an optimal multivalent vaccine formulation, while understanding the immunological responses associated with protection against a *Bpm* challenge. We synthesized and intranasally delivered a glycoconjugate moiety on AuNPs using several *Burkholderia*-specific antigens along with the lipopolysaccharide (LPS) from *B. thailandensis*. Immunization with a combination formulation containing OpcP and

OpcP1 (AuNP-Combo2-LPS) afforded complete protection against lethality. Animals immunized with the AuNP-Combo2-LPS had robust antigen-specific lung IgA responses and serum IgG, with elevated IgG_{2c} titers. In addition, sera from AuNP-Combo2-LPS immunized mice promotes antibody-dependent opsonophagocytosis and reduced bacterial survival in primary macrophages. Splenocytes from AuNP-Combo2-LPS immunized mice showed elevated levels of IFNγ, TNFα, IL-2, IL-17A, and IL-10, upon antigen restimulation. Overall, our study shows that AuNP-coupled glycoconjugate vaccine immunization is associated with antigen-specific humoral and cell-mediated responses associated with protection against *Bpm*. Our data highlights the identification of several protective antigens against *Bpm* and expands on the rationale for the delivery of multiple antigens using an AuNP platform as a means of inducing both humoral and cell-mediated responses.

RESULTS

Immunization with AuNP-OpcP-LPS or AuNP-OpcP1-LPS provides protection against an intranasal challenge with *Bpm* K96243.

To test the protective properties of several immunogenic proteins when delivered intranasally, we conducted an *in vivo* protection study against an inhalational challenge of *Bpm* K96243, using six previously identified proteins (165) (Fig 1A). We recombinantly expressed and purified each protein by affinity chromatography (Hcp1, OmpW, OpcP, OpcP1, FlgL, and Hemagglutinin [HA]) and coupled them to the surface of 15 nm gold nanoparticle (AuNPs) (Fig 1). In addition, we coupled the lipopolysaccharide (LPS) of *B. thailandensis* to incorporate a repeating glycoconjugate moiety onto AuNPs (Fig. 1). Then, we intranasally (i.n.) immunized C57BL/6 mice with three doses at two-week intervals, with individual AuNP-protein-LPS candidates containing 10 μg of protein, 10 μg of LPS, and 20 μg of CpG (final concentrations; Fig. 6A). A group of mice also received a

combination of equal ratios of each individually coupled antigen (AuNP-Combo1-LPS). Three weeks after receiving the last immunization, animals were challenged with 6 lethal-dose 50 equivalents (LD_{50}) of *Bpm* K96243. Animals immunized with AuNP-OpcP-LPS or AuNP-OpcP1-LPS showed 30% and 90% protection, respectively, against a lethal inhalational dose of *Bpm* K96243 by day 35 post-infection (Fig 6B). However, no significant protection was afforded by the AuNP-Combo1-LPS formulation or the conjugates containing candidates Hcp1, FlgL, OmpW, or HA (Fig. 6B). The lung, liver, and spleen of surviving animals were collected at day 35 days post-infection, and animals vaccinated with AuNP-OpcP-LPS or AuNP-OpcP1-LPS showed little to no bacterial counts in the three organs (Fig. 6C-E). Only a single animal had colonization in the spleen with 1×10^5 bacteria (Fig. 6C). These results demonstrate the ability of AuNP-OpcP-LPS or AuNP-OpcP1-LPS to protect against a lethal dose of *Bpm* K96243 when delivered intranasally.

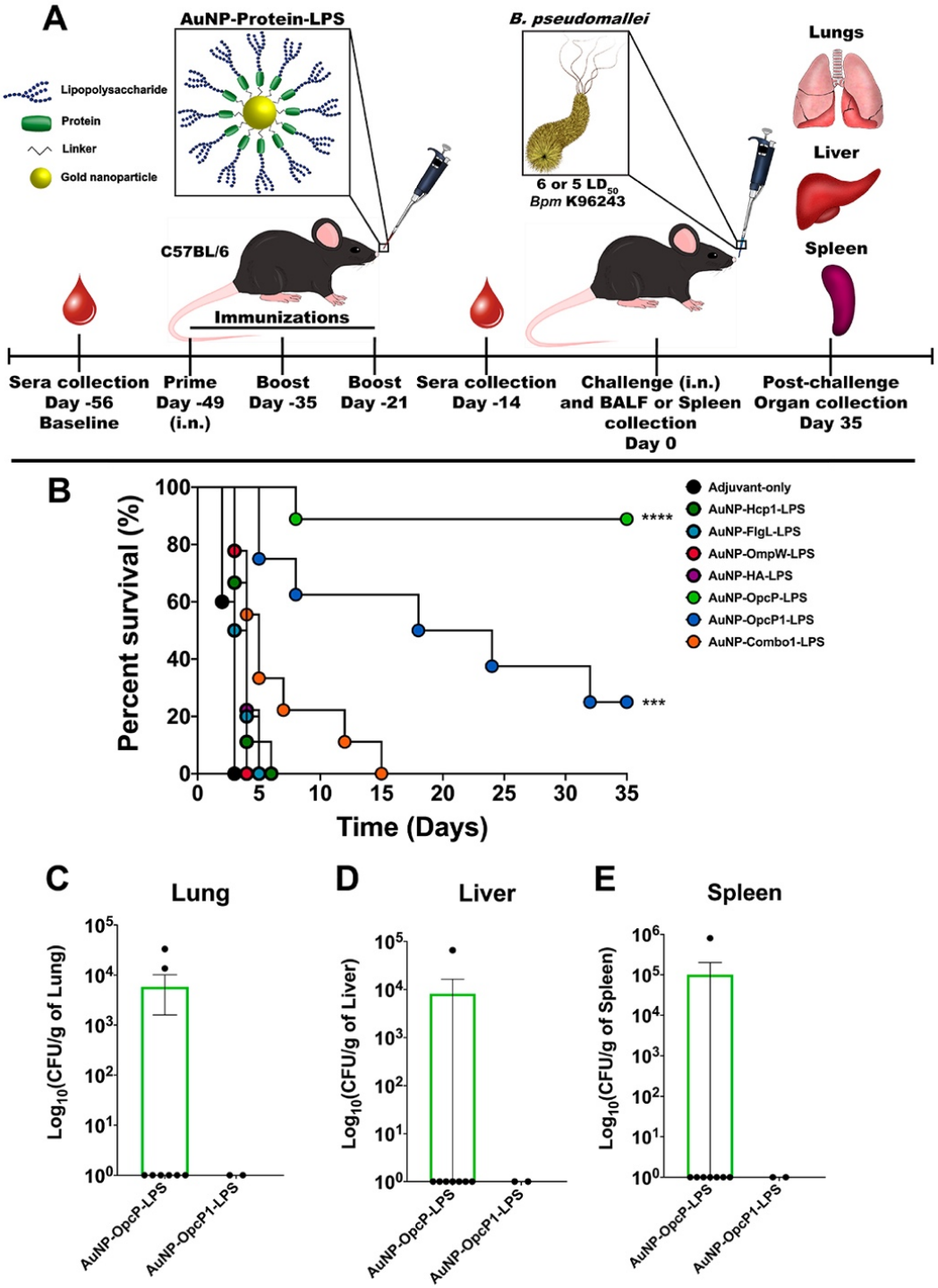
A
AuNP-Protein-LPS
Lipopolysaccharide
Protein
Linker
Gold nanoparticle
B. pseudomallei
6 or 5 LD50
Bpm K96243
Lungs
Liver
Spleen
C57BL/6
Immunizations
Sera collection Day -56 Baseline
Prime Day -49 (i.n.)
Boost Day -35
Boost Day -21
Sera collection Day -14
Challenge (i.n.) and BALF or Spleen collection Day 0
Post-challenge Organ collection Day 35
B
Percent survival (%)
Time (Days)
Adjuvant-only
AuNP-Hcp1-LPS
AuNP-FlgL-LPS
AuNP-OmpW-LPS
AuNP-HA-LPS
AuNP-OpcP-LPS
AuNP-OpcP1-LPS
AuNP-Combo1-LPS
****
***
C
Lung
Log10(CFU/g of Lung)
D
Liver
Log10(CFU/g of Liver)
E
Spleen
Log10(CFU/g of Spleen)
AuNP-OpcP-LPS
AuNP-OpcP1-LPS

Figure 6. Increase survival from AuNP-OpcP-LPS or AuNP-OpcP1-LPS immunized mice against a lethal intranasal challenge with *Bpm* K96243.
(A) Graphical representation of the vaccination and challenge timeline. C57BL/6 mouse (n = 10) were immunized intranasally 3× in two-week intervals with formulations containing 10 μg of protein, 10 μg of LPS, and 20 μg of CpG ODN 2395. A combination formulation (AuNP-Combo1-LPS) included equivalent amounts of protein (Hcp1, OmpW, OpcP, OpcP1, FlgL, and HA) from each candidate for a total of 10 μg of protein. **(B)** Three-weeks after the last vaccination, animals were challenged with 6 LD_{50} (9.0×10^4 CFU per mouse) of *Bpm* K96243, the **(C)** lungs, **(D)** livers, and **(E)** spleens of surviving animals were collected at 35 days post-infection to evaluate bacterial infection. Bacterial load was determined per gram of tissue, and representative panels for colonization are shown on log scale. All colonization data are shown as means ± standard errors of the means (SEM) of results determined per group. Statistical analyses were determined using the Kaplan-Meier method, followed by log-rank test. Levels of significance compared to the adjuvant-only group: ***$p < 0.001$, ****$p < 0.0001$.

Immunization with refined AuNP-Combo2-LPS formulation containing OpcP/OpcP1 provides enhanced protection against inhalational *Bpm* challenge.

Based on our initial experiment showing a significant increase in protection afforded by the AuNP-OpcP-LPS or AuNP-OpcP1-LPS nanovaccines, we further investigated the protective properties of a combination of these formulations. We performed similar immunization scheme of three doses in two-week intervals with subsequent lethal challenge with *Bpm* K96243. To evaluate immunization-induced pathology in tissues, the lung, liver, and spleen from three representative animals were evaluated two weeks after receiving the last immunization. All tissues from the three different vaccines appeared unremarkable (Fig 7). Animals immunized with individual AuNP-OpcP-LPS or AuNP-OpcP1-LPS had a significant increase in survival following a 5 LD_{50} challenge of *Bpm* K96243, with 90% and 80% protection at day 35 post-infection (Fig. 8A). Further, animals that received a combination formulation with equivalent amounts of AuNP-OpcP-LPS and AuNP-OpcP1-LPS showed complete protection against lethality, with 100% of animals surviving to day 35 post-infection (Fig. 8A). Although related in molecular weight, we found that OpcP and OpcP1 only share a 39% identity and 54% similarity. We collected

the lungs, livers, and spleens or surviving animals to assess bacterial infection and histopathology from surviving animals. Mice immunized with individual AuNP-OpcP-LPS or AuNP-OpcP1-LPS showed some bacterial colonization, with the highest numbers being $1x10^3$ CFU/g of tissue in the lungs (Fig. 8B). However, most animals, except for one in each group, did not have any colonization of the liver (Fig. 8B), and only one mouse from the AuNP-OpcP-LPS immunization group showed spleen colonization (Fig. 8C). Animals immunized with the AuNP-Combo2-LPS formulation showed lower lung and liver bacterial counts and only a single mouse displayed some colonization in the spleen (Fig. 8C-D).

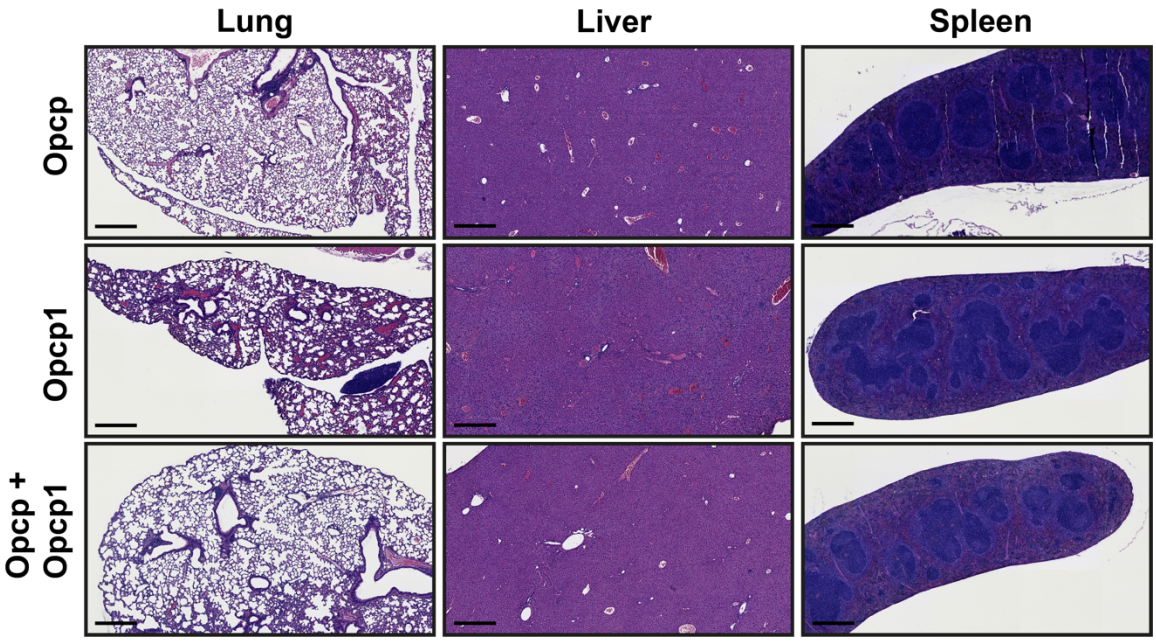

Figure 7. Histopathology analysis from vaccinated-only mice.
Histopathological analysis from lungs, livers, and spleens of a representative mouse animals immunized intranasally with AuNP-OpcP-LPS (top panels), AuNP-OpcP1-LPS (middle panels), or AuNP-Combo-LPS (lower panels). Two-weeks after the last immunization, organs from three representative animals were harvested and fixed in 10% formalin. The tissues were fixed, sectioned, and stained with H&E. All animal tissue sections showed similar findings as reported in the post-challenge groups but to a lesser degree. Images are representative of three mice. Scale bar 500 μm.

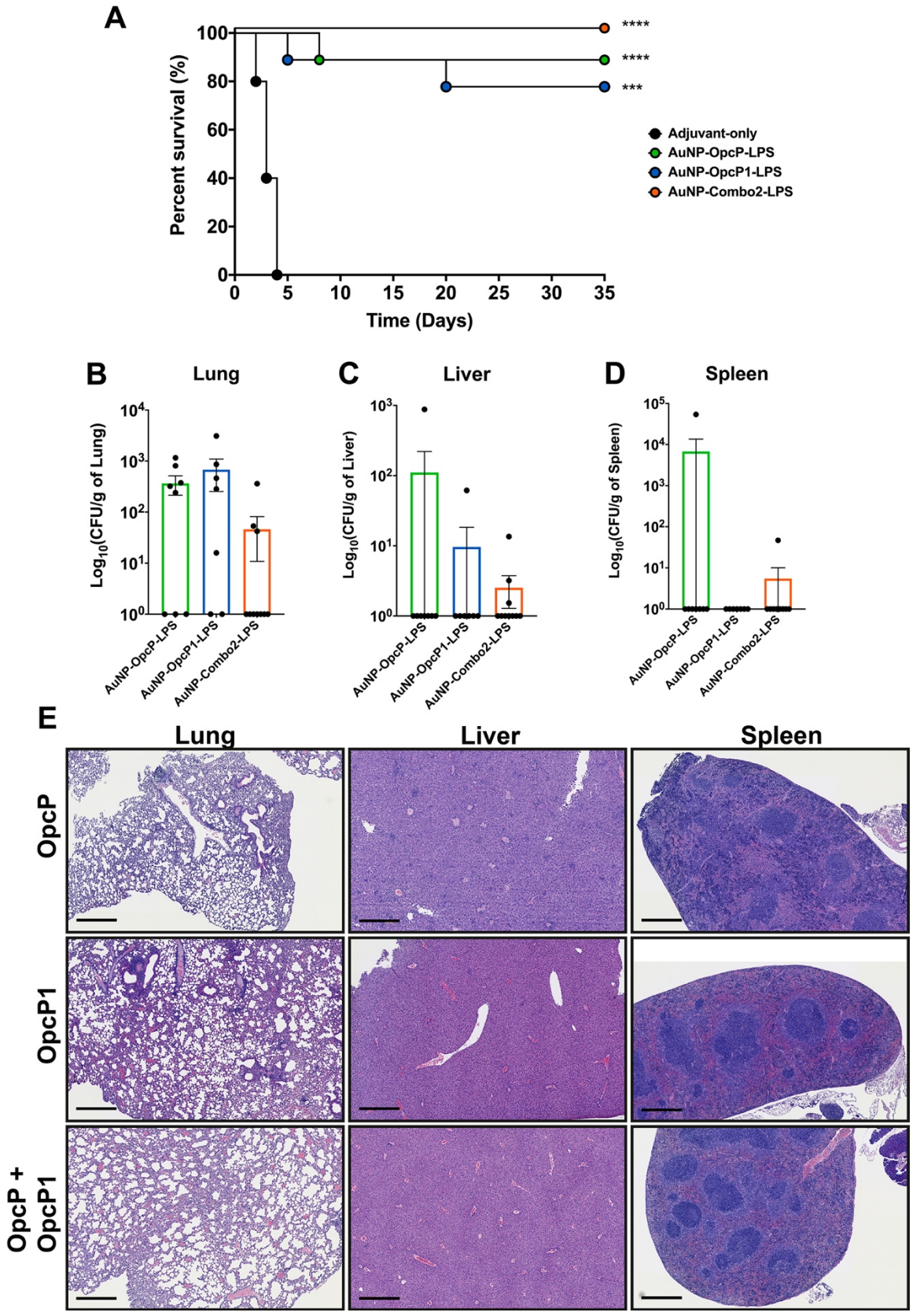
A
Percent survival (%)
Time (Days)
****
****
***
Adjuvant-only
AuNP-OpcP-LPS
AuNP-OpcP1-LPS
AuNP-Combo2-LPS
B
Lung
Log10(CFU/g of Lung)
C
Liver
Log10(CFU/g of Liver)
D
Spleen
Log10(CFU/g of Spleen)
AuNP-OpcP-LPS
AuNP-OpcP1-LPS
AuNP-Combo2-LPS
E
Lung
Liver
Spleen
OpcP
OpcP1
OpcP + OpcP1

Figure 8. Intranasal immunization with optimized formulation (AuNP-Combo2-LPS) provides enhanced protection against inhalational melioidosis.
C57BL/6 mice (n = 10) were immunized as described in figure 1. The AuNP-Combo2-LPS vaccinated group contained equivalent amounts of protein (OpcP and Opcp1) from each candidate for a total of 10 μg of protein. (A) After intranasal challenge with 5 LD_{50} (7.5 × 104 CFU per mouse) of *Bpm* K96243, (B) lungs, (C) livers, and (D) spleens of surviving animals were collected at 35 days post-infection, and bacterial enumeration performed. Bacterial load was determined per gram of tissue, and representative panels for colonization are shown on a log scale. (E) Histopathological analysis from lungs, livers, and spleens of a representative mouse from each surviving group. Lung sections from the AuNP-OpcP-LPS vaccination group showed increased pathological findings, compared to the AuNP-OpcP1-LPS and AuNP-Combo2-LPS groups. The liver sections from the AuNP-OpcP-LPS immunization group showed the most inflammation and evidence of liver injury, compared with the other groups. Spleen sections from surviving animals all showed similar histopathological findings, with the most pronounced in the AuNP-OpcP-LPS vaccine group. At the endpoint of the experiment, tissues were harvested from three mice of the 10 survivors. The tissues were fixed, sectioned, and stained with H&E. Images are representative of three mice. Scale bar 500 μm. All colonization data are shown as means ± standard errors of the means (SEM) of results determined per group. Statistical analyses were determined using the Kaplan-Meier method, followed by log-rank test. Levels of significance compared to the adjuvant-only group: ***$p < 0.0005$, ****$p < 0.0001$.

Histopathology analysis of the lung sections from the AuNP-OpcP-LPS vaccination group showed increased interstitial pneumonia and lung consolidation when compared to the OpcP1 and combo groups (Fig. 8E, left panels). In addition, AuNP-OpcP-LPS immunized mice had more parabronchial and perivascular lymphoid aggregates when compared to the other groups, post challenge (Fig. 8E, left panels). The liver sections from the AuNP-OpcP-LPS immunization group showed the most inflammation and evidence of liver injury (Fig. 8E, center panels). There was mixed portal and lobular inflammation that consisted of both lymphocytes and neutrophils (Fig. 8E, center panels). Two of three mice showed extramedullary hematopoiesis, which is evidence of liver injury. Livers from these animals also had granulomatous inflammation that was composed of activated histiocytes (Fig. 8E, center panels). These features were minimal to absent in the OpcP1 and combo groups, post challenge. The sections of spleen from the different immunization groups all

showed similar histopathologic changes, although AuNP-OpcP-LPS immunized mice had increased expansion of the marginal zone and atrophy of the germinal centers when compared to the other groups (Fig. 8E, right panels). Similar histologic findings were observed in all the groups; however, these were at varying degrees and most pronounced in the AuNP-OpcP-LPS group (Fig. 8E, right panels). Together, these results demonstrate that the AuNP-Combo2-LPS vaccine provides complete protection against lethality, with bacterial infection contained in the lung of infected mice.

Individual AuNP-protein-LPS formulations elicit robust protein- and LPS-specific humoral responses but lower OpcP and OpcP1 antibody titers from the AuNP-Combo1-LPS formulation.

The protection differences between individual and combination vaccines warranted the analysis of the antigen-specific immune responses occurring between the different formulations. We first analyzed antigen-specific total IgG responses from individual and AuNP-Combo1-LPS formulations against each antigen. Immunization with individual AuNP-protein-LPS candidates showed significantly higher total antigen-specific IgG titers against their corresponding protein or LPS from the AuNP-OpcP-LPS and AuNP-Opcp1-LPS groups (Fig. 9A, B). In addition, the AuNP-Combo1-LPS was also able to produce elevated LPS-specific total IgG titers (Fig. 9B). To evaluate differences between the individual vaccine formulations and the AuNP-Combo1-LPS group, we measured IgG titers against each protein. Animals immunized with the AuNP-Combo1-LPS formulation showed similar IgG titers against Hcp1 (Fig. 9C), OmpW (Fig. 9D), FlgL (Fig. 9G), and HA (Fig. 9H). However, total IgG titers from the AuNP-Combo1-LPS vaccine showed lower OpcP- and OpcP1-specific titers (Fig. 9 E-F). Together these results confirm that AuNP-protein-LPS vaccination induce robust antigen-specific humoral responses and may explain the reduce protective capacity of the AuNP-Combo1-LPS formulation.

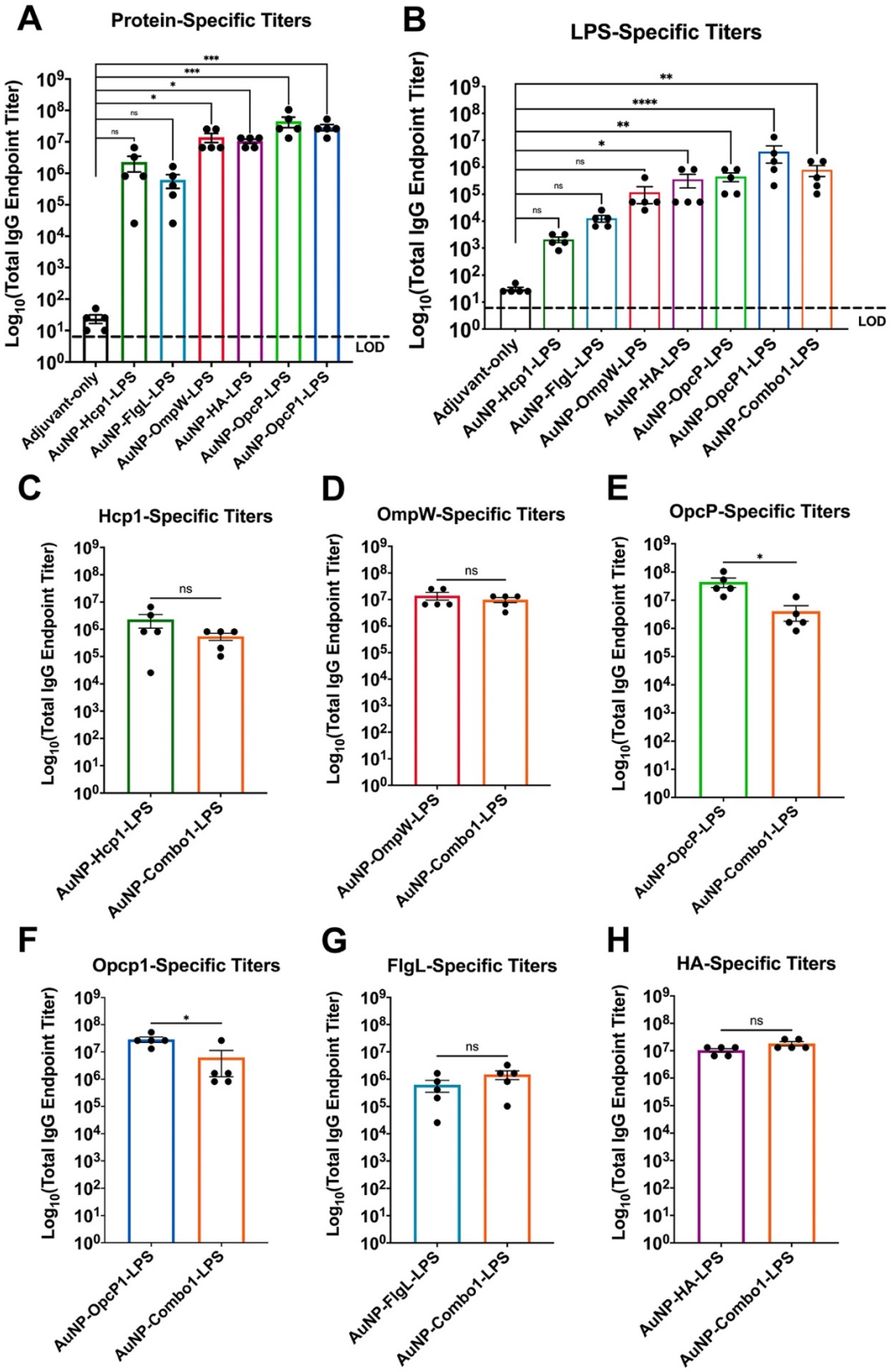
A
Protein-Specific Titers
Log10(Total IgG Endpoint Titer)
LOD
Adjuvant-only
AuNP-Hcp1-LPS
AuNP-FlgL-LPS
AuNP-OmpW-LPS
AuNP-HA-LPS
AuNP-OpcP-LPS
AuNP-OpcP1-LPS
B
LPS-Specific Titers
AuNP-Combo1-LPS
C
Hcp1-Specific Titers
D
OmpW-Specific Titers
E
OpcP-Specific Titers
F
Opcp1-Specific Titers
G
FlgL-Specific Titers
H
HA-Specific Titers
ns

Figure 9. Immunization with individual AuNP-protein-LPS candidates results in robust systemic antigen-specific specific humoral responses but reduced OpcP- and OpcP1-specific antibody response from AuNP-Combo1-LPS vaccination. Total-protein and LPS-specific IgG antibody responses. **(A)** Protein- and **(B)** LPS-specific total IgG titers were assessed by ELISA, with endpoint titers defined as twice the standard deviation (SD) of the levels measured for naive sera. **(C-H)** Sera samples taken from the mice immunized with the AuNP-Combo1-LPS formulation were used to assay protein-specific total IgG antibody titers. All antibody data are expressed as mean ± SEM of results from at least 5 mice per group and analyzed in triplicate. Significant differences between total IgG protein- or LPS-specific titers were determined using a one-way ANOVA followed by Tukey's pos hoc test. Significant differences between individual and combo1 total IgG titers were determined via Student's *t*-test. Non-significant (ns). $*p < 0.05$, $**p < 0.01$, $***p < 0.001$.

AuNP-Combo2-LPS formulation induces robust antigen-specific serum antibody response and promotes opsonophagocytosis by primary macrophages.

Given the protection differences afforded by the two different vaccine combinations, we analyzed the antigen-specific total and isotypic antibody differences. We measured total IgG antibody responses elicited by the individual vaccine formulations, as well as from the AuNP-Combo2-LPS. Animals immunized with the different formulations showed robust total protein-specific IgG responses with antibody titers of $10^7 – 10^8$ (Fig. 10 A, B). Also, LPS-specific serum IgG titers showed a robust response in mice immunized with individual formulation with titers of 10^6 (Fig. 10C). Importantly, we showed that the protein- and LPS-specific humoral response was maintained in animals immunized with the AuNP-Combo2-LPS vaccine (Fig. 10 A-C). Furthermore, protein-specific isotype titers showed higher IgG_{2c} levels than IgG_1 in animals immunized with either individual formulations or the AuNP-Combo2-LPS (Fig. 10 D, E). However, no significant differences in LPS-specific isotype titers were observed from the different immunization groups (Fig. 11). To test the functionality of this serum antibodies, we analyzed whether the antibodies promote antibody-mediated bacterial opsonophagocytosis. Primary murine macrophages were infected with *Bpm* that was previously incubated with immune serum from the vaccination groups.

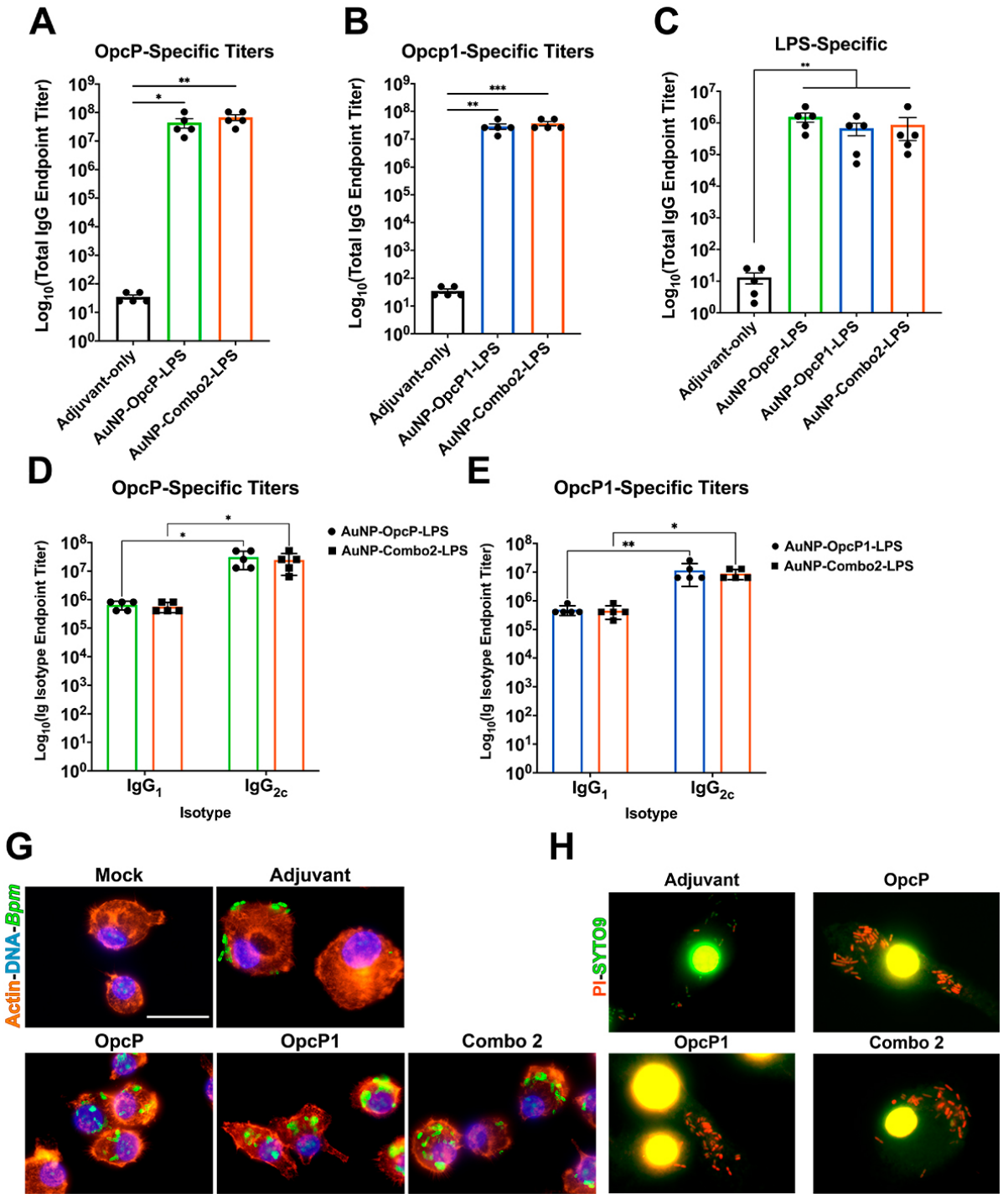
A
OpcP-Specific Titers
Log10(Total IgG Endpoint Titer)
Adjuvant-only
AuNP-OpcP-LPS
AuNP-Combo2-LPS
B
Opcp1-Specific Titers
Log10(Total IgG Endpoint Titer)
Adjuvant-only
AuNP-OpcP1-LPS
AuNP-Combo2-LPS
C
LPS-Specific
Log10(Total IgG Endpoint Titer)
Adjuvant-only
AuNP-OpcP-LPS
AuNP-OpcP1-LPS
AuNP-Combo2-LPS
D
OpcP-Specific Titers
AuNP-OpcP-LPS
AuNP-Combo2-LPS
Log10(Ig Isotype Endpoint Titer)
IgG1
IgG2c
Isotype
E
OpcP1-Specific Titers
AuNP-OpcP1-LPS
AuNP-Combo2-LPS
Log10(Ig Isotype Endpoint Titer)
IgG1
IgG2c
Isotype
G
Mock
Adjuvant
Actin-DNA-Bpm
OpcP
OpcP1
Combo 2
H
Adjuvant
OpcP
PI-SYTO9
OpcP1
Combo 2

Figure 10. Immunization with optimized AuNP-Combo2-LPS formulation elicits sustained antigen-specific humoral responses associated with increased opsonophagocytosis by macrophages.
Protein- and LPS-specific IgG and isotype antibody responses. (A) OpcP- (B) OpcP1- and (C) LPS-specific total IgG titers were assessed by ELISA, with endpoint titers defined as twice the standard deviation (SD) of the levels measured for naive sera. (D) OpcP and (E) OpcP-specific IgG1 and IgG2c isotype antibody titers. Sera samples taken from the mice immunized with the AuNP-Combo2-LPS formulation were used to assay protein- and LPS-specific total IgG as well as isotype antibody titers. (F) Fluorescence microscopy analysis of primary murine macrophages 2 h after Bpm K96243 infection in the presence of immune serum (from OpcP, OpcP1, and Combo2 vaccinated groups). After infection, cells were fixed, permeabilized, and stained with phalloidin-rhodamine (actin), DAPI (bacteria and cell nuclei), and examined by immunofluorescence (sera anti-LPS followed by a rabbit anti-mouse Alexa Fluor-488). (G) LIVE/DEADTM BacLight^{TM}-stained primary murine macrophages infected with Bpm K96243 for 2 h in the presence of sera from each immunization group. Panels below each group represent magnifications (10×) of the images on top. Images were taken using an Olympus BX51 upright fluorescence microscope (60×) and processed using Image J software. Scale bars 25 μm. All antibody data are expressed as mean ± SEM of results from at least 5 mice per group and analyzed in triplicate. Significant differences between total IgG protein- or LPS-specific titers were determined using a one-way ANOVA followed by Tukey's pos hoc test. *$p < 0.05$, **$p < 0.01$, ***$p < 0.001$.

After infection, macrophages were fixed, permeabilized, and analyzed using immunofluorescence microscopy. A higher number of bacteria were internalized by macrophages in the presence of serum from animals immunized with AuNP-OpcP-LPS, AuNP-OpcP1-LPS, or AuNP-Combo2-LPS, compared to bacteria incubated with naïve serum (Fig. 10G). Using bacterial live/dead staining, we evaluated internalization of the bacteria by macrophages. After 2 h of infection, most of the internalized bacteria by macrophages in the presence of immune sera were non-viable, compared to naïve sera, as visualized by the incorporation of propidium iodide (Fig. 10H). These data demonstrate that the AuNP-Combo2-LPS formulation induce a strong antigen-specific antibody response, promoting opsonophagocytic activity and inducing higher IgG_{2c} titers.

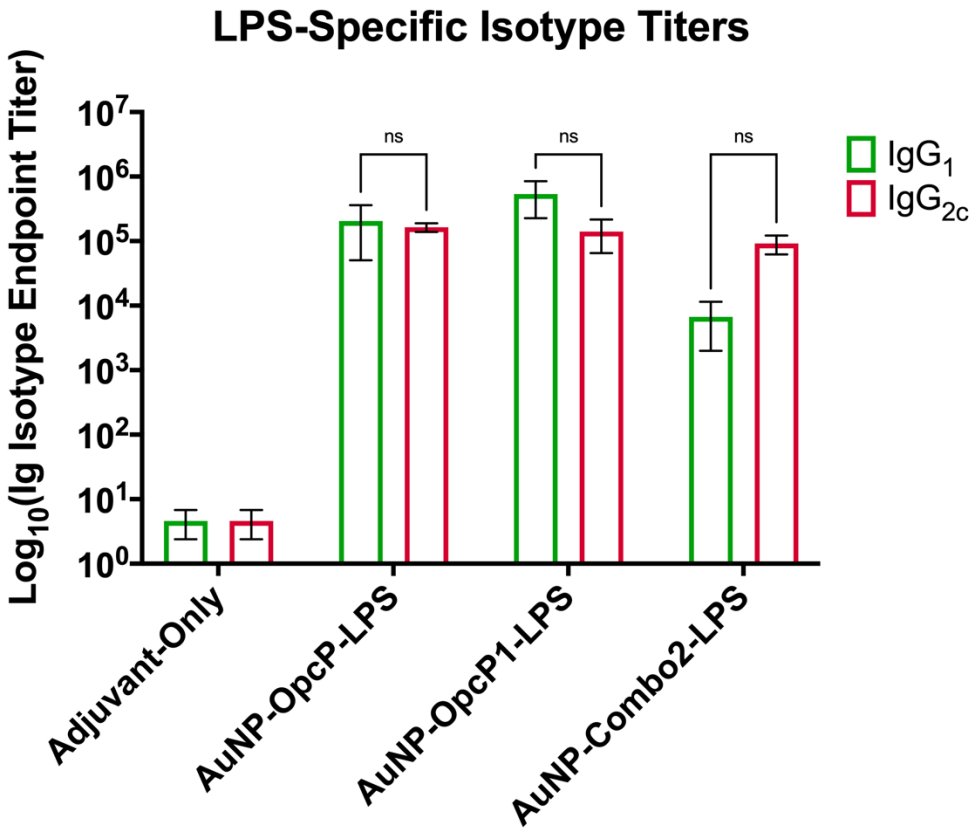

Figure 11. LPS-specific isotype titers in serum of AuNP-linked glycoconjugate immunized mice.
Sera from immunized animals was collected two-weeks after the last immunization. LPS-specific IgG_1 and IgG_{2c} antibody isotype titers were assessed by ELISA, with endpoint titers defined as twice the standard deviation (SD) of the levels measured for naive sera (adjuvant-only). All antibody data are expressed as mean ± SEM of results from at least 5 mice per group and analyzed in triplicate. Significant differences between LPS-specific isotype titers were determined using a two-way ANOVA followed by Tukey's pos hoc test. Not-significant (ns).

Intranasal immunization with AuNP-Combo2-LPS induces robust antigen-specific lung IgG and IgA responses.

We measured IgG and IgA antibody responses in the bronchioalveolar lavage fluid (BALF) of immunized mice to understand tissue-specific protective responses. Antigen-specific lung total IgG (Fig. 12A-C) and IgA titers (Fig. 12 D-F) were evaluated three-weeks after the final intranasal immunization. Animals receiving individual formulations (AuNP-OpcP-LPS or AuNP-OpcP1-LPS) showed strong antigen-specific total IgG responses in

the lung (Fig. 12 A-C) with levels around 10^6 for protein-specific and 10^3 for LPS-specific responses (Fig. 12 A-C). Similarly, animals immunized with single formulations showed robust antigen-specific lung IgA responses with titers of 10^5 and 10^4 against protein or LPS, respectively, as compared to control mice (Fig. 12 D-F). These antigen-specific IgG and IgA responses were equivalent to those seen in animals immunized with the AuNP-Combo2-LPS (Fig 12 A-F). These results validate that the gold nanovaccine induces strong humoral responses in the lung after intranasal immunization.

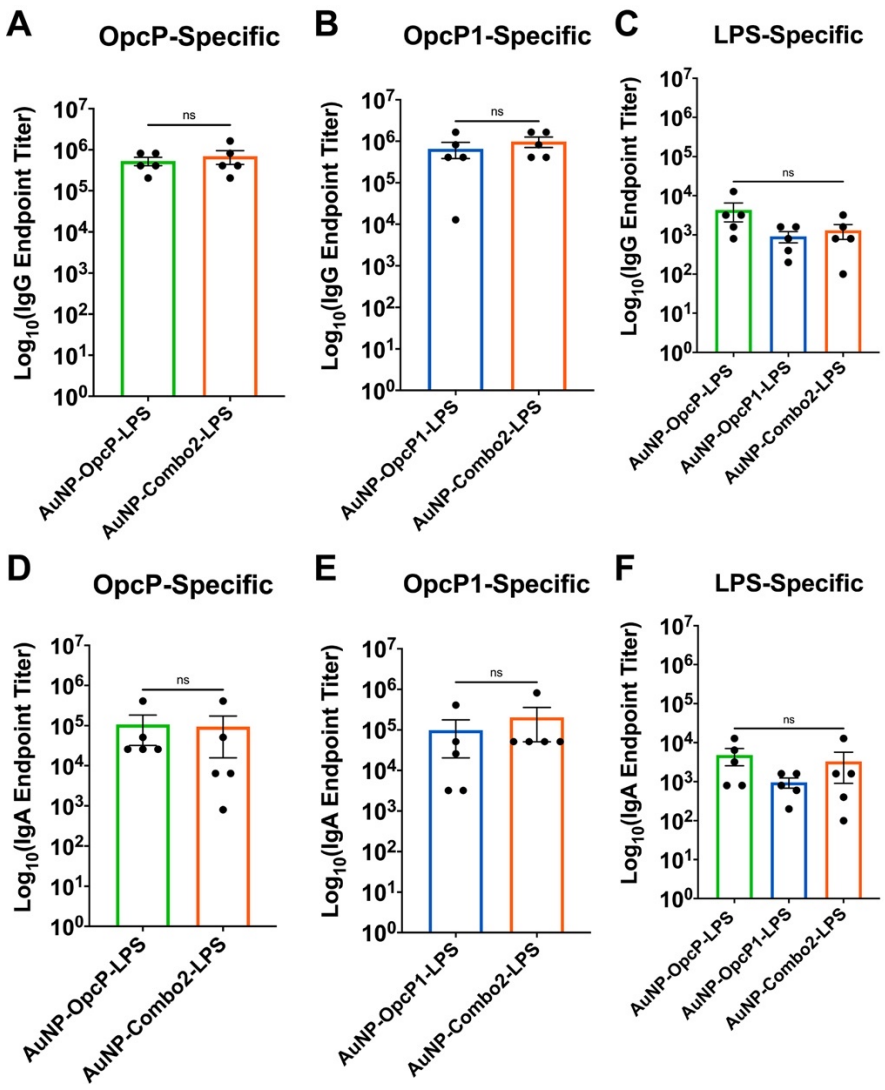

Figure 12. Immunization with optimized AuNP-Combo2-LPS formulation elicits robust lung total IgG and IgA responses.
Total IgG and IgA protein-specific antibody responses was analyzed from BALF of immunized animals two-weeks after the last immunization. **(A-C)** OpcP, OpcP1, and LPS-specific total IgG titers were assessed by ELISA, with endpoint titers defined as twice the standard deviation (SD) of the levels measured from adjuvant-only immunized animals. **(D-F)** OpcP, OpcP1, and LPS-specific IgA sera responses were analyzed by ELISA. Sera samples taken from the mice immunized with the AuNP-Combo2-LPS formulation were used to assay protein-specific total IgG and IgA antibody titers. All antibody data are expressed as mean ± SEM of results from at least 5 mice per group and analyzed in triplicate. Significant differences between total IgG and IgA protein for protein-specific titers were determined by a Student's *t*-test and LPS-specific titers were determined using a one-way ANOVA followed by Tukey's pos hoc test. Not-significant (ns).

Gold-linked glycoconjugate (AuNP-Combo2-LPS) vaccine induces an antigen-specific mixed T_H1-T_H17-biased cytokine response to protein restimulation.

Given our previous observations showing induction of a T_H1-biased response with antibody IgG_{2c} subtype after AuNP-Combo2-LPS immunization, we determined if gold-linked glycoconjugate vaccine activate antigen-specific T cell responses. Spleens from AuNP-Combo2-LPS or adjuvant-only immunized mice (n=5) were collected on day 21 post immunization and single cell suspensions were cultured in the presence of different antigens. Splenocytes from AuNP-Combo2-LPS or adjuvant-only immunized animals were stimulated with OpcP, OpcP1, *Bth* LPS, a combination of OpcP+LPS or OpcP1+LPS, αCD3/αCD28 antibody-conjugated beads, or mock (media control). Five days after restimulation, cell supernatants were collected and used to measure the production of cytokines. Our results show a significant increase in IL-2, IFNγ, TNFα, IL-17A, and IL-10 cytokine production in response to OpcP or OpcP1 restimulation (Fig. 13 A-E). In contrast, no significant higher differences were seen after the addition of LPS to either OpcP or OpcP1 (Fig. 13 A-E). Furthermore, no protein- or LPS-specific significant differences in IL-4 production from splenocytes upon restimulation were measured (Fig.13 F). These data further demonstrate induction of a mixed protein-specific T_H1-T_H17-biased response after intranasal vaccination with AuNP-Combo2-LPS.

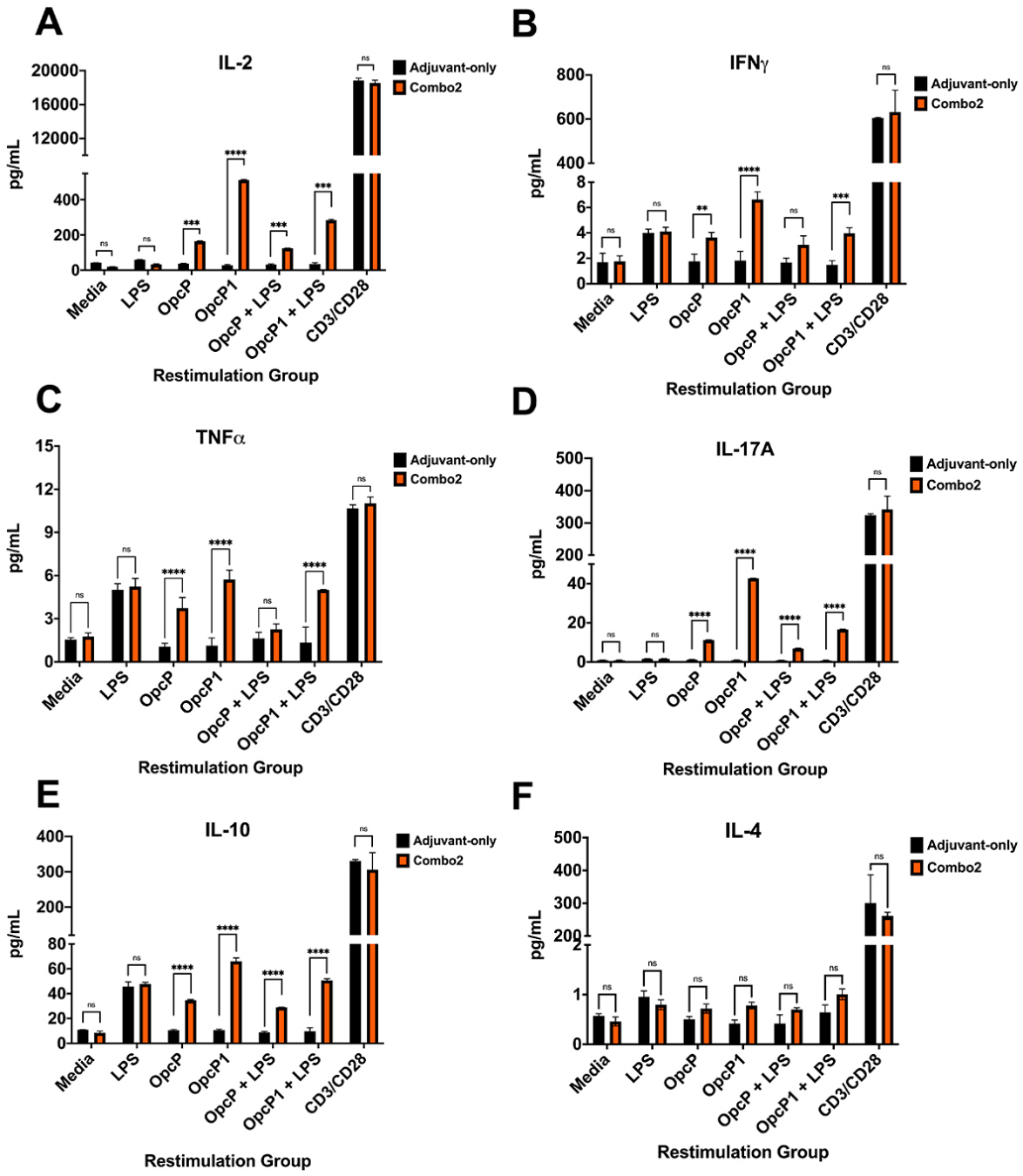
A
IL-2
pg/mL
Adjuvant-only
Combo2
Media
LPS
OpcP
OpcP1
OpcP + LPS
OpcP1 + LPS
CD3/CD28
Restimulation Group
B
IFNγ
C
TNFα
D
IL-17A
E
IL-10
F
IL-4

Figure 13. Mice immunized with AuNP-Combo2-LPS produce a robust antigen-specific T_H1-T_H17 cytokine profile correlated with antigen-specific responses. Antigen-specific cytokine profile production from AuNP-Combo2-LPS splenocyte upon stimulation threw-weeks post immunization. Supernatants were analyzed for production of (A) IL-2, (B) IFNγ, (C) TNFα, (D) IL-17A, (E) IL-10, and (F) IL-4. Mice (five per group) were immunized with 10 μg of protein and 10 μg LPS adjuvanted with 20 μg of CpG. Two boosts were given on days 28, and 49 and spleens were harvested three weeks after the final boost. Spleen cells from AuNP-Combo2-LPS immunized mice were stimulated for 5 days with protein, LPS, or both. Splenocytes stimulated media, or anti-CD3/CD28 antibodies served as controls. Supernatants were assayed for cytokine expression using a murine BioPlex ELISA kit. All cytokine data are expressed as mean ± SEM of results from at least 5 mice per group and analyzed in triplicate. Significant differences were determined using a two-way ANOVA followed by Tukey's pos hoc test. *$p < 0.05$, **$p < 0.01$, ***$p < 0.001$, ****$p < 0.0001$.

DISCUSSION

Current evidence indicates that protection against melioidosis, both in humans and animal models, requires robust humoral and cellular adaptive immunity (72, 181, 201–204, 186–188, 190, 193–195, 200). However, efficient vaccine delivery platforms capable of eliciting robust, long-lasting, and specific immune responses while maintaining a safe profile are limited (11, 12, 14, 199). The development of potent and safe vaccine platforms that help promote cellular immunity against intracellular bacterial remains a challenge and warrants further investigation. Nanoparticle-based vaccines, mainly those utilizing gold nanoparticles, offer a means of delivering multiple antigens on the same surface with greater efficacy to lymphoid organs in comparison to soluble antigens (11, 12, 50, 51, 181, 199). Although the mechanisms promoting increased immune responses are not fully understood, they involve enhancing antigen stability to cross mucosal barriers and increase antigen processing and presentation upon antigen-presenting cell (APC) internalization (11, 12, 50, 51, 181, 199). The stable conjugation of a protein-LPS moiety onto the surface of AuNPs seeks to preserve important antigenic molecular structures critical for eliciting robust humoral and cell-mediated immunity in a multivalent display of antigens in a rigid surface. The design of an AuNP-delivered glycoconjugate vaccine seeks to elicit robust

immune responses against multiple antigens to increase the protective efficacy and security of this vaccine platform (51, 56, 181). To exploit this idea, we covalently conjugated a protein-LPS glycoconjugate motif on the surface of 15 nm AuNPs via a small hydrophobic linker (16-MHDA). The lipopolysaccharide (LPS) of *Bth*, composed of the O-antigen molecule (OAg) and the lipid A moiety, were coupled to AuNP-protein conjugates to broaden the protective response (203–205). The LPS of *Bth,* a T-cell independent antigen is expected to engage T cell help allowing for B cell memory development and the production of antibody responses (177). The lipid A region of the *Bth* LPS structure could act as an adjuvant by stimulating the production of inflammatory cytokines (Fig. 13) (176, 204, 205). Furthermore, the final vaccine formulation contained the toll-like receptor 9 (TLR9) agonist, CpG ODN 2395, to augment and divert the immunogenicity of the protein or LPS antigens to a T_H1-biased response (12).

Given that inhalational exposure with *Bpm* presents the most lethal route of infection, a vaccine that elicits robust mucosal responses is needed to fully protect against inhalational challenge and represent the most appealing strategy for inducing specific immune responses in mucosal tissues (72). However, vaccines that can be delivered mucosally presented challenges of antigen uptake, rapid clearance, size restriction for amenability to cross the epithelium, few mucosal adjuvants available, etc. (59). Therefore, AuNPs ameliorate some of the mucosal subunit vaccines' challenges by affording a safe platform for antigen stability, uptake, and delivery. Therefore, we synthesized individual gold-linked glycoconjugates using six *Burkholderia*-specific protein antigens that were derived from our previous predictions using bio- and immuno-informatic reverse vaccinology analysis (165). We found that several of these candidates provided increased protection in a murine model of glanders (*B. mallei* infection) and promoted different protection levels when delivered using a similar immunization route (165, 206). However, we wanted to evaluate their protective efficacy against *Bpm*, develop a refined formulation, and analyze which humoral and cellular immune response are elicited. We found that two

of these antigens, namely OpcP or OpcP1, provided a significant increase in protection against *Bpm*, but a combination of these in equal ratios (AuNP-Combo2-LPS) afforded 100% mice survival against inhalational melioidosis. Most of the surviving animals had bacterial infection contained in the lung, and few pathological lesions to mention as compared to the individual AuNP-protein-LPS formulations. The absence of sterilizing immunity could be due to the complex lifestyle of *Bpm,* which requires numerous and redundant virulence mechanisms, or the need to broaden the protective response using other conserved and immunogenic antigens. While OpcP (BPSS0879) and OpcP1 (BPSS0708) only share 39% in amino acid sequence identity, both proteins are predicted to form porins in the bacterial outer membrane (OM). Interestingly, OpcP is an abundant porin in the OM of *Bpm*, comprising up to 11% of its total OM proteins (180). Future studies should aim at defining the function of this protein and the implications in antigen processing. Nonetheless, our data provided the rationale for analyzing the antigen-specific protective marker differences between OpcP and OpcP1.

One of the main objectives in this chapter was to demonstrate that gold-coupled glycoconjugate vaccines induce robust antigen-specific humoral responses after intranasal delivery. Our results showed that AuNP-OpcP-LPS and AuNP-OpcP1-LPS were associated with the highest percent survival and maintained strong total IgG responses against protein and LPS antigen alone. However, we observed reduced antigen-specific IgG titers when given in a formulation containing six antigens (AuNP-Combo1-LPS). A reduced immune response against our leading candidates could provide a plausible explanation for the inability of the AuNP-Combo1-LPS formulation to provide full protection against a *Bpm* challenge. Our refined vaccine formulation AuNP-Combo2-LPS showed that antigen-specific serum IgG titers were equivalent against both protein and LPS compared to the individual vaccines. Our data demonstrate the ability of glycoconjugate-coupled AuNPs to elicit strong humoral responses against three distinct antigens. This observation is important, as melioidosis convalescent patients have higher OAg-specific

antibody titers correlated with a higher degree of survival (181, 189, 202). Our data also demonstrates the ability of AuNP-Combo2-LPS intranasal vaccination to elicit systemic IgG and lung IgA responses, correlating with protection. This is critical as melioidosis survivors have higher LPS-specific IgA titers compared to non-survivors (181). These results further highlight that gold-linked glycoconjugate intranasal vaccine immunization induce strong systemic and mucosal humoral responses. This also suggests that humoral protective immunity could protect against bacteria at different stages of infection, including inhibition of bacterial adherence onto the mucosal epithelium, preventing subsequent dissemination. Bacterial opsonophagocytosis in the presence of absence of immune sera showed an increased in bacterial uptake when sera from AuNP-OpcP-LPS or AuNP-OpcP1-LPS was added, a function that was also observed with the AuNP-Combo2-LPS formulation. The sera effect was confirmed by the reduced bacterial viability within macrophages. It has been previously shown that sera from convalescent melioidosis patients promotes antibody-dependent bacterial uptake and bacterial clearance (202). Our observations strengthen the hypothesis that humoral responses are an essential correlate of protection in melioidosis patients.

To analyze isotypic antibody differences as measure of immune biased responses, we measured IgG_{2c} and IgG_1 isotype titers from individual and AuNP-Combo2-LPS formulations. Higher IgG_{2c} antibody titers in C57BL6 mice are associated with the induction of a T_H1-biased response, given that this mouse genetic background does not express the IgG_{2a} isoform (183, 184). Our isotype differences, with higher protein-specific IgG_{2c} titers, suggest a T_H1-biased immune response, as has been reported previously (184). It has been shown that cell-mediated immunity is important for protecting many intracellular pathogens, including *Bpm* (66). The correlation of cell-mediated immunity, especially the production of IFNγ, with human melioidosis survival prompted the analysis of its induction by our gold-linked glycoconjugate vaccines. Our results from splenocytes of immunized animals exogenously re-stimulated with antigen demonstrate that protein-

specific T-cell responses may contribute to the protection afforded by these vaccines. In response to protein restimulation, splenocytes from AuNP-Combo2-LPS produce higher levels of IFNγ, IL-2, TNFα, IL-17A, and IL-10. Interestingly, human peripheral blood mononuclear cells (PBMCs) from diabetic melioidosis patients showed reduced IL-17 production upon restimulation, suggesting that IL-17 might be playing a significant role in response to *Bpm* infection (193). Furthermore, the induction of a mixed T_H1-T_H17 response has previously been observed in other *Burkholderia* vaccines, including a live-attenuated *B. mallei* vaccine (CLH001: Δ*tonB*/Δ*hcp1*) generated by our own group (98, 170). The importance of IFNγ as well as IL-17 has broad implications in vaccine design, as both are important in promoting optimal macrophage activation for intracellular pathogen killing and antibody production, respectively (207–209).

Future studies should focus on determining the role of effector T_H17 cells in protection against *Bpm* infection. This response could provide an important correlation between gold-linked glycoconjugate vaccines and the ability to elicit robust humoral and cell-mediated immunity (39). Future studies should determine the tissue-specific T-cell-mediated responses and epitope mapping of both OpcP/OpcP1 antigens. In summary, we generated an optimized vaccine strategy against inhalational melioidosis. The resulting optimized combination vaccine (AuNP-Combo2-LPS) displayed full protection against a lethal *Bpm* K96243 challenge with unremarkable tissue pathology. We showed that delivery of individual or a combination of gold-coupled glycoconjugates induced robust antigen-specific humoral responses both systemically and at mucosal sites. Finally, we showed that splenocytes from immunized mice produced a protein-specific mixed T_H1-T_H17 upon antigen re-stimulation. Our study provides a vaccine strategy against *Bpm* and an immune stimulatory platform to induce strong humoral and T cell-mediated immunity.

Chapter 9: A Nanovaccine Against Enterohemorrhagic *Escherichia coli* O157:H7

INTRODUCTION

Diarrheal diseases are one of the leading causes of morbidity and mortality, especially among children under the age of five. A significant proportion of diarrheal disease is caused by pathogenic *E. coli* (210). Due in part to their pathogenic mechanisms, clinical symptomology, and virulence factors, diarrheagenic *E. coli* are classified into different pathotypes (136, 137). Enterohemorrhagic *E. coli* (EHEC), particularly serotype O157:H7, is a unique human pathogen which is associated with severe complications and high mortality as compared to other pathotypes. In addition, the primary reservoir for EHEC includes ruminants and the main route of infection involves ingestion of contaminated food products which often result in outbreaks. Infections caused by EHEC can range from acute self-resolving diarrheal episodes to hemorrhagic colitis that can progress to the hemolytic-uremic syndrome (HUS) (136, 137). The production of Shiga toxins (Stx) is one of the defining characteristics of EHEC O157:H7 pathogenesis and the key virulence factor associated with HUS. However, the first step in the pathogenic process of EHEC is the adherence to intestinal epithelial cells (IECs) (210, 211). To colonize the intestinal mucosa, EHEC O157:H7 is known to utilize a myriad of pili and/or fimbria to attach to IECs (211). Subsequently, EHEC binding results in an intimate attachment to the surface of IECs and injection of virulence factors using its Type 3 Secretion System (T3SS) apparatus. The translocated virulence factors are responsible for the formation of histological changes known as attaching and effacing (A/E) lesions on epithelial cells. These lesions are characterized by the disruption of the microvilli and the accumulation of actin below the site of bacterial adherence to create a "cup-like structure" (136). The genetic factors

necessary for the biogenesis of a functional T3SS, and many of its effectors are located on a pathogenicity island called the Locus of Enterocyte Effacement (LEE) (212).

Despite the pathogenic processes and the likelihood to cause severe disease and sequelae in humans, there are no specific treatment options available to combat EHEC infections. In fact, the conventional use of antibiotics only aggravates the disease because it promotes and exacerbates the expression of gene products encoding the Stx toxins (Stx1 and Stx2) which are located within a lambdoid phage. This process induces bacterial lysis, allowing for the release and dissemination of Stx into the intestine and other organs (138). Therefore, the development of new strategies to control infections caused by EHEC are necessary. A viable alternative to prevent infection is the development of vaccines; however, there are no approved human vaccines against this pathogen. The advances in vaccine development have included different platforms and approaches such as live attenuated, whole cell killed, subunit, toxoids, polysaccharide, and polysaccharide-protein conjugates (145, 213). Previous studies have focused on the development of vaccines based on proteins encoded in the LEE pathogenicity island, such as the intimin adhesin and the T3SS component EspA (214), as well as other peptides (215), different fusion constructs containing the subunit A and B of Stx1 and Stx2 (216), or avirulent bacterial ghost cells derived from EHEC O157:H7 (154). These different vaccine candidates have shown variable success in various *in vivo* murine models of infection.

Recently, gold nanoparticles (AuNPs) have received attention due to their potential use over traditional vaccine platforms (217). The location of AuNPs in lymphoid tissues and cells (175, 218), the capacity of coupling to a variety of biomolecules (21, 217, 219), their stability, and their safety (21, 217) (essential for the development and synthesis of vaccines), provides a multifaceted focus for the design of this new vaccine platform. Previously, we identified two immunogenic protein candidates specific for EHEC using a reverse vaccinology approach. These candidates were tested using a DNA vaccine vector and demonstrated variable degrees of protection (213, 220, 221). Therefore, the objective

of this study was to conjugate these two EHEC O157:H7 antigen candidates to the AuNP platform and assess whether the nanovaccines can induce protective responses *in vitro* and *in vivo*. Our work proposes to bridge the properties of subunit vaccination with those of synthetic nanomaterials to enhance immune responses to vaccines against pathogenic *E. coli*. We have developed a multidisciplinary pipeline for the identification of antigens and efficient delivery of nanovaccines that can be used against other pathogenic bacterial organisms.

RESULTS

Purification of immunogenic proteins and coupling of AuNP vaccines.

Using information from a comparative bio-immunoinformatic analysis performed in our laboratory, two O157:H7-specific candidates were selected based on their predicted immunogenicity, bacterial surface location and human MHC allele coverage, and because they were previously demonstrated to be protective when used as DNA vaccines (213, 221). To use these proteins as subunit vaccine candidates, we selected a gold nanoparticle (AuNP) platform to display the antigens and to immunize mice subcutaneously. AuNPs have gained interest as vaccine scaffolds because they have been used to incorporate, stabilize, and increase the immunogenicity of subunit vaccine candidates (175). We purified two proteins, LomW (933W phage-encoded outer membrane protein) and EscC (Type 3 secretion system structural protein) under native conditions using affinity chromatography to allow efficient conjugation onto the AuNP surface. The His-tagged proteins were visualized by Coomassie stain and western blot (Fig. 14A). To consistently synthesize spherical 15 nm AuNPs, the Turkevich method (167) was used, and the resulting particles were visualized using transmission electron microscopy (Fig. 14B). The protein candidates were immobilized on the AuNP surface by adding 16-mercaptohexaundecanoic acid (MHDA) which is a small linker with a thiol group that readily binds AuNP and

possess a carboxylic acid on the distal end used to covalently attach biomolecules (47). We confirmed the conjugation of these proteins to MHDA-coupled AuNPs by UV-Vis spectroscopy as seen by the wavelength displacement to 529 nm and 530 nm upon addition of LomW and EscC, respectively (Fig. 14C). This red shift (2 nm and 3 nm for LomW and EscC, respectively) after the addition of proteins onto the AuNPs allowed us to characterize the stable coupling of AuNP-protein platform for subsequent *in vivo* studies.

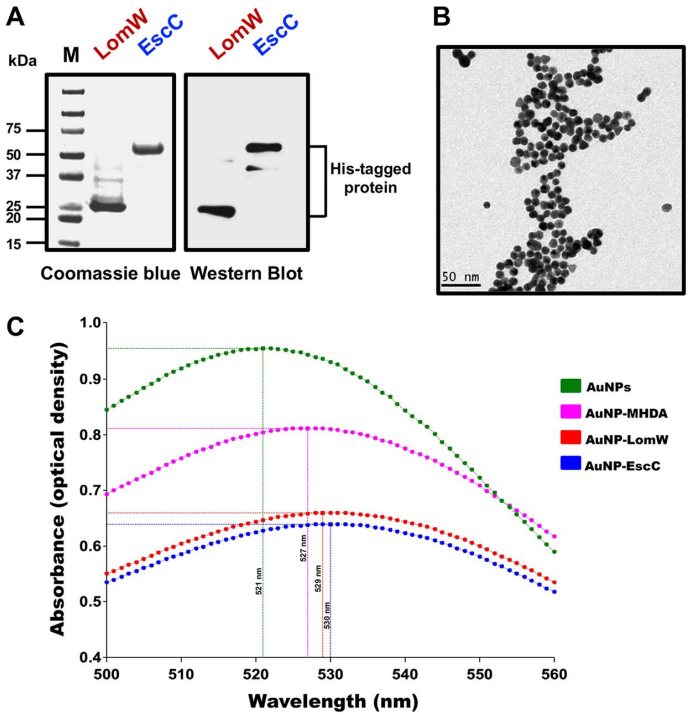

Figure 14. Purification and characterization of AuNP platform after conjugation to LomW and EscC.
(A) Coomassie stained gel and western blot with anti-His shows the purity of LomW (28 kDa) and EscC (56 kDa). Purification of His-tagged recombinant protein from *E. coli* BL21 using Co2+-affinity chromatography. (B) Transmission electron micrograph of bare AuNPs showing its consistent size and shape. Bar shows 50 nm reference scale. (C) Absorption spectrum of non-conjugated AuNPs (green), AuNPs with MHDA linker (pink), and AuNPs after covalent conjugation with LomW (red) and EscC (blue). Displacement shows a red shift after successful conjugation of protein.

Reduced gastrointestinal colonization in AuNP-EscC and AuNP-LomW immunized animals.

After confirming the proper coupling of stable AuNP-protein conjugates, we assessed the protective efficacy and multivalency of AuNPs vaccines (nanovaccines) in an *in vivo* murine model of *E. coli* infection. Mice were immunized subcutaneously (s.c.) using the scheme displayed in Fig. 15.

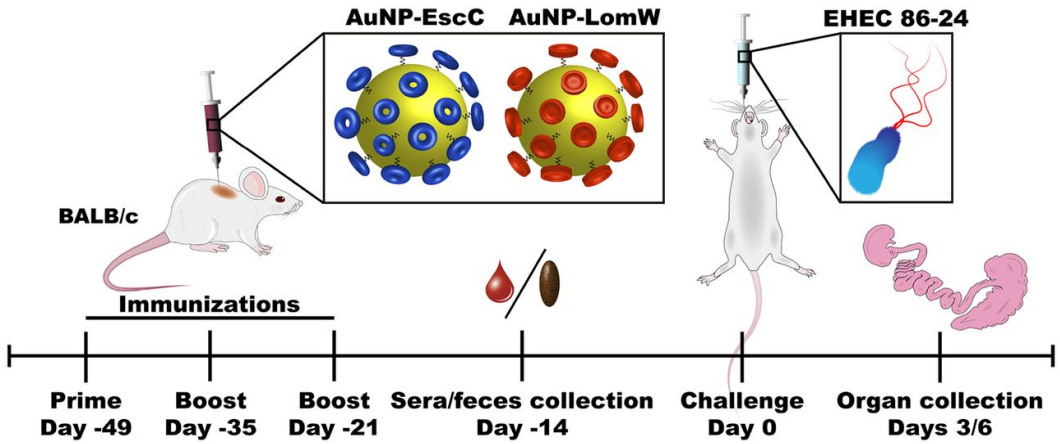

Figure 15. Timeline of vaccination schedule.
Subcutaneous vaccination schematic in BALB/c mice and gavage challenge with EHEC O157:H7 strain 86-24, followed by blood, feces, and organ collection.

BALB/c mice received three immunizations in two-week intervals containing a total of 10 µg of protein conjugated onto AuNPs and combined with adjuvants. A group of mice received a combination formulation containing approximately 5 µg of each AuNP-conjugated candidate. Serum and fecal samples were collected two weeks after the last immunization to evaluate humoral responses. Mice were then challenged via gavage three weeks after the last immunization with 3 x 10^9 CFU of EHEC O157:H7 (strain 86-24). At three- and six-days post-challenge, we collected the large intestine and cecum and evaluated bacterial colonization. Immunization with either AuNP-LomW, AuNP-EscC, or AuNP-Combination (AuNP-LomW + AuNP-EscC) resulted in a significant reduction in colonization in both the cecum and large intestine at three days post challenge (Fig. 16).

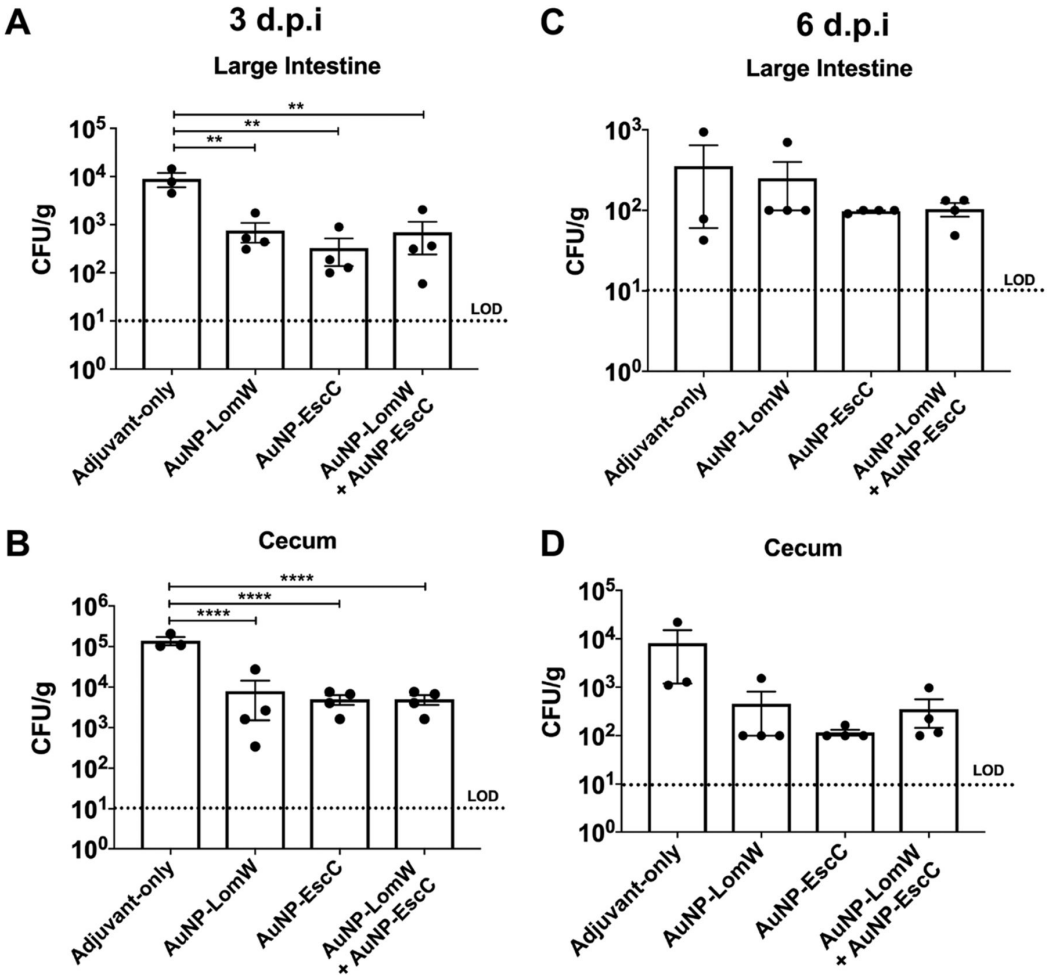

Figure 16. Reduced bacterial colonization from AuNP-protein vaccinated mice. After challenge via gavage with 3×10^9 CFU of EHEC 86-24, large intestines and ceca from BALB/c mice (n=8) were collected at **(A-B)** 3 and **(C-D)** 6 days post-infection. Organs were processed, diluted, and plated on MacConkey agar plates for bacterial enumeration. Bacterial load was determined per gram of tissue. All colonization data is shown as mean ± SEM from per group. Significant differences in organ colonization were determined via one-way ANOVA followed by Tukey's *post hoc* test: *, P<0.05, **, P<0.001; ***, P<0.0001.

In all three immunization groups, there was a significant reduction in colonization in both the large intestine (Fig. 16A) and the cecum (Fig. 16B) at 3 days post infection (d.p.i.). We saw a similar pattern of reduced colonization at 6 d.p.i. (Fig 16C and D) but differences were smaller because animals had begun to clear the wild type bacteria from the

gastrointestinal (GI) tract (Fig. 17). These results confirmed the vaccine properties of our AuNP-protein immunization in the reduction of EHEC colonization *in vivo*.

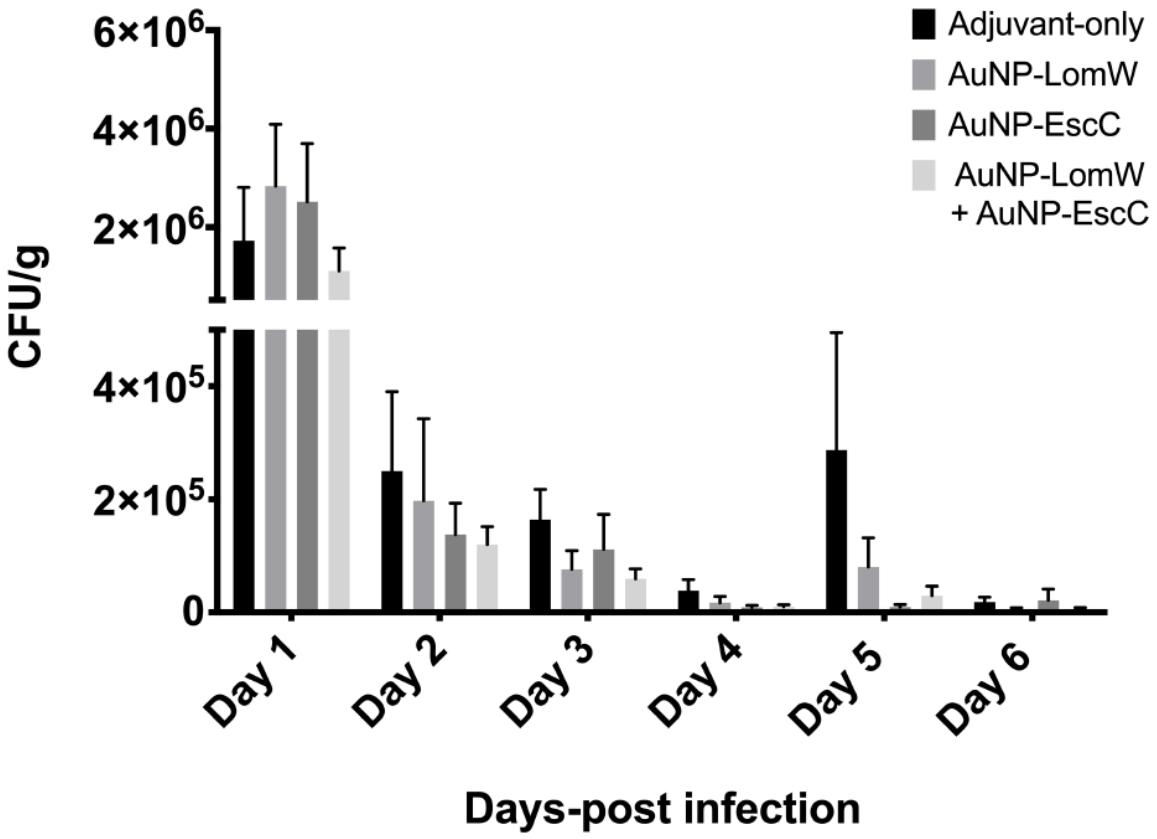

Figure 17. EHEC O157:H7 bacterial counts in feces after infection.
Excretion of EHEC O157:H7 was determined as CFU/g of feces for the first 6 days post challenge. The results are expressed as means ± the SEM from eight mice in each group. Fecal pellets were collected in pre-weighted 1 mL of PBS tubes and weighted after sample collection. After processing and diluting in PBS, fecal samples were plated on MacConkey Agar plates and incubated at 37°C prior to counting.

AuNP-protein immunization resulted in robust humoral mediated immunity.

To evaluate the immunogenicity of the AuNP-LomW and AuNP-EscC nanovaccines, we evaluated the production of protein-specific total IgG and secretory IgA (sIgA) responses in immunized mice. Using the serum and fecal samples collected after the last immunization, we compared the total IgG endpoint titers from AuNP-LomW, AuNP-EscC,

and combination formulations against each antigen. The IgG end-point titers against LomW and EscC were significantly higher for all three vaccine formulations as compared to the adjuvant-only immunized mice group (Fig. 18 A and B). The levels of serum IgG demonstrate the ability of AuNP-protein vaccination to elicit strong systemic antigen-specific IgG responses. Likewise, the total fecal sIgA endpoint titers were significantly higher for LomW and EscC in both vaccine groups (Fig. 18 C and D).

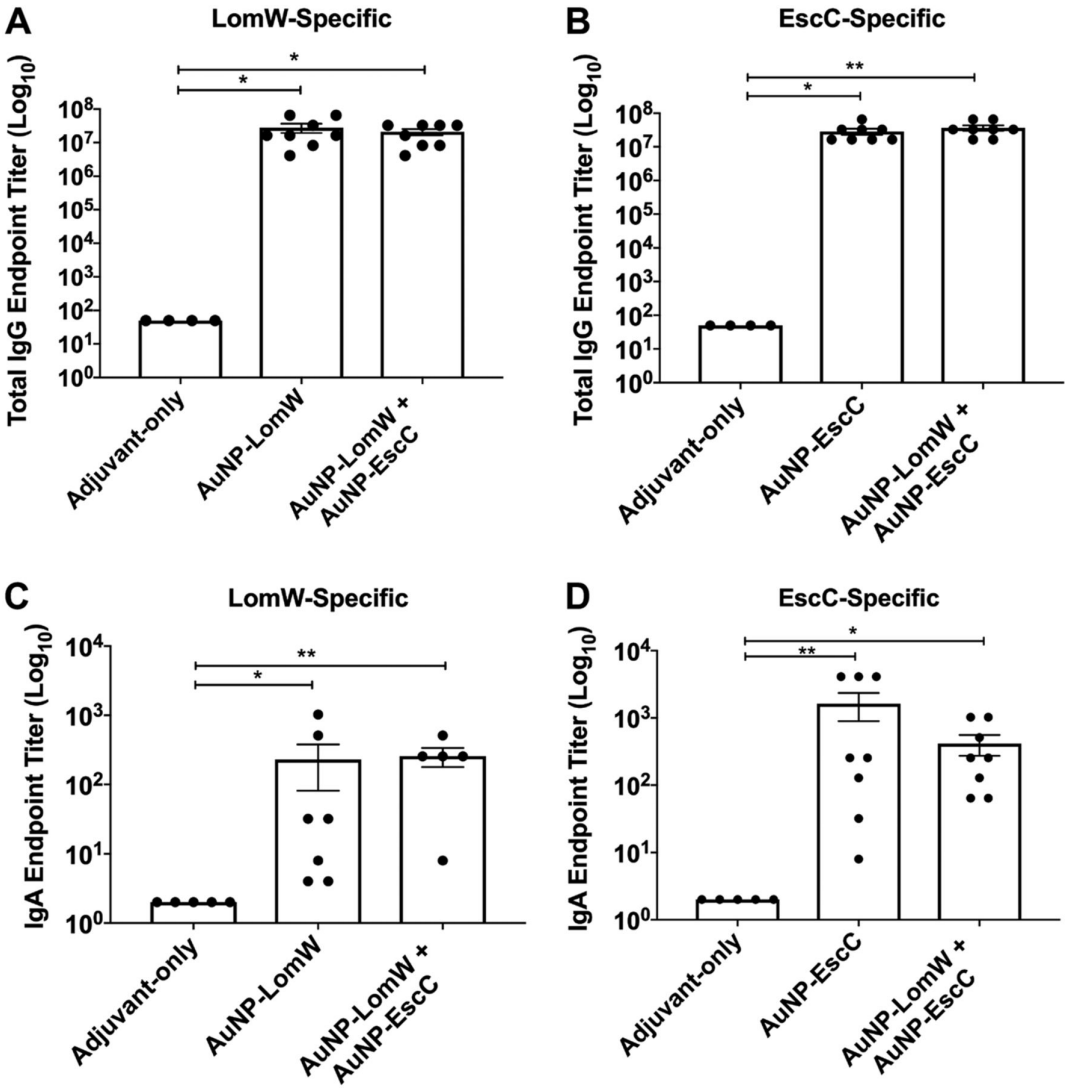

Figure 18. Antibody responses after AuNP-protein immunization.
(A) LomW-specific total IgG titers and **(C)** secretory IgA, as well as **(B)** EscC-specific total IgG antibody responses and **(D)** secretory IgA were assessed via ELISA, with endpoint titers determined as twice the SD from naïve sera. Sera and fecal samples were collected two-weeks post last immunization. Samples taken from the mice immunized with the combination formulation were used to assay anti-LomW and anti-EscC antibody titers. All antibody data is expressed as mean ± SEM from (n=8) per group. Significant differences in IgG and IgA titers were determined via one-way ANOVA followed by Tukey's *post hoc* test: *, $P<0.05$, **, $P<0.001$; ***, $P<0.0001$.

The levels of sIgA confirm that AuNP-protein immunization elicited strong mucosal IgA responses irrespective of the vaccination route. These results demonstrate that AuNP-LomW, AuNP-EscC, and AuNP-combination can elicit strong IgG and sIgA responses. Next, we evaluated the functionality of these antibody responses during *in vitro* experiments by determining whether serum antibodies were able to mediate inhibition of the adherence and establishment of infection.

Antibodies from AuNP-immunization decreased bacterial adherence to intestinal epithelial cells.

The capacity of antibodies to neutralize pathogens in mucosal surfaces is important for host protection, especially against enteric bacteria. To assess the functionality of these antibodies, we tested whether serum was able to inhibit bacterial adherence to human intestinal epithelial cells (IECs; Caco-2). Using 10% of serum from AuNP-vaccinated mice, we quantified adherence of EHEC to IECs and detected a reduction of approximately 98% when EHEC (MOI = 10) was incubated prior to infection with AuNP-LomW, AuNP-EscC, or combination sera (Fig. 19A). In contrast, serum from animals that were vaccinated with the adjuvant-only control or serum from naïve animals had about a 20% reduction in bacterial adherence (Fig. 19A). To calculate adhered bacteria, the different samples were all compared to the input inoculum.

To further analyze the neutralizing capacity of antibodies found in the immune serum, an *in vitro* assay was performed to evaluate adherence of EHEC to Caco-2 cells. One of the hallmark pathogenic mechanisms during EHEC infection is the intimate adherence onto the epithelial surface and the formation of polymerized actin pedestals (136, 137).

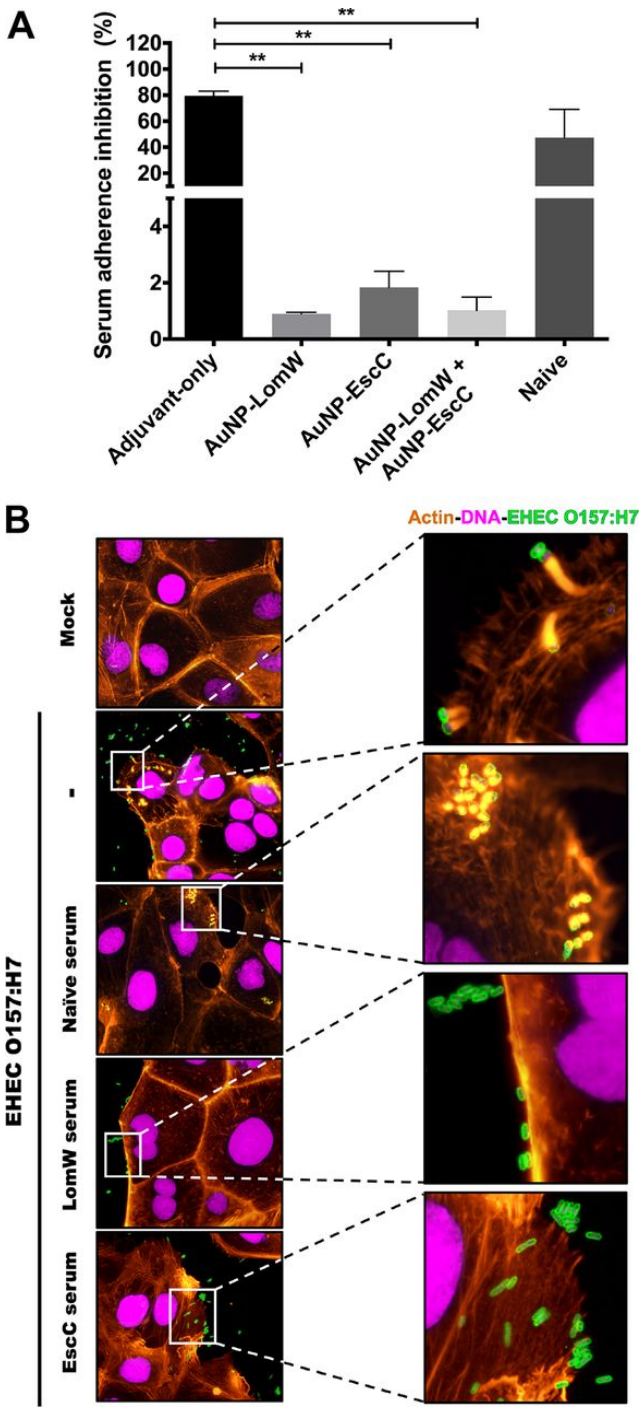

Figure 19. Serum from AuNP-protein immunized mice reduces EHEC 86-24 adherence and pedestal formation on Caco-2 intestinal epithelial cells.
EHEC 86-24 bacterial cells (1×10^7 CFU) were incubated in the presence of inactivated immunized serum (10% of final volume) from AuNP-LomW, AuNP-EscC, and AuNP-LomW + AuNP-EscC for 1 h at 37°C. Serum from naïve or adjuvant-only immunization served as controls. After incubation, bacteria were used to infect Caco-2 cells for 2 h. **(A)** After infection, cell monolayers were washed, detached, and diluted to enumerate adhered bacteria. All adherence data is expressed as mean ± SEM from two independent experiments using sera from (n=8) mice per group. Significant differences were determined via one-way ANOVA followed by Tukey's *post hoc* test: *, P<0.05, **, P<0.001; ***, P<0.0001. **(B)** Fluorescence microscopy analysis of Caco-2 cells after EHEC infection in the presence of immune serum (from vaccinated groups). After infection, cells were fixed and stained with phalloidin-rhodamine (actin), DAPI (bacteria and nuclei), or EHEC by immunofluorescence (anti-EHEC primary antibody conjugated to FITC). Panels on the right present a magnification of images on left. Magnified view shows the formation of actin pedestals and bacterial adherence pattern.

To visualize bacterial adherence and the rearrangement of actin cytoskeleton, Caco-2 cells were labeled with fluorescent actin stain (FAS), nuclei labeled with DAPI, and a commercial antibody was used to detect EHEC. In the case of EHEC infected cells and using fluorescence microscopy, we observed a diffuse adherence pattern and the accumulation of polymerized actin beneath the site of bacterial attachment (Fig. 19B).

In contrast, immune serum from vaccinated mice inhibited the formation of actin pedestal structures and reduced the number of bacteria attached to host cells (Fig. 19B). These results corroborate our quantitative analysis and further demonstrate a reduction in bacterial adherence in the presence of immune serum (Fig. 19A). Overall, we found that serum from AuNP-vaccinated mice significantly reduce the attachment of EHEC to IECs, thereby preventing the formation of actin pedestals.

We then tested whether the serum from vaccinated mice was able to block the adherence of other pathotypes which share some of the antigens coupled to the nanovaccines. Enteroaggregative *E. coli* (EAEC) O104:H4 is a hybrid strain that was associated with numerous HUS cases during the German outbreak in 2011, and which

possess EAEC virulence factors but also encodes for Shiga toxin (222). On the other hand, enteropathogenic *E. coli* (EPEC), like EHEC, carries the LEE pathogenicity island which encodes for the T3SS components required for A/E lesion formation. A bioinformatic comparison confirmed that EscC and LomW of EHEC are highly conserved proteins between either EPEC (EscC) or EAEC (LomW) (Table 1). Therefore, we tested whether antibodies against these proteins conferred cross-protective anti-adhesive properties *in vitro* against other pathotypes. A characteristic aggregative adherence pattern in a stack-brick conformation and a cytotoxic effect represented by contraction of the actin cytoskeleton followed by detachment from the substratum are associated with EAEC pathogenesis (136, 137). We observed that these adhesive properties were affected during EAEC infection in the presence of LomW-specific serum (Fig. 20A). In the case of EPEC, infection is characterized by a localized adherence pattern leading to the establishment of microcolonies and subsequent formation of actin pedestals. Unlike EHEC, where a complete abolishment on the formation of actin pedestals was observed, EscC-specific serum partially reduced bacterial adherence and the formation of pedestals (Fig. 20B). These results indicate that: 1) a reduction in the adherence for both pathotypes was achieved; 2) the presence of LomW-specific antibodies can prevent aggregative adherence and cytotoxicity during EAEC infection, while EscC-specific antibodies reduced adherence and to a lesser extent the formation of pedestals during EPEC infection.

Table 1: Homology of EHEC O157:H7 EscC and LomW among EPEC and EAEC/EHEC pathotypes.

Pathotype	**EscC**	**LomW**	**Homology/Identity to EHEC O157:H7 strain 86-24**
EPEC O127:H6	✓		100%/99.8%
EAEC/EHEC O104:H4		✓	100%/100%

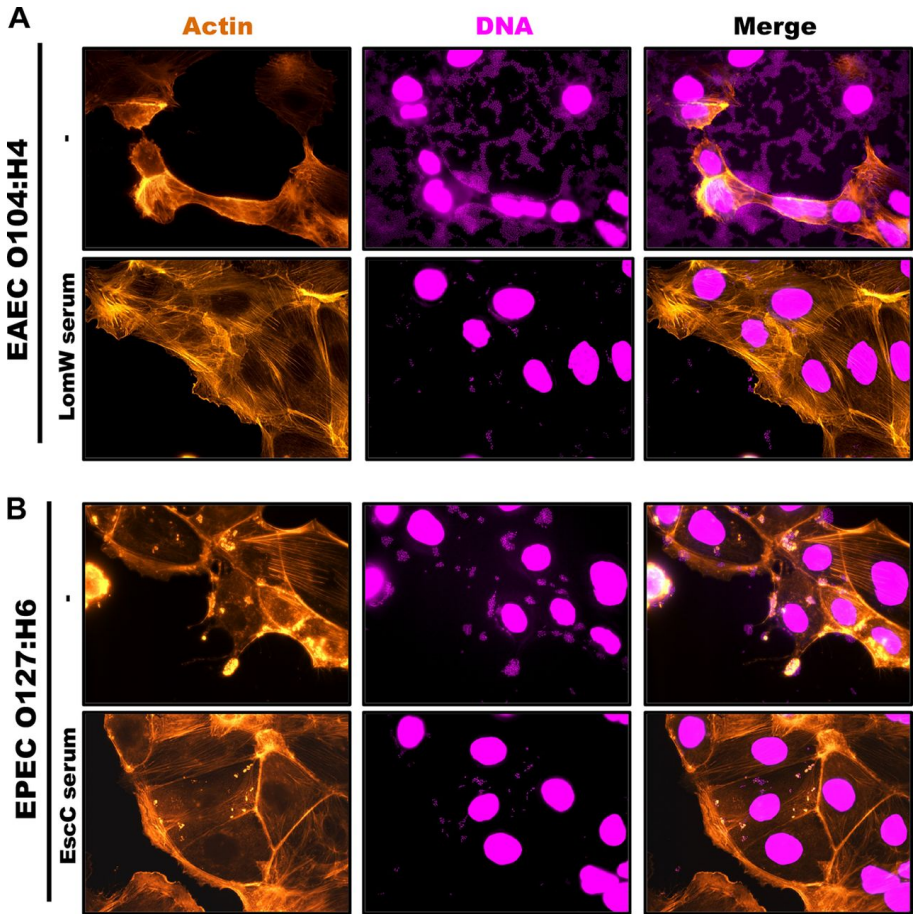

Figure 20. Cross-protective effect from immune serum from AuNP-protein vaccinated mice reduces adherence and cytotoxic effect induced by EAEC or EPEC on Caco-2 intestinal epithelial cells.
Infection of Caco-2 cells was carried out as mentioned in the previous image. **(A)** EAEC O104:H4 was incubated in the presence or absence of AuNP-LomW immune serum for 1 h. After incubation, bacteria were used to infect Caco-2 cells for 2 h and stained for fluorescence microscopy. **(B)** EPEC O127:H6 was incubated in the presence or absence of AuNP-EscC immune serum prior to infection in Caco-2 cells. After infection, cells were fixed and stained as previously described.

Bactericidal activity of AuNP-immunized serum is antigen-specific and involves the classical complement pathway.

We then evaluated whether the serum from vaccinated mice had bactericidal activity. To test the activity by complement-mediated killing, we quantified the percentage of EHEC killing in the presence of active or inactive serum, and inactive serum supplemented with a source of complement. In the presence of active serum from the three AuNP-immunized

mice groups, we observed almost complete killing but did not see a significant difference in percentage of bacterial killing between the 3 groups. In contrast, we noticed a significant reduction in bacterial killing from inactivated AuNP-LomW and AuNP-EscC immunized serum (Fig. 21A). Further, the bacterial killing effect was restored for the AuNP-EscC inactivated serum when an exogenous complement source was added, and to some extent, for the serum of AuNP-LomW, and AuNP combination (Fig. 21A). To corroborate that complement-mediated killing is the mechanism used to damage the integrity of the bacterial membrane and achieve bacterial clearance, we used a LIVE/DEAD BacLight assay to monitor bacterial viability as a function of the membrane integrity. SYTO9 is a green, fluorescent dye that can enter all bacterial cells, whereas Propidium Iodide (PI) is a red dye that only enters bacteria when the membrane is damaged. We observed an increase in the number of red-stained bacterial cells in the presence of sera from AuNP-LomW, AuNP-EscC, and AuNP combination, indicating the loss of membrane integrity (Fig. 21B). In contrast, the majority of untreated EHEC, or those bacteria treated with naïve serum, showed green, fluorescent signal (Fig. 21B). This suggest that the bactericidal activity from the serum of AuNP-proteins is antigen-specific and supports the engagement of the classical complement pathway as a mechanism of bacterial killing *in vitro*.

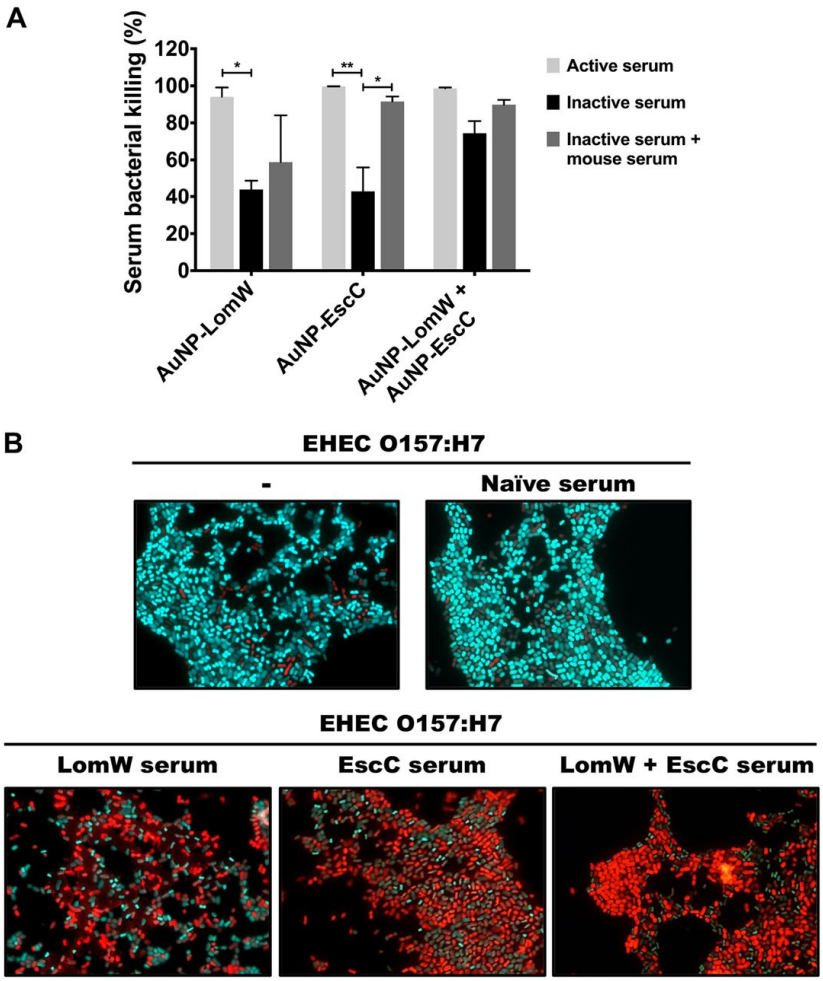

Figure 21. Serum bactericidal activity of immune serum from AuNP-protein vaccinated mice is antigen dependent.
EHEC 86-24 (1×10^7 CFU) was incubated with 10% of activate, inactive, and inactive + exogenous complement source. Bacteria were incubated in the presence of serum using 10% of serum for 1 h at 37°C. **(A)** Viable CFU counts were determined by plating on LB agar plates. Bacterial killing was normalized using bacteria surviving after exposure with adjuvant-only serum. Data is expressed as mean ± SEM from two independent experiments using sera from (n=8) mice per group. Significant differences were determined via one-way ANOVA followed by Tukey's *post hoc* test: *, $P<0.05$, **, $P<0.001$; ***, $P<0.0001$. **(B)** LIVE/DEAD BacLight assay using SYTO9 to stain live bacteria (cyan color) while propidium iodide (red color) stain dead bacteria. EHEC 86-24 (1×10^7 CFU) was incubated in the presence of AuNP-immune and naïve serum for 1 h at 37°C prior to staining.

DISCUSSION

The current interest in AuNPs for biomedical applications has been a result of their natural properties, including stabilization of antigens and enhancing uptake by antigen presenting cells (47, 223). The use of AuNPs has been exploited for the delivery of antigens in several models, including viral diseases and cancer (47, 48, 63, 223, 224). However, there are few reports of AuNP functionalization with bacterial antigens (58, 157). We have previously used AuNPs for the construction of nanovaccines against other bacterial pathogens (55, 165, 225). Therefore, we sought to exploit the natural properties of AuNPs by coupling two EHEC O157:H7-specific antigens and assessing their protective properties both *in vivo* and *in vitro*. Both LomW and EscC were identified by an extensive bio-immunoinformatic analysis and were predicted to contain several immunogenic epitopes, and our laboratory has previously shown that they can provide some level of protection against EHEC colonization when delivered as a DNA vaccine (213, 220, 221). Therefore, we decided to investigate whether we could use the AuNP platform to potentiate the delivery of these antigenic protein candidates and increase their protective effect. Based on our prior experience, we were able to demonstrate that AuNPs form stable scaffolds capable of conjugating different proteins (LomW and EscC) on their surface, allowing for stabilization and efficient antigen delivery.

As extensively demonstrated, EHEC O157:H7 colonization onto intestinal epithelial cells is characterized by the formation of tight interactions with epithelial cells, also known as attaching and effacing (A/E) lesions (137). In recent years, EHEC has not received much attention for the development of vaccine candidates because attention has re-focused to other pathogenic *E. coli* strains (145, 213). Nonetheless, studies examining vaccine candidates in cattle against EHEC have focused on various virulence factors including colonization factors, T3SS structural proteins, or Shiga toxin (Stx) (153, 226). Although promising, these attempts have shown variable degrees of success. In the present

study, we observed a significant reduction in EHEC colonization to the large intestine and cecum of mice that were immunized with AuNP-LomW, AuNP-EscC, and the combination nanovaccine. These results indicate that AuNP-protein immunization elicits a protective immune response capable of neutralizing EHEC, thus preventing the colonization of the mouse GI tract. A previous study highlighted the importance of outer membrane proteins as immunogenic antigens recognized by HUS patients and with antibodies present in their sera (227). Among the proteins that were identified to be reactive in HUS patient sera are the flagella protein (FliC) and outer membrane structural components (OmpF, OmpC), all of them displaying both IgG and IgA reactivity (227). It is plausible to propose that other surface exposed proteins, like LomW and EscC, might be reactive during disease progression; thus, a nanovaccine intervention that elicits both systemic and mucosal antibodies might prevent the development of HUS.

The function of the LomW protein in EHEC pathogenesis is not characterized, but if expressed, the protein is predicted to be translocated to the bacterial outer membrane as a component of the 933W phage machinery, a genetic region that also encodes the Shiga toxin genes (228). The presence of LomW on the bacterial outer membrane needs further investigation, but if this occurs during infection, the antigen becomes an ideal target for vaccination because it can be readily recognized by antibodies as demonstrated in our experiments. On the other hand, EscC is a structural protein component of the type 3 secretion system (T3SS), known to participate in the formation of a ring on the bacterial outer membrane (229). The reduction of EHEC adherence to IECs in the presence of EscC-specific antibodies strongly suggests that such inhibition interferes with early events prior to intimate attachment. Previously, it was demonstrated that vaccination with structural T3SS components reduced bacterial fecal shedding (230). Our data confirm those results but in addition, we now provide evidence demonstrating that serum can block the formation of actin pedestals on the surface of intestinal cells, which represent a direct effect on the pathogenic mechanism of EHEC and potentially, other A/E lesion forming pathogens. In

addition, it has been demonstrated that antibodies that inactivate the T3SS inhibit the injection of effector molecules that mediate other bacterial pathogenic mechanisms (230). The absence of actin pedestals in the presence of antigen-specific serum confirms the inhibition of an important pathogenic EHEC mechanism. Although we do not know the mechanism mediating the anti-LomW effect, our results indicate that antibodies against both EscC and LomW allow for inhibition of EHEC early events during adhesion, prior to the intimate attachment to IECs and the subsequent pathogenic process.

Despite differences in the pathogenic mechanisms between diverse *E. coli* pathogroups, there are shared homologous proteins linked to disease; therefore, the components that constitute these bacterial systems would be ideal antigens in the development of cross-protective vaccine candidates. Here, we describe the high sequence conservation of LomW between EAEC O104:H4 and EHEC, as well as EscC between EPEC O127:H6 and EHEC (Table 1). Our cross-protective *in vitro* studies demonstrated inhibition of bacterial adherence to IECs as well as pedestal formation and cell cytotoxicity in EPEC and EAEC, respectively, and indicates that development of a multi-*E. coli* vaccine might be feasible. In the case of EAEC O104:H4, the characteristic aggregative adherence pattern and cell cytotoxicity (characterized by cell rounding and detachment from the substratum) is interrupted by serum from AuNP-LomW immunized mice. For *E. coli* O127:H6 (EPEC), the characteristic localized adherence pattern was reduced in the presence of AuNP-EscC; however, the formation of actin pedestals was not completely abolished. These indicate variable effects associated with heterologous mechanisms in colonization, including the participation of additional pathotype-specific virulence factors. Further studies to increase the cross-protective effect with other pathotypes is needed to advance a multivalent vaccine.

Humoral responses play a major role in controlling extracellular pathogens, especially enteric organisms that colonize the GI tract (231). Protective immune responses against EHEC are mediated by a T_H2-biased humoral immune response that includes

neutralizing IgA antibodies; however, IgG has also been shown to play a role (232, 233). The route of vaccination is important because the type and location (systemic vs. mucosal) of the immune responses dictate the protective outcome of a vaccine. Mucosal immunization against EHEC is associated with sIgA, although there have also been several candidates whose protection is correlated with IgG levels (153, 232, 233). Systemic immunization routes, such as subcutaneous vaccination have reported high levels of IgG as a protective mechanism in the absence of IgA (153). However, few vaccine candidates have been able to induce robust IgG and IgA responses. In our study, we demonstrated that subcutaneous immunization with the AuNP vaccine results in high serum IgG and fecal sIgA responses. Interestingly, the differences in the magnitude of titers between IgG and IgA could be the result of antibody fluctuations in fecal pellets or the time of collection. In addition to the neutralization activity, we demonstrated the bactericidal properties of serum from AuNP-protein immunized mice. We showed that antigen-specific serum from vaccinated mice damages the bacterial membrane, thus indicating activation of the classical complement pathway. These results prove the functionality of serum antibodies in mediating bacterial killing. Previously, oral immunization with a live-attenuated *Salmonella* strain expressing *E. coli* O157:H7 intimin was shown to elicit humoral and mucosal humoral responses (153). Our results corroborate some of those findings, including the involvement of both mucosal and systemic humoral responses in reducing intestinal colonization. However, we now demonstrate that AuNPs elicit robust antigen-specific serum IgG and mucosal IgA responses without the need of a live-attenuated vaccine platform.

In summary, we have demonstrated that our AuNP-vaccine platform can induce protective immune responses both *in vivo* and *in vitro* while coupling specific antigens targeting EHEC adhesion and colonization. We have also demonstrated the functionality of these immune responses *in vitro*. This subunit vaccine platform can induce strong humoral responses in response to each antigen as well as in combination. We propose that

conjugating antigens on the surface of synthetic AuNPs is a viable approach for the design of effective bacterial vaccines.

CONCLUSIONS AND FUTURE DIRECTIONS

This study's main objective was to generate a broadly protective subunit vaccine against *B. pseudomallei* and *B. mallei* pathogens. To achieve this goal, I evaluated several AuNP-linked glycoconjugates using the LPS of *B. thailandensis* and several *B. mallei*-specific proteins previously identified via a reverse vaccinology approach. In this work, I have shown that different gold-linked glycoconjugates provide varying degrees of protection against *B. mallei* infection in a mouse model of glanders. I have also shown that a refined gold-linked glycoconjugate formulation containing three different protein antigens, OpcP, OmpW, and Hemagglutinin, provides 100% protection by 35 days post-infection against lethality in a mouse model of glanders.

Furthermore, I have shown that these conserved antigens in *B. pseudomallei* also afford different degrees of protection in a mouse model of melioidosis. Like in the glanders model of infection, I showed that immunization with a refined formulation containing two antigens, OpcP and OpcP1, afforded complete protection against *B. pseudomallei* infection murine melioidosis model and was associated with a lower bacterial infection in the livers and spleens of surviving animals. In this work, I have shown the ability of different gold-linked glycoconjugates to induce robust antigen-specific humoral responses, with combination formulations having similar antigen-specific antibody responses against different antigens as single gold-linked glycoconjugates. I have also shown that protective antigens are associated with the induction of a T_H1-biased immune response with increased macrophage opsonophagocytosis and reduced bacterial viability. Also, I have shown that splenocytes from vaccinated animals produced a mixed T_H1-T_H17 cytokine production upon protein re-stimulation associated with protection. These results highlight the ability of a gold-linked glycoconjugate to promote humoral and cell-mediated immunity, correlated with protection against a mouse model of melioidosis. The studies presented here show a subunit vaccine platform that induce protective responses against two

intracellular pathogens with complex lifestyles. Future studies should include characterizing the epitopes of OpcP and Opcp1 to identify the most immunogenic regions which could be synthesized and delivered more effectively. Furthermore, future studies should focus on analyzing the durability of these correlates of protection and the tissue-specific memory or effector cell populations and their mechanism of protection.

Using a similar vaccination strategy, I also showed the ability of EHEC O157:H7-specific AuNP-delivered vaccine candidates to induce robust systemic IgG and mucosal IgA humoral responses. These responses were associated with reduced bacterial colonization in the gut of immunized mice. In addition, we showed that serum from immunized animals had antigen-specific bactericidal activity and inhibited bacterial adherence *in vitro*. These results highlight the potential for AuNP-delivered nanovaccines to protect against intracellular and extracellular bacterial pathogens. Future studies should include testing various vaccination routes and comparing the effectiveness of this vaccine and the role of adjuvant-codelivery in a single AuNP that can help provide increase protection. In the era of multidrug resistance, vaccines against these bacterial pathogens offer a means to prevent and combat some of the most challenging global health threats humanity has faced.

Furthermore, the studies presented here sought to exploit the use of a synthetic vaccine platform to deliver a multivalent vaccine and enhance protection against several bacterial pathogens. Also, this study highlights the use of nanovaccine technologies in the development of effective antibacterial vaccines. However, with increasing understanding of vaccine platforms that target specific cells or tissue compartments and specific adjuvants, vaccinology's future looks bright and will have implications against other disease models outside of infectious disease. Overall, I think the results summarize in this dissertation are a starting point for a gold-delivered multivalent vaccine as an effective strategy to protect against *B. mallei*, *B. pseudomallei*, and pathogenic *E. coli*.

References

1. Plotkin S. 2014. History of vaccination. Proc Natl Acad Sci U S A 111:12283–12287.
2. Milligan GN, Barrett AD. 2012. Vaccinology: An Essential Guide, 3rd ed. Wiley-Blackwell.
3. Siegrist CA. 2008. Vaccine immunology. Vaccines 2:14–32.
4. Shapiro-Shapin CG. 2010. Pearl Kendrick, grace eldering, and the Pertussis Vaccine. Emerg Infect Dis 16:1273–1278.
5. Rappuoli R. 2000. Reverse vaccinology. Curr Opin Microbiol 3:445–450.
6. Delany I, Rappuoli R, Seib KL. 2013. Vaccines, Reverse Vaccinology, and Bacterial Pathogenesis. Cold Spring Harb Perspect Med 3.
7. Capecchi B, Serruto D, Adu-Bobie J, Rappuoli R, Pizza M. 2004. The genome revolution in vaccine research. Curr Issues Mol Biol 6:17–28.
8. Sette A, Rappuoli R. 2010. Reverse vaccinology: Developing vaccines in the era of genomics. Immunity 33:530–541.
9. Polack FP, Thomas SJ, Kitchin N, Absalon J, Gurtman A, Lockhart S, Perez JL, Pérez Marc G, Moreira ED, Zerbini C, Bailey R, Swanson KA, Roychoudhury S, Koury K, Li P, Kalina W V., Cooper D, Frenck RW, Hammitt LL, Türeci Ö, Nell H, Schaefer A, Ünal S, Tresnan DB, Mather S, Dormitzer PR, Şahin U, Jansen KU, Gruber WC. 2020. Safety and Efficacy of the BNT162b2 mRNA Covid-19 Vaccine. N Engl J Med 383:2603–2615.
10. Jackson LA, Anderson EJ, Rouphael NG, Roberts PC, Makhene M, Coler RN, McCullough MP, Chappell JD, Denison MR, Stevens LJ, Pruijssers AJ, McDermott A, Flach B, Doria-Rose NA, Corbett KS, Morabito KM, O'Dell S, Schmidt SD, Swanson PA, Padilla M, Mascola JR, Neuzil KM, Bennett H, Sun W, Peters E, Makowski M, Albert J, Cross K, Buchanan W, Pikaart-Tautges R, Ledgerwood JE, Graham BS, Beigel JH. 2020. An mRNA Vaccine against SARS-CoV-2 — Preliminary Report. N Engl J Med 383:1920–1931.
11. Bachmann MF, Jennings GT. 2010. Vaccine delivery: A matter of size, geometry, kinetics and molecular patterns. Nat Rev Immunol 10:787–796.
12. De Temmerman ML, Rejman J, Demeester J, Irvine DJ, Gander B, De Smedt SC. 2011. Particulate vaccines: On the quest for optimal delivery and immune response. Drug Discov Today 16:569–582.
13. Cobb BA, Wang Q, Tzianabos AO, Kasper DL. 2004. Polysaccharide processing and presentation by the MHCII pathway. Cell 117:677–687.
14. Smith DM, Simon JK, Baker JR. 2013. Applications of nanotechnology for immunology. Nat Rev Immunol 13:592–605.

15. Burgdorf S, Kurts C. 2008. Endocytosis mechanisms and the cell biology of antigen presentation. Curr Opin Immunol 20:89–95.

16. Hemmi H, Zaidi N, Wang B, Matos I, Fiorese C, Lubkin A, Zbytnuik L, Suda K, Zhang K, Noda M, Kaisho T, Steinman RM, Idoyaga J. 2012. Treml4, an Ig Superfamily Member, Mediates Presentation of Several Antigens to T Cells *In Vivo*, Including Protective Immunity to HER2 Protein. J Immunol by guest Sept J Immunol 8:1147–1155.

17. Blum JS, Wearsch PA, Cresswell P. 2013. Pathways of Antigen Processing. Annu Rev Immunol 31:443–73.

18. Zupančič E, Curato C, Paisana M, Rodrigues C, Porat Z, Viana AS, Afonso CAM, Pinto J, Gaspar R, Moreira JN, Satchi-Fainaro R, Jung S, Florindo HF. 2017. Rational design of nanoparticles towards targeting antigen-presenting cells and improved T cell priming. J Control Release 258:182–195.

19. Song C, Noh YW, Lim YT. 2016. Polymer nanoparticles for cross-presentation of exogenous antigens and enhanced cytotoxic T-lymphocyte immune response. Int J Nanomedicine 11:3753–3764.

20. Bozzacco L, Trumpfheller C, Siegal FP, Mehandru S, Markowitz M, Carrington M, Nussenzweig MC, Piperno AG, Steinman RM. 2007. DEC-205 receptor on dendritic cells mediates presentation of HIV gag protein to CD8+ T cells in a spectrum of human MHC I haplotypes. Proc Natl Acad Sci 104:1289–1294.

21. Zhou Q, Zhang Y, Du J, Li Y, Zhou Y, Fu Q, Zhang J, Wang X, Zhan L. 2016. Different-Sized Gold Nanoparticle Activator/Antigen Increases Dendritic Cells Accumulation in Liver-Draining Lymph Nodes and CD8+ T Cell Responses. ACS Nano 10:2678–2692.

22. Heit A, Schmitz F, O'Keeffe M, Staib C, Busch DH, Wagner H, Huster KM. 2005. Protective CD8 T cell immunity Triggered by CpG-Protein Conjugates Competes with the Efficacy of Live Vaccines. J Immunol 174:4373–4380.

23. Luo M, Wang H, Wang Z, Cai H, Lu Z, Li Y, Du M, Huang G, Wang C, Chen X, Porembka MR, Lea J, Frankel AE, Fu YX, Chen ZJ, Gao J. 2017. A STING-activating nanovaccine for cancer immunotherapy. Nat Nanotechnol 12:648–654.

24. Wang C, Zhu W, Wang B-Z. 2017. Dual-linker gold nanoparticles as adjuvanting carriers for multivalent display of recombinant influenza hemagglutinin trimers and flagellin improve the immunological responses *in vivo* and *in vitro*. Int J Nanomedicine 12:4747–4762.

25. Hoving JC, Wilson GJ, Brown GD. 2014. Signalling C-type lectin receptors, microbial recognition and immunity. Cell Microbiol 16:185–194.

26. Graham DB, Stephenson LM, Lam SK, Brim K, Lee HM, Bautista J, Gilfillan S, Akilesh S, Fujikawa K, Swat W. 2007. An ITAM-signaling pathway controls cross-presentation of particular but not soluble antigens in dendritic cells. J Exp Med 204:2889–2897.

27. Rappuoli R. 2018. Glycoconjugate vaccines: Principles and mechanisms. Sci

Transl Med 10:1–7.

28. Smith DM, Simon JK, Baker JR. 2013. Applications of nanotechnology for immunology. Nat Rev Immunol 13:592–605.

29. Moyer TJ, Zmolek AC, Irvine DJ, Moyer TJ, Zmolek AC, Irvine DJ. 2016. Beyond antigens and adjuvants: formulating future vaccines. J Clin Invest 126:799–808.

30. Zhang W, Wang L, Liu Y, Chen X, Liu Q, Jia J, Yang T, Qiu S, Ma G. 2014. Immune responses to vaccines involving a combined antigen-nanoparticle mixture and nanoparticle-encapsulated antigen formulation. Biomaterials 35:6086–6097.

31. Kool M, Fierens K, Lambrecht BN. 2012. Alum adjuvant: Some of the tricks of the oldest adjuvant. J Med Microbiol 61:927–934.

32. Del Giudice G, Rappuoli R, Didierlaurent AM. 2018. Correlates of adjuvanticity: A review on adjuvants in licensed vaccines. Semin Immunol 39:14–21.

33. Avci FY, Kasper DL. 2010. How Bacterial Carbohydrates Influence the Adaptive Immune System. Annu Rev Immunol 28:107–130.

34. Geijtenbeek TBH, Gringhuis SI. 2009. Signalling through C-type lectin receptors: shaping immune responses. Nat Rev Immunol 9:465–479.

35. Zhao L, Seth A, Wibowo N, Zhao CX, Mitter N, Yu C, Middelberg APJ. 2014. Nanoparticle vaccines. Vaccine 32:327–337.

36. Song W, Anselmo AC, Huang L. 2019. Nanotechnology intervention of the microbiome for cancer therapy. Nat Nanotechnol 14:1093–1103.

37. Chattopadhyay S, Chen JY, Chen HW, Jack Hu CM. 2017. Nanoparticle Vaccines Adopting Virus-like Features for Enhanced Immune Potentiation. Nanotheranostics 1:244–260.

38. Lin LC-W, Chattopadhyay S, Lin J-C, Hu C-MJ. 2018. Advances and Opportunities in Nanoparticle- and Nanomaterial-Based Vaccines against Bacterial Infections. Adv Healthc Mater 7:1–26.

39. Marques Neto LM, Kipnis A, Junqueira-Kipnis AP. 2017. Role of Metallic Nanoparticles in Vaccinology: Implications for Infectious Disease Vaccine Development. Front Immunol 8:1–10.

40. Bhattacharyya S, Kudgus RA, Bhattacharya R, Mukherjee P. 2011. Inorganic Nanoparticles in Cancer Therapy. Pharm Res 28:237–259.

41. Du J, Zhang YS, Hobson D, Hydbring P. 2017. Nanoparticles for immune system targeting. Drug Discov Today 22:1295–1301.

42. Pugazhendhi A, Edison TNJI, Karuppusamy I, Kathirvel B. 2018. Inorganic nanoparticles: a potential cancer therapy for human welfare. Int J Pharm 539:104–111.

43. Saptarshi SR, Duschl A, Lopata AL. 2013. Interaction of nanoparticles with proteins: Relation to bio-reactivity of the nanoparticle. J Nanobiotechnology 11:1–

12.

44. Crisponi G, Nurchi VM, Lachowicz JI, Peana M, Medici S, Zoroddu MA. 2017. Toxicity of Nanoparticles: Etiology and Mechanisms, p. 511–546. *In* Antimicrobial Nanoarchitectonics. Elsevier.

45. Silva JM, Vandermeulen G, Oliveira VG, Pinto SN, Rodrigues C, Salgado A, Afonso CA, Viana AS, Jérôme C, Silva LC, Graca L, Préat V, Florindo HF. 2014. Development of functionalized nanoparticles for vaccine delivery to dendritic cells: a mechanistic approach. Nanomedicine 9:2639–2656.

46. Ferreira RC, Neves H, Pinto JF, Lopes CM. 2017. Overview on Inhalable Nanocarriers for Respiratory Immunization. Curr Pharm Des 23:6160–6181.

47. Thobhani S, Attree S, Boyd R, Kumarswami N, Noble J, Szymanski M, Porter RA. 2010. Bioconjugation and characterisation of gold colloid-labelled proteins. J Immunol Methods 356:60–69.

48. Gao W, Fang RH, Thamphiwatana S, Luk BT, Li J, Angsantikul P, Zhang Q, Hu CMJ, Zhang L. 2015. Modulating Antibacterial Immunity via Bacterial Membrane-Coated Nanoparticles. Nano Lett 15:1403–1409.

49. Pissuwan D, Cortie CH, Valenzuela SM, Cortie MB. 2010. Functionalised gold nanoparticles for controlling pathogenic bacteria. Trends Biotechnol 28:207–213.

50. Niikura K, Matsunaga T, Suzuki T, Kobayashi S, Yamaguchi H, Orba Y, Kawaguchi A, Hasegawa H, Kajino K, Ninomiya T, Ijiro K, Sawa H. 2013. Gold Nanoparticles as a Vaccine Platform: Influence of Size and Shape on Immunological Responses *in Vitro* and *in Vivo*. ACS Nano 7:3926–3938.

51. Climent N, García I, Marradi M, Chiodo F, Miralles L, Maleno MJ, Gatell JM, García F, Penadés S, Plana M. 2018. Loading dendritic cells with gold nanoparticles (GNPs) bearing HIV-peptides and mannosides enhance HIV-specific T cell responses. Nanomedicine Nanotechnology, Biol Med 14:339–351.

52. Chiodo F, Marradi M, Park J, Ram AFJ, Penadés S, van Die I, Tefsen B. 2014. Galactofuranose-Coated Gold Nanoparticles Elicit a Pro-inflammatory Response in Human Monocyte-Derived Dendritic Cells and Are Recognized by DC-SIGN. ACS Chem Biol 9:383–389.

53. MacParland SA, Tsoi KM, Ouyang B, Ma XZ, Manuel J, Fawaz A, Ostrowski MA, Alman BA, Zilman A, Chan WCW, McGilvray ID. 2017. Phenotype Determines Nanoparticle Uptake by Human Macrophages from Liver and Blood. ACS Nano 11:2428–2443.

54. Chen YS, Hung YC, Lin WH, Huang GS. 2010. Assessment of gold nanoparticles as a size-dependent vaccine carrier for enhancing the antibody response against synthetic foot-and-mouth disease virus peptide. Nanotechnology 21:195101.

55. Gregory AE, Williamson ED, Prior JL, Butcher WA, Thompson IJ, Shaw AM, Titball RW. 2012. Conjugation of *Y. pestis* F1-antigen to gold nanoparticles improves immunogenicity. Vaccine 30:6777–6782.

56. Safari D, Marradi M, Chiodo F, Th Dekker HA, Shan Y, Adamo R, Oscarson S,

Rijkers GT, Lahmann M, Kamerling JP, Penadés S, Snippe H. 2012. Gold nanoparticles as carriers for a synthetic *Streptococcus pneumoniae* type 14 conjugate vaccine. Nanomedicine 7:651–662.

57. Rodriguez E, Rio -Del, Marradi M, Calderon-Gonzalez R, Frande-Cabanes E, Penadés S, Petrovsky N, Alvarez-Dominguez C. 2015. A gold glyco-nanoparticle carrying a listeriolysin O peptide and formulated with Advax delta inulin adjuvant induces robust T-cell protection against listeria infection. Vaccine 33:1465–1473.

58. Dakterzada F, Mobarez AM, Habibi Roudkenar M, Mohsenifar A. 2016. Induction of humoral immune response against *Pseudomonas aeruginosa* flagellin (1-161) using gold nanoparticles as an adjuvant. Vaccine 34:1472–1479.

59. Marasini N, Skwarczynski M, Toth I. 2017. Intranasal delivery of nanoparticle-based vaccines. Ther Deliv 8:151–167.

60. Tonigold M, Mailänder V. 2016. Endocytosis and intracellular processing of nanoparticles in dendritic cells: routes to effective immunonanomedicines. Nanomedicine 11:2625–2630.

61. Wang C, Zhu W, Luo Y, Wang BZ. 2018. Gold nanoparticles conjugating recombinant influenza hemagglutinin trimers and flagellin enhanced mucosal cellular immunity. Nanomedicine Nanotechnology, Biol Med 14:1349–1360.

62. Kang S, Ahn S, Lee J, Kim JY, Choi M, Gujrati V, Kim H, Kim J, Shin E-C, Jon S. 2017. Effects of gold nanoparticle-based vaccine size on lymph node delivery and cytotoxic T-lymphocyte responses. J Control Release 256:56–67.

63. Fogli S, Montis C, Paccosi S, Silvano A, Michelucci E, Berti D, Bosi A, Parenti A, Romagnoli P. 2017. Inorganic nanoparticles as potential regulators of immune response in dendritic cells. Nanomedicine (Lond) 12:1647–1660.

64. Currie BJ. 2004. *Burkholderia pseudomallei* and *Burkholderia mallei*: Melioidosis and Glanders, p. 2869–2879. *In* Mandell, GL, Bennett, JE, Dolin, R (eds.), Principles and Practice of Infectious Diseases, 6th ed. Churchill Livingstone.

65. Dvorak GD, Spickler AR. 2008. Glanders. J Am Vet Med Assoc 233:570–577.

66. Wiersinga WJ, Virk HS, Torres AG, Currie BJ, Peacock SJ, Dance DAB, Limmathurotsakul D. 2018. Melioidosis. Nat Rev Dis Prim 4:17107.

67. Galyov EE, Brett PJ, DeShazer D. 2010. Molecular Insights into *Burkholderia mallei* and *Burkholderia pseudomallei* Pathogenesis. Annu Rev Microbiol 64:495–517.

68. Wiersinga WJ, Currie BJ, Peacock SJ. 2012. Melioidosis. N Engl J Med 367:1035–1044.

69. Limmathurotsakul D, Golding N, Dance DAB, Messina JP, Pigott DM, Moyes CL, Rolim DB, Bertherat E, Day NPJ, Peacock SJ, Hay SI. 2016. Predicted global distribution of *Burkholderia pseudomallei* and burden of melioidosis. Nat Microbiol 1:15008.

70. Khan I, Wieler LH, Melzer F, Elschner MC, Muhammad G, Ali S, Sprague LD,

Neubauer H, Saqib M. 2013. Glanders in Animals: A Review on Epidemiology, Clinical Presentation, Diagnosis and Countermeasures. Transbound Emerg Dis 60:204–221.

71. Khakhum N, Tapia D, Torres AG. 2019. *Burkholderia mallei* and Glanders, p. 161–184. *In* Singh, SK, Kuhn, JH (eds.), Defense Against Biological Attacks. Springer Nature Switzerland, Cham, Switzerland.

72. Aschenbroich SA, Lafontaine ER, Hogan RJ. 2017. Melioidosis and glanders modulation of the innate immune system: barriers to current and future vaccine approaches. Expert Rev Vaccines 15:1163–1181.

73. Currie BJ. 2015. Melioidosis: Evolving concepts in epidemiology, pathogenesis, and treatment. Semin Respir Crit Care Med 36:111–125.

74. Estes DM, Dow SW, Schweizer HP, Torres AG. 2010. Present and future therapeutic strategies for melioidosis and glanders. Expert Rev Anti Infect Ther 8:325–338.

75. Morici L, Torres AG, Titball RW. 2019. Novel multi-component vaccine approaches for *Burkholderia pseudomallei*. Clin Exp Immunol 196:178–188.

76. Lipsitz R, Garges S, Aurigemma R, Baccam P, Blaney D, Cheng A, Currie B, Dance D, Gee J, Larsen J, Limmathurotsakul D, Morrow M, Norton R, O'Mara E, Peacock S, Pesik N, Rogers L, Schweizer H, Steinmetz I, Tan G, Tan P, Wiersinga W, Wuthiekanun V, Smith T. 2010. Workshop on Treatment of and Postexposure Prophylaxis for *Burkholderia pseudomallei* and *B. mallei* Infection, 2010. Emerg Infect Dis 18.

77. Saiprom N, Amornchai P, Wuthiekanun V, Day NPJ, Limmathurotsakul D, Peacock SJ, Chantratita N. 2015. Trimethoprim/sulfamethoxazole resistance in clinical isolates of *Burkholderia pseudomallei* from Thailand. Int J Antimicrob Agents 45:557–559.

78. Chaowagul W, Suputtamongkul Y, Smith MD, White NJ. 1997. Oral fluoroquinolones for maintenance treatment of melioidosis. Trans R Soc Trop Med Hyg 91:599–601.

79. Barnes KB, Hamblin KA, Richards MI, Laws TR, Vente A, Atkins HS, Harding S V. 2017. Demonstrating the Protective Efficacy of the Novel Fluoroquinolone Finafloxacin against an Inhalational Exposure to *Burkholderia pseudomallei*. Antimicrob Agents Chemother 61:1–17.

80. Chan E, Martelli P, Hui S, Teng JLL, Lau SKP, Woo PCY. 2018. *In Vitro* Susceptibility of Ceftolozane-Tazobactam against *Burkholderia pseudomallei*. Antimicrob Agents Chemother 62:1–2.

81. Sengyee S, Saiprom N, Paksanont S, Limmathurotsakul D, Wuthiekanun V, Chantratita N. 2017. Susceptibility of Clinical Isolates of *Burkholderia pseudomallei* to a Lipid A Biosynthesis Inhibitor. Am J Trop Med Hyg 97:62–67.

82. Bommineni GR, Kapilashrami K, Cummings JE, Lu Y, Knudson SE, Gu C, Walker SG, Slayden RA, Tonge PJ. 2016. Thiolactomycin-Based Inhibitors of

Bacterial β-Ketoacyl-ACP Synthases with *in vivo* Activity. J Med Chem 59:5377–5390.

83. Kreisberg JF, Ong NT, Krishna A, Joseph TL, Wang J, Ong C, Ooi HA, Sung JC, Siew CC, Chang GC, Biot F, Cuccui J, Wren BW, Chan J, Sivalingam SP, Zhang LH, Verma C, Tan P. 2013. Growth Inhibition of Pathogenic Bacteria by Sulfonylurea Herbicides. Antimicrob Agents Chemother 57:1513–1517.

84. Cummings JE, Kingry LC, Rholl DA, Schweizer HP, Tonge PJ, Slayden RA. 2014. The *Burkholderia pseudomallei* Enoyl-Acyl Carrier Protein Reductase FabI1 is Essential for *In Vivo* Growth and Is the Target of a Novel Chemotherapeutic with Efficacy. Antimicrob Agents Chemother 58:931–935.

85. Cummings JE, Beaupre AJ, Knudson SE, Liu N, Yu W, Neckles C, Wang H, Khanna A, Bommineni GR, Trunck LA, Schweizer HP, Tonge PJ, Slayden RA. 2014. Substituted Diphenyl Ethers as a Novel Chemotherapeutic Platform against *Burkholderia pseudomallei*. Antimicrob Agents Chemother 58:1646–1651.

86. Laws TR, Taylor AW, Russell P, Williamson D. 2019. The treatment of melioidosis: is there a role for repurposed drugs? A proposal and review. Expert Rev Anti Infect Ther 17:957–967.

87. Mima T, Kvitko BH, Rholl DA, Page MGP, Desarbre E, Schweizer HP. 2011. *In vitro* activity of BAL30072 against *Burkholderia pseudomallei*. Int J Antimicrob Agents 38:157–159.

88. Bandeira T de JPG, Brilhante RSN, Rocha MFG, Moreira CA, Cordeiro R de A, Ribeiro JF, Castelo-Branco D de SCM, Sidrim JJC. 2013. *In vitro* antimicrobial susceptibility of clinical and environmental strains of *Burkholderia pseudomallei* from Brazil. Int J Antimicrob Agents 42:375–377.

89. Scarff JM, Waidyarachchi SL, Meyer CJ, Lane DJ, Chai W, Lemmon MM, Liu J, Butler MM, Bowlin TL, Lee RE, Panchal RG. 2019. Aminomethyl spectinomycins: a novel antibacterial chemotype for biothreat pathogens. J Antibiot (Tokyo) 72:693–701.

90. Barnes KB, Steward J, Thwaite JE, Lever MS, Davies CH, Armstrong SJ, Laws TR, Roughley N, Harding S V., Atkins TP, Simpson AJH, Atkins HS. 2013. Trimethoprim/sulfamethoxazole (co-trimoxazole) prophylaxis is effective against acute murine inhalational melioidosis and glanders. Int J Antimicrob Agents 41:552–557.

91. Siritongsuk P, Hongsing N, Thammawithan S, Daduang S, Klaynongsruang S, Tuanyok A, Patramanon R. 2016. Two-phase bactericidal mechanism of silver nanoparticles against *Burkholderia Pseudomallei*. PLoS One 11:1–22.

92. Ruiz SI, El-Gendy N, Bowen LE, Berkland C, Bailey MM. 2016. Formulation and Characterization of Nanocluster Ceftazidime for the Treatment of Acute Pulmonary Melioidosis. J Pharm Sci 105:3399–3408.

93. Ruiz SI, Bowen LE, Bailey MM, Berkland C. 2018. Pulmonary Delivery of Ceftazidime for the Treatment of Melioidosis in a Murine Model. Mol Pharm

15:1371–1376.

94. Castelo-Branco DSCM, Riello GB, Vasconcelos DC, Guedes GMM, Serpa R, Bandeira TJPG, Monteiro AJ, Cordeiro RA, Rocha MFG, Sidrim JJC, Brilhante RSN. 2016. Farnesol increases the susceptibility of *Burkholderia pseudomallei* biofilm to antimicrobials used to treat melioidosis. J Appl Microbiol 120:600–606.

95. Koh GCKW, Limmathurotsakul D. 2010. Gamma interferon supplementation for melioidosis. Antimicrob Agents Chemother 54:4520.

96. Propst KL, Troyer RM, Kellihan LM, Schweizer HP, Dow SW. 2010. Immunotherapy Markedly Increases the Effectiveness of Antimicrobial Therapy for Treatment of *Burkholderia pseudomallei* Infection. Antimicrob Agents Chemother 54:1785–1792.

97. Waag DM. 2015. Efficacy of Postexposure Therapy against Glanders in Mice. Antimicrob Agents Chemother 59:2236–2241.

98. Khakhum N, Bharaj P, Myers JN, Tapia D, Kilgore PB, Ross BN, Walker DH, Endsley JJ, Torres AG. 2019. *Burkholderia pseudomallei* Δ*tonB* Δ*hcp1* Live Attenuated Vaccine Strain Elicits Full Protective Immunity against Aerosolized Melioidosis Infection. mSphere 4:1–13.

99. Hatcher CL, Mott TM, Muruato LA, Sbrana E, Torres AG. 2016. *Burkholderia mallei* CLH001 Attenuated Vaccine Strain Is Immunogenic and Protects against Acute Respiratory Glanders. Infect Immun 84:2345–2354.

100. Marchetti R, Dillon MJ, Burtnick MN, Hubbard MA, Kenfack MT, Blériot Y, Gauthier C, Brett PJ, AuCoin DP, Lanzetta R, Silipo A, Molinaro A. 2015. *Burkholderia pseudomallei* Capsular Polysaccharide Recognition by a Monoclonal Antibody Reveals Key Details toward a Biodefense Vaccine and Diagnostics against Melioidosis. ACS Chem Biol 10:2295–2302.

101. AuCoin DP, Reed DE, Marlenee NL, Bowen RA, Thorkildson P, Judy BM, Torres AG, Kozel TR. 2012. Polysaccharide Specific Monoclonal Antibodies Provide Passive Protection against Intranasal Challenge with *Burkholderia pseudomallei*. PLoS One 7:e35386.

102. Peddayelachagiri B V., Paul S, Makam SS, Urs RM, Kingston JJ, Tuteja U, Sripathy MH, Batra H V. 2014. Functional characterization and evaluation of *in vitro* protective efficacy of murine monoclonal antibodies BURK24 and BURK37 against *Burkholderia pseudomallei*. PLoS One 9:e90930.

103. Ceballos-Olvera I, Sahoo M, Miller MA, del Barrio L, Re F. 2011. Inflammasome-dependent pyroptosis and IL-18 Protect against *Burkholderia pseudomallei* Lung Infection while IL-1β is Deleterious. PLoS Pathog 7:e1002452.

104. Weehuizen TAF, Lankelma JM, De Jong HK, De Boer OJ, Roelofs JJTH, Day NP, Gram H, De Vos AF, Wiersinga WJ. 2016. Therapeutic administration of a monoclonal anti-IL-1β antibody protects against experimental melioidosis. Shock 46:566–574.

105. Zhang S, Feng S-H, Li B, Kim H-Y, Rodriguez J, Tsai S, Lo S-C. 2011. *In Vitro*

and *In Vivo* Studies of Monoclonal Antibodies with Prominent Bactericidal Activity against *Burkholderia pseudomallei* and *Burkholderia mallei*. Clin Vaccine Immunol 18:825–834.

106. Kim HY, Tsai S, Lo SC, Wear DJ, Izadjoo MJ. 2011. Production and Characterization of Chimeric Monoclonal Antibodies against *Burkholderia pseudomallei* and *B. mallei* Using the DHFR Expression System. PLoS One 6:e19867.

107. Zimmerman SM, Dyke JS, Jelesijevic TP, Michel F, Lafontaine ER, Hogan RJ. 2017. Antibodies against *In Vivo*-Expressed Antigens Are Sufficient To Protect against Lethal Aerosol Infection with *Burkholderia mallei* and *Burkholderia pseudomallei*. Infect Immun 85:e00102-17.

108. Easton A, Ashraful Haque, Chu K, Patel N, Lukaszewski RA, Krieg AM, Titball RW, Bancroft GJ. 2011. Combining Vaccination and Postexposure CpG Therapy Provides Optimal Protection Against Lethal Sepsis in a Biodefense Model of Human Melioidosis. J Infect Dis 204:636–644.

109. Judy BM, Taylor K, Deeraksa A, Johnston RK, Endsley JJ, Vijayakumar S, Aronson JF, Estes DM, Torres AG. 2012. Prophylactic Application of CpG Oligonucleotides Augments the Early Host Response and Confers Protection in Acute Melioidosis. PLoS One 7:e34176.

110. Puangpetch A, Anderson R, Huang YY, Sermswan RW, Chaicumpa W, Sirisinha S, Wongratanacheewin S. 2012. Cationic Liposomes Extend the Immunostimulatory Effect of CpG Oligodeoxynucleotide against *Burkholderia pseudomallei* Infection in BALB/c Mice. Clin Vaccine Immunol 19:675–683.

111. Puangpetch A, Anderson R, Huang YY, Saengsot R, Sermswan RW, Wongratanacheewin S. 2014. Comparison of the protective effects of killed *Burkholderia pseudomallei* and CpG oligodeoxynucleotide against live challenge. Vaccine 32:5983–5988.

112. Koh GCKW, Weehuizen TA, Breitbach K, Krause K, de Jong HK, Kager LM, Hoogendijk AJ, Bast A, Peacock SJ, van der Poll T, Steinmetz I, Wiersinga WJ. 2013. Glyburide Reduces Bacterial Dissemination in a Mouse Model of Melioidosis. PLoS Negl Trop Dis 7:e2500.

113. Koh GCKW, Maude RR, Schreiber MF, Limmathurotsakul D, Wiersinga WJ, Wuthiekanun V, Lee SJ, Mahavanakul W, Chaowagul W, Chierakul W, White NJ, Van Der Poll T, Day NPJ, Dougan G, Peacock SJ. 2011. Glyburide is anti-inflammatory and associated with reduced mortality in melioidosis. Clin Infect Dis 52:717–725.

114. Hamon Y, Luciani M-F, Becq F, Verrier B, Rubartelli A, Chimini G. 1997. Interleukin-1β Secretion Is Impaired by Inhibitors of the Atp Binding Cassette Transporter, ABC1. Blood 90:2911–2915.

115. Wilson WJ, Afzali MF, Cummings JE, Legare ME, Tjalkens RB, Allen CP, Slayden RA, Hanneman WH. 2016. Immune Modulation as an Effective Adjunct Post-exposure Therapeutic for *B. pseudomallei*. PLoS Negl Trop Dis 10:e0005065.

116. Asakrah S, Nieves W, Mahdi Z, Agard M, Zea AH, Roy CJ, Morici LA. 2013. Post-Exposure Therapeutic Efficacy of COX-2 Inhibition against *Burkholderia pseudomallei*. PLoS Negl Trop Dis 7:e2212.

117. Skyberg JA, Rollins MCF, Holderness JS, Marlenee NL, Schepetkin IA, Goodyear A, Dow SW, Jutila MA, Pascual DW. 2012. Nasal Acai Polysaccharides Potentiate Innate Immunity to Protect gainst Pulmonary *Francisella tularensi*s and *Burkholderia pseudomallei* Infections. PLoS Pathog 8:e1002587.

118. Cortés-Vieyra R, Bravo-Patiño A, Valdez-Alarcón JJ, Juárez MC, Finlay BB, Baizabal-Aguirre VM. 2012. Role of glycogen synthase kinase-3 beta in the inflammatory response caused by bacterial pathogens. J Inflamm (United Kingdom) 9:23.

119. Tay TF, Maheran M, Too SL, Hasidah MS, Ismail G, Embi N. 2012. Glycogen synthase kinase-3β inhibition improved survivability of mice infected with *Burkholderia pseudomallei*. Trop Biomed 29:551–567.

120. Maniam P, Nurul Aiezzah Z, Mohamed R, Embi N, Hasidah MS. 2015. Regulatory role of GSK3β in the activation of NF-ϰB and modulation of cytokine levels in *Burkholderia pseudomallei*-infected PBMC isolated from streptozotocininduced diabetic animals. Trop Biomed 32:36–48.

121. Alam S, Javor S, Degardin M, Ajami D, Rebek M, Kissner TL, Waag DM, Rebek J, Saikh KU. 2015. Structure-Based Design and Synthesis of a Small Molecule that Exhibits Anti-inflammatory Activity by Inhibition of MyD88-mediated Signaling to Bacterial Toxin Exposure. Chem Biol Drug Des 86:200–209.

122. Mahlapuu M, Håkansson J, Ringstad L, Björn C. 2016. Antimicrobial Peptides: An Emerging Category of Therapeutic Agents. Front Cell Infect Microbiol 6:1–12.

123. Ganz T. 2003. Defensins: Antimicrobial peptides of innate immunity. Nat Rev Immunol 3:710–720.

124. Madhongsa K, Pasan S, Phophetleb O, Nasompag S, Thammasirirak S, Daduang S, Taweechaisupapong S, Lomize AL, Patramanon R. 2013. Antimicrobial Action of the Cyclic Peptide Bactenecin on *Burkholderia pseudomallei* Correlates with Efficient Membrane Permeabilization. PLoS Negl Trop Dis 7:e2267.

125. Abdelbaqi S, Deslouches B, Steckbeck J, Montelaro R, Reed DS. 2016. Novel engineered cationic antimicrobial peptides display broad-spectrum activity against *Francisella tularensis*, *Yersinia pestis* and *Burkholderia pseudomallei*. J Med Microbiol 65:188–194.

126. Samy RP, Thwin MM, Stiles BG, Satyanarayana-Jois S, Chinnathambi A, Zayed M, Alharbi SA, Siveen KS, Sikka S, Kumar AP, Sethi G, Lim LHK. 2015. Novel phospholipase A2 inhibitors from python serum are potent peptide antibiotics. Biochimie 111:30–44.

127. Salmond GPC, Fineran PC. 2015. A century of the phage: past, present and future. Nat Rev Microbiol 13:777–786.

128. Levin BR, Bull JJ. 2004. Population and evolutionary dynamics of phage therapy.

Nat Rev Microbiol 2:166–173.

129. Yordpratum U, Tattawasart U, Wongratanacheewin S, Sermswan RW. 2011. Novel lytic bacteriophages from soil that lyse *Burkholderia pseudomallei*. FEMS Microbiol Lett 314:81–88.

130. Kulsuwan R, Wongratanacheewin S, Wongratanacheewin RS, Yordpratum U, Tattawasart U. 2014. Lytic capability of bacteriophages (Family Myoviridae) on *Burkholderia pseudomallei*. Southeast Asian J Trop Med Public Health 45:1344–1353.

131. Khakhum N, Yordpratum U, Boonmee A, Tattawasart U, Rodrigues JLM, Sermswan RW. 2016. Identification of the *Burkholderia pseudomallei* bacteriophage ST79 lysis gene cassette. J Appl Microbiol 121:364–372.

132. Kvitko BH, Cox CR, Deshazer D, Johnson SL, Voorhees KJ, Schweizer HP. 2012. ϕX216, a P2-like bacteriophage with broad *Burkholderia pseudomallei* and *B. mallei* strain infectivity. BMC Microbiol 12:289.

133. Guang-Han O, Leang-Chung C, Vellasamy KM, Mariappan V, Li-Yen C, Vadivelu J. 2016. Experimental phage therapy for *Burkholderia pseudomallei* infection. PLoS One 11:e0158213.

134. Kamjumphol W, Chareonsudjai P, Chareonsudjai S. 2018. Antibacterial activity of chitosan against *Burkholderia pseudomallei*. Microbiologyopen 7:e00534.

135. Dedrick RM, Guerrero-Bustamante CA, Garlena RA, Russell DA, Ford K, Harris K, Gilmour KC, Soothill J, Jacobs-Sera D, Schooley RT, Hatfull GF, Spencer H. 2019. Engineered bacteriophages for treatment of a patient with a disseminated drug-resistant *Mycobacterium abscessus*. Nat Med 25:730–733.

136. Croxen MA, Law RJ, Scholz R, Keeney KM, Wlodarska M, Finlay BB. 2013. Recent Advances in Understanding Enteric Pathogenic *Escherichia coli*. Clin Microbiol Rev 26:822–880.

137. Kaper JB, Nataro JP, Mobley HLT. 2004. Pathogenic *Escherichia coli*. Nat Rev Microbiol 2:123–140.

138. Nguyen Y, Sperandio V. 2012. Enterohemorrhagic *E. coli* (EHEC) pathogenesis. Front Cell Infect Microbiol 2:1–7.

139. Goldwater PN, Bettelheim KA. 2012. Treatment of enterohemorrhagic *Escherichia coli* (EHEC) infection and hemolytic uremic syndrome (HUS). BMC Med 10:12.

140. Sanchez-Villamil J, Navarro-Garcia F. 2015. Role of virulence factors on host inflammatory response induced by diarrheagenic *Escherichia coli* pathotypes. Future Microbiol 10:1009–1033.

141. Snedeker KG, Shaw DJ, Locking ME, Prescott RJ. 2009. Primary and secondary cases in *Escherichia coli* O157 outbreaks: A statistical analysis. BMC Infect Dis 9:144.

142. Boerlin P, McEwen SA, Boerlin-Petzold F, Wilson JB, Johnson RP, Gyles CL.

1999. Associations between Virulence Factors of Shiga Toxin-Producing *Escherichia coli* and Disease in Humans. J Clin Microbiol 37:497–503.

143. Neely MN, Friedman DI. 1998. Functional and genetic analysis of regulatory regions of coliphage H- 19B: Location of shiga-like toxin and lysis genes suggest a role for phage functions in toxin release. Mol Microbiol 28:1255–1267.

144. Zhang X, McDaniel AD, Wolf LE, Keusch GT, Waldor MK, Acheson DWK. 2000. Quinolone Antibiotics Induce Shiga Toxin-Encoding Bacteriophages, Toxin Production, and Death in Mice. J Infect Dis 181:664–670.

145. Rojas-Lopez M, Monterio R, Pizza M, Desvaux M, Rosini R. 2018. Intestinal Pathogenic *Escherichia coli*: Insights for Vaccine Development. Front Microbiol 9:440.

146. Bitzan M, Poole R, Mehran M, Sicard E, Brockus C, Thuning-Roberson C, Rivière M. 2009. Safety and Pharmacokinetics of Chimeric Anti-Shiga Toxin 1 and Anti-Shiga Toxin 2 Monoclonal Antibodies in Healthy Volunteers. Antimicrob Agents Chemother 53:3081–3087.

147. Rocha LB, Luz DE, Moraes CTP, Caravelli A, Fernandes I, Guth BEC, Horton DSPQ, Piazza RMF. 2012. Interaction between Shiga Toxin and Monoclonal Antibodies: Binding Characteristics and *in Vitro* Neutralizing Abilities. Toxins (Basel) 4:729–747.

148. López EL, Contrini MM, Glatstein E, Ayala SG, Santoro R, Allende D, Ezcurra G, Teplitz E, Koyama T, Matsumoto Y, Sato H, Sakai K, Hoshide S, Komoriya K, Morita T, Harning R, Brookman S. 2010. Safety and Pharmacokinetics of Urtoxazumab, a Humanized Monoclonal Antibody, against Shiga-Like Toxin 2 in Healthy Adults and in Pediatric Patients Infected with Shiga-like Toxin-Producing *Escherichia coli*. Antimicrob Agents Chemother 54:239–243.

149. Watanabe-Takahashi M, Sato T, Dohi T, Noguchi N, Kano F, Murata M, Hamabata T, Natori Y, Nishikawa K. 2010. An Orally Applicable Shiga Toxin Neutralizer Functions in the Intestine To Inhibit the Intracellular Transport of the Toxin. Infect Immun 78:177–183.

150. Stearns-Kurosawa DJ, Collins V, Freeman S, Debord D, Nishikawa K, Oh SY, Leibowitz CS, Kurosawa S. 2011. Rescue from lethal Shiga toxin 2-induced renal failure with a cell-permeable peptide. Pediatr Nephrol 26:2031–2039.

151. Li X, Wu P, Cheng S, Lv X. 2012. Synthesis and Assessment of Globotriose-Chitosan Conjugate, a Novel Inhibitor of Shiga Toxins Produced by *Escherichia coli*. J Med Chem 55:2702–2710.

152. Liu J, Sun Y, Feng S, Zhu L, Guo X, Qi C. 2009. Towards an attenuated enterohemorrhagic *Escherichia coli* O157:H7 vaccine characterized by a deleted *ler* gene and containing apathogenic Shiga toxins. Vaccine 27:5929–5935.

153. Oliveira AF, Cardoso SA, dos Reis Almeida FB, de Oliveira LL, Pitondo-Silva A, Gomes Soares S, Hanna ES. 2012. Oral immunization with attenuated *Salmonella* vaccine expressing *Escherichia coli* O157: H7 *intimin* gamma triggers both

systemic and mucosal humoral immunity in mice. Microbiol Immunol 56:513–522.

154. Cai K, Gao X, Li T, Hou X, Wang Q, Liu H, Xiao L, Tu W, Liu Y, Shi J, Wang H. 2010. Intragastric immunization of mice with enterohemorrhagic *Escherichia coli* O157:H7 bacterial ghosts reduces mortality and shedding and induces a Th2-type dominated mixed immune response. Can J Microbiol 56:389–398.

155. Cheng Y, Feng Y, Luo P, Gu J, Yu S, Zhang W jun, Liu Y qing, Wang Q xu, Zou Q ming, Mao X hu. 2009. Fusion Expression and Immunogenicity of EHEC EspA-Stx2A1 protein: Implications for the Vaccine Development. J Microbiol 47:498–505.

156. Gansheroff LJ, Wachtel MR, O'Brien AD. 1999. Decreased Adherence of Enterohemorrhagic *Escherichia coli* to HEp-2 Cells in the Presence of Antibodies That Recognize the C-terminal Region of Intimin. Infect Immun 67:6409–6417.

157. Gao X, Cai K, Shi J, Liu H, Hou X, Tu W, Xiao L, Wang Q, Wang H. 2009. Immunogenicity of a novel Stx2B-Stx1B fusion protein in a mice model of Enterohemorrhagic *Escherichia coli* O157:H7 infection. Vaccine 27:2070–2076.

158. Amani J, Mousavi SL, Rafati S, Salmanian AH. 2009. *In silico* analysis of chimeric *espA*, *eae* and *tir* fragments of *Escherichia coli* O157:H7 for oral immunogenic applications. Theor Biol Med Model 6:1–11.

159. Amani J, Mousavi SL, Rafati S, Salmanian AH. 2011. Immunogenicity of a plant-derived edible chimeric EspA, Intimin and Tir of *Escherichia coli* O157:H7 in mice. Plant Sci 180:620–627.

160. Amani J, Salmanian AH, Rafati S, Mousavi SL. 2010. Immunogenic properties of chimeric protein from *espA*, *eae* and *tir* genes of *Escherichia coli* O157:H7. Vaccine 28:6923–6929.

161. Konadu EY, Parke JC, Tran HT, Bryla DA, Robbins JB, Szu SC. 1998. Investigational vaccine for *Escherichia coli* O157: Phase 1 study of O157 O-specific polysaccharide-*Pseudomonas aeruginosa* recombinant exoprotein A conjugates in adults. J Infect Dis 177:383–387.

162. Huang D, Zhou H, Gao J. 2015. Nanoparticles modulate autophagic effect in a dispersity-dependent manner. Sci Rep 5:14361.

163. Hutter J, Lepenies B. 2015. Carbohydrate-Based Vaccines: An Overview, p. 259–281. *In* Lepenies, B (ed.), Carbohydrate-Based Vaccines. Springer, Clifton, N.J.

164. Bernocchi B, Carpentier R, Betbeder D. 2017. Nasal nanovaccines. Int J Pharm 530:128–138.

165. Muruato LA, Tapia D, Hatcher CL, Kalita M, Brett PJ, Gregory AE, Samuel JE, Titball RW, Torres AG. 2017. Use of Reverse Vaccinology in the Design and Construction of Nanoglycoconjugate Vaccines against *Burkholderia pseudomallei*. Clin Vaccine Immunol 24:e00206-17.

166. Burtnick MN, Heiss C, Schuler AM, Azadi P, Brett PJ, Morici LA, Titball R, Wooten RM. 2012. Development of novel O-polysaccharide based

glycoconjugates for immunization against glanders. Front Cell Infect Microbiol 2:148.

167. Turkevich J, Stevenson PC, Hillier J. 1951. A study of the nucleation and growth process in the synthesis of colloidal gold. Discuss Faraday Soc 55–75.

168. Sanchez-Villamil JI, Tapia D, Torres AG. 2019. Development of a gold nanoparticle vaccine against enterohemorrhagic *Escherichia coli* O157:H7. MBio 10:e01869-19.

169. Schindelin J, Arganda-Carreras I, Frise E, Kaynig V, Longair M, Pietzsch T, Preibisch S, Rueden C, Saalfeld S, Schmid B, Tinevez JY, White DJ, Hartenstein V, Eliceiri K, Tomancak P, Cardona A. 2012. Fiji: An open-source platform for biological-image analysis. Nat Methods 9:676–682.

170. Khakhum N, Bharaj P, Myers JN, Tapia D, Walker DH, Endsley JJ, Torres AG. 2019. Evaluation of *Burkholderia mallei* Δ*tonB* Δ*hcp1* (CLH001) as a live attenuated vaccine in murine models of glanders and melioidosis. PLoS Negl Trop Dis 13:e0007578.

171. Boyd MA, Tennant SM, Saague VA, Simon R, Muhsen K, Ramachandran G, Cross AS, Galen JE, Pasetti MF, Levine MM. 2014. Serum Bactericidal Assays To Evaluate Typhoidal and Nontyphoidal Salmonella Vaccines. Clin Vaccine Immunol 21:712–721.

172. Mountzouros KT, Howell AP. 2000. Detection of Complement-Mediated Antibody-Dependent Bactericidal Activity in a Fluorescence-Based Serum Bactericidal Assay for Group B *Neisseria meningitidis*. J Clin Microbiol 38:2878–2884.

173. Tapia D, Sanchez-Villamil JI, Torres AG. 2019. Emerging role of biologics for the treatment of melioidosis and glanders. Expert Opin Biol Ther 19:1319–1332.

174. Titball RW, Burtnick MN, Bancroft GJ, Brett P. 2017. *Burkholderia pseudomallei* and *Burkholderia mallei* vaccines: Are we close to clinical trials? Vaccine 35:5981–5989.

175. Ahmad S, Zamry AA, Tan HTT, Wong KK, Lim JK, Mohamud R. 2017. Targeting dendritic cells through gold nanoparticles: A review on the cellular uptake and subsequent immunological properties. Mol Immunol 91:123–133.

176. Sengyee S, Yoon SH, Eoin West T, Ernst RK, Chantratita N. 2019. Lipopolysaccharides from different *Burkholderia* species with different lipid a structures induce toll-like receptor 4 activation and react with melioidosis patient sera. Infect Immun 87:1–15.

177. Avci FY, Li X, Tsuji M, Kasper DL. 2011. A mechanism for glycoconjugate vaccine activation of the adaptive immune system and its implications for vaccine design. Nat Med 17:1602–1609.

178. Waag DM, McCluskie MJ, Zhang N, Krieg AM. 2006. A CpG Oligonucleotide Can Protect Mice from a Low Aerosol Challenge Dose of *Burkholderia mallei*. Infect Immun 74:1944–1948.

179. Steinhagen F, Kinjo T, Bode C, Klinman DM. 2011. TLR-based immune adjuvants. Vaccine 29:3341–3355.

180. Schell MA, Zhao P, Wells L. 2011. Outer Membrane Proteome of *Burkholderia pseudomallei* and *Burkholderia mallei* From Diverse Growth Conditions. J Proteome Res 10:2417–2424.

181. Pumpuang A, Phunpang R, Ekchariyawat P, Dulsuk A, Loupha S, Kwawong K, Charoensawat Y, Thiansukhon E, Day NPJ, Burtnick MN, Brett PJ, West TE, Chantratita N. 2019. Distinct classes and subclasses of antibodies to hemolysin co-regulated protein 1 and O-polysaccharide and correlation with clinical characteristics of melioidosis patients. Sci Rep 9:13972.

182. Gregory AE, Judy BM, Qazi O, Blumentritt CA, Brown KA, Shaw AM, Torres AG, Titball RW. 2015. A gold nanoparticle-linked glycoconjugate vaccine against *Burkholderia mallei*. Nanomedicine Nanotechnology, Biol Med 11:447–456.

183. Martin RM, Silva A, Lew AM. 1997. The Igh-1 sequence of the non-obese diabetic (NOD) mouse assigns it to the IgG2c isotype. Immunogenetics 46:167–168.

184. Nazeri S, Zakeri S, Mehrizi AA, Sardari S, Djadid ND. 2020. Measuring of IgG2c isotype instead of IgG2a in immunized C57BL/6 mice with *Plasmodium vivax* TRAP as a subunit vaccine candidate in order to correct interpretation of Th1 versus Th2 immune response. Exp Parasitol 216:107944.

185. Limmathurotsakul D, Golding N, Dance DAB, Messina JP, Pigott DM, Moyes CL, Rolim DB, Bertherat E, Day NPJ, Peacock SJ, Hay SI. 2016. Predicted global distribution of *Burkholderia pseudomallei* and burden of melioidosis. Nat Microbiol 1:15008.

186. Jenjaroen K, Chumseng S, Sumonwiriya M, Ariyaprasert P, Chantratita N, Sunyakumthorn P, Hongsuwan M, Wuthiekanun V, Fletcher HA, Teparrukkul P, Limmathurotsakul D, Day NPJ, Dunachie SJ. 2015. T-Cell Responses Are Associated with Survival in Acute Melioidosis Patients. PLoS Negl Trop Dis 9:e0004152.

187. Kronsteiner B, Chaichana P, Sumonwiriya M, Jenjaroen K, Chowdhury FR, Chumseng S, Teparrukkul P, Limmathurotsakul D, Day NPJ, Klenerman P, Dunachie SJ. 2019. Diabetes alters immune response patterns to acute melioidosis in humans. Eur J Immunol 49:1092–1106.

188. Kaewarpai T, Ekchariyawat P, Phunpang R, Wright SW, Dulsuk A, Moonmueangsan B, Morakot C, Thiansukhon E, Day NPJ, Lertmemongkolchai G, West TE, Chantratita N. 2020. Longitudinal profiling of plasma cytokines in melioidosis and their association with mortality: a prospective cohort study. Clin Microbiol Infect 26:783.e1-783.e8.

189. Chaichana P, Jenjaroen K, Chumseng S, Sumonwiriya M, Rongkard P, Kronsteiner B, Teparrukkul P, Limmathurotsakul D, Day NPJ, Chantratita N, Dunachie SJ. 2021. Role of *Burkholderia pseudomallei*-Specific IgG2 in Adults with Acute Melioidosis, Thailand. Emerg Infect Dis 27:463–470.

190. Nithichanon A, Rinchai D, Buddhisa S, Saenmuang P, Kewcharoenwong C, Kessler B, Khaenam P, Chetchotisakd P, Maillere B, Robinson J, Reynolds CJ, Boyton RJ, Altmann DM, Lertmemongkolchai G. 2018. Immune Control of *Burkholderia pseudomallei*-Common, High-Frequency T-Cell Responses to a Broad Repertoire of Immunoprevalent Epitopes. Front Immunol 9:484.

191. Lauw FN, Simpson AJH, Prins JM, Smith MD, Kurimoto M, van Deventer SJH, Speelman P, Chaowagul W, White NJ, van der Poll T. 1999. Elevated Plasma Concentrations of Interferon (IFN)–γ and the IFN-γ–Inducing Cytokines Interleukin (IL)–18, IL-12, and IL-15 in Severe Melioidosis. J Infect Dis 180:1878–1885.

192. Haque A, Easton A, Smith D, O'Garra A, Van Rooijen N, Lertmemongkolchai G, Titball RW, Bancroft GJ. 2006. Role of T cells in innate and adaptive immunity against murine *Burkholderia pseudomallei* infection. J Infect Dis 193:370–379.

193. Pongcharoen S, Ritvirool PN, Sanguansermsri D, Chanchan P, Jienmongkol P, Butkhamchot P, Warnnissorn P, Banchuin N, Sirisinha S. 2008. Reduced Interleukin-17 Expression of *Burkholderia pseudomallei*-Infected Peripheral Blood Mononuclear Cells of Diabetic Patients. Asian Pacific J Allergy Immunol 26:63–69.

194. Nithichanon A, Gourlay LJ, Bancroft GJ, Ato M, Takahashi Y, Lertmemongkolchai G. 2017. Boosting of post-exposure human T-cell and B-cell recall responses *in vivo* by *Burkholderia pseudomallei*-related proteins. Immunology 151:98–109.

195. Suwannasaen D, Mahawantung J, Chaowagul W, Limmathurotsakul D, Felgner PL, Davies H, Bancroft GJ, Titball RW, Lertmemongkolchai G. 2011. Human Immune Responses to *Burkholderia pseudomallei* Characterized by Protein Microarray Analysis. J Infect Dis 203:1002–1011.

196. Lee K, Conboy M, Park HM, Jiang F, Kim HJ, Dewitt MA, Mackley VA, Chang K, Rao A, Skinner C, Shobha T, Mehdipour M, Liu H, Huang W, Lan F, Bray NL, Li S, Corn JE, Kataoka K, Doudna JA, Conboy I, Murthy N. 2017. Nanoparticle delivery of Cas9 ribonucleoprotein and donor DNA *in vivo* induces homology-directed DNA repair. Nat Biomed Eng 1:889–901.

197. Paul AM, Shi Y, Acharya D, Douglas JR, Cooley A, Anderson JF, Huang F, Bai F. 2014. Delivery of antiviral small interfering RNA with gold nanoparticles inhibits dengue virus infection in vitro. J Gen Virol 95:1712–1722.

198. Hirai T, Yoshioka Y, Izumi N, Ichihashi KI, Handa T, Nishijima N, Uemura E, Sagami KI, Takahashi H, Yamaguchi M, Nagano K, Mukai Y, Kamada H, Tsunoda SI, Ishii KJ, Higashisaka K, Tsutsumi Y. 2016. Metal nanoparticles in the presence of lipopolysaccharides trigger the onset of metal allergy in mice. Nat Nanotechnol 11:808–816.

199. Fallarini S, Paoletti T, Battaglini CO, Ronchi P, Lay L, Bonomi R, Jha S, Mancin F, Scrimin P, Lombardi G. 2013. Factors affecting T cell responses induced by fully synthetic glyco-gold-nanoparticles. Nanoscale 5:390–400.

200. Kessler B, Rinchai D, Kewcharoenwong C, Nithichanon A, Biggart R, Hawrylowicz CM, Bancroft GJ, Lertmemongkolchai G. 2017. Interleukin 10 inhibits pro-inflammatory cytokine responses and killing of *Burkholderia pseudomallei*. Sci Rep 7:42791.

201. Ulett GC, Ketheesan N, Hirst RG. 1998. Macrophage-lymphocyte interactions mediate anti-*Burkholderia pseudomallei* activity. FEMS Immunol Med Microbiol 21:283–286.

202. Chaichana P, Kronsteiner B, Rongkard P, Teparrukkul P, Limmathurotsakul D, Chantratita N, Day NPJ, Fletcher HA, Dunachie SJ. 2020. Serum From Melioidosis Survivors Diminished Intracellular *Burkholderia pseudomallei* Growth in Macrophages: A Brief Research Report. Front Cell Infect Microbiol 10:442.

203. Nelson M, Prior JL, Lever MS, Jones HE, Atkins TP, Titball RW. 2004. Evaluation of lipopolysaccharide and capsular polysaccharide as subunit vaccines against experimental melioidosis. J Med Microbiol 53:1177–1182.

204. Scott AE, Burtnick MN, Stokes MGM, Whelan AO, Williamson ED, Atkins TP, Prior JL, Brett PJ. 2014. *Burkholderia pseudomallei* Capsular Polysaccharide Conjugates Provide Protection against Acute Melioidosis. Infect Immun 82:3206–3213.

205. Ngugi SA, Ventura V V., Qazi O, Harding S V., Kitto GB, Estes DM, Dell A, Titball RW, Atkins TP, Brown KA, Hitchen PG, Prior JL. 2010. Lipopolysaccharide from *Burkholderia thailandensis* E264 provides protection in a murine model of melioidosis. Vaccine 28:7551–77555.

206. Tapia D, Sanchez-Villamil JI, Torres AG. 2020. Multicomponent gold nano-glycoconjugate as a highly immunogenic and protective platform against *Burkholderia mallei*. npj Vaccines 5:82.

207. Shibui A, Shimura E, Nambu A, Yamaguchi S, Leonard WJ, Okumura K, Sugano S, Sudo K, Nakae S. 2012. Th17 cell-derived IL-17 is dispensable for B cell antibody production. Cytokine 59:108–114.

208. Pasquevich KA, Ibañez AE, Coria LM, Samartino CG, Estein SM, Zwerdling A, Barrionuevo P, Oliveira FS, Seither C, Warzecha H, Oliveira SC, Giambartolomei GH, Cassataro J. 2011. An oral Vaccine Based on U-Omp19 Induces Protection against *B. abortus* Mucosal Challenge by Inducing an Adaptive IL-17 Immune Response in Mice. PLoS One 6:e16203.

209. Ahmed M, Smith DM, Hamouda T, Rangel-Moreno J, Fattom A, Khader SA. 2017. A novel nanoemulsion vaccine induces mucosal Interleukin-17 responses and confers protection upon *Mycobacterium tuberculosis* challenge in mice. Vaccine 35:4983–4989.

210. GBD 2013 M, Causes of Death C. 2015. Global, regional, and national age-sex specific all-cause and cause-specific mortality for 240 causes of death, 1990-2013: A systematic analysis for the Global Burden of Disease Study 2013. Lancet 385:117–171.

211. Farfan MJ, Torres AG. 2012. Molecular Mechanisms that Mediate Colonization of Shiga Toxin-Producing *Escherichia coli* Strains. Infect Immun 80:903–913.

212. Elliott SJ, Sperandio V, Giron JA, Shin S, Mellies JL, Wainwright L, Hutcheson SW, McDaniel TK, Kaper JB. 2000. The Locus of Enterocyte Effacement (LEE)-Encoded Regulator Controls Expression of Both LEE- and Non-LEE-Encoded Virulence Factors in Enteropathogenic and Enterohemorrhagic *Escherichia coli*. Infect Immun 68:6115–6126.

213. García-Angulo VA, Kalita A, Kalita M, Lozano L, Torres AG. 2014. Comparative genomics and immunoinformatics approach for the identification of vaccine candidates for enterohemorrhagic *Escherichia coli* O157:H7. Infect Immun 82:2016–2026.

214. Gu J, Liu Y, Yu S, Wang H, Wang Q, Yi Y, Zhu F, Yu X jie, Zou Q, Mao X. 2009. Enterohemorrhagic *Escherichia coli* trivalent recombinant vaccine containing EspA, intimin and Stx2 induces strong humoral immune response and confers protection in mice. Microbes Infect 11:835–841.

215. Wan C song, Zhou Y, Yu Y, Peng L juan, Zhao W, Zheng X li. 2011. B-cell epitope KT-12 of enterohemorrhagic *Escherichia coli* O157:H7: A novel peptide vaccine candidate. Microbiol Immunol 55:247–253.

216. Cai K, Gao X, Li T, Wang Q, Hou X, Tu W, Xiao L, Tian M, Liu Y, Wang H. 2011. Enhanced immunogenicity of a novel Stx2Am-Stx1B fusion protein in a mice model of enterohemorrhagic *Escherichia coli* O157:H7 infection. Vaccine 29:946–952.

217. Cruz LJ, Tacken PJ, Zeelenberg IS, Srinivas M, Bonetto F, Weigelin B, Eich C, De Vries IJ, Figdor CG. 2014. Tracking Targeted Bimodal Nanovaccines: Immune Responses and Routing in Cells, Tissue, and Whole Organism. Mol Pharm 11:4299–4313.

218. Reddy ST, Van Der Vlies AJ, Simeoni E, Angeli V, Randolph GJ, O'Neil CP, Lee LK, Swartz MA, Hubbell JA. 2007. Exploiting lymphatic transport and complement activation in nanoparticle vaccines. Nat Biotechnol 25:1159–1164.

219. Tao W, Ziemer KS, Gill HS. 2014. Gold nanoparticle-M2e conjugate formulated with CpG induces protective immunity against influenza A virus. Nanomedicine (Lond) 9:237–251.

220. Kalita A, Kalita M, Torres AG. 2015. Exploiting the power of OMICS approaches to produce *E. coli* O157 vaccines. Gut Microbes 5:770–774.

221. Tapia D, Ross BN, Kalita A, Kalita M, Hatcher CL, Muruato LA, Torres AG. 2016. From *In silico* Protein Epitope Density Prediction to Testing *Escherichia coli* O157:H7 Vaccine Candidates in a Murine Model of Colonization. Front Cell Infect Microbiol 6:94.

222. Buchholz U, Bernard H, Werber D, Bohmer M, Remschmidt C, Wilking H, Delere Y, an der Heiden M, Adlhoch C, Dreesman J, Ehlers J, Ethelberg S, Faber M, Frank C, Fricke G, Greiner M, Hohle M, Ivarsson S, Jark U, Kirchner M, Koch J,

Krause G, Luber P, Rosner B, Stark K, Kuhne M. 2011. German Outbreak of *Escherichia coli* O104:H4 Associated with Sprouts. N Engl J Med 365:1763–1770.

223. McCarthy DP, Hunter ZN, Chackerian B, Shea LD, Miller SD. 2014. Targeted immunomodulation using antigen-conjugated nanoparticles. Wiley Interdiscip Rev Nanomedicine Nanobiotechnology 6:298–315.

224. Walkey CD, Chan WCW. 2012. Understanding and controlling the interaction of nanomaterials with proteins in a physiological environment. Chem Soc Rev 41:2780–2799.

225. Torres AG, Gregory AE, Hatcher CL, Vinet-Oliphant H, Morici LA, Titball RW, Roy CJ. 2015. Protection of non-human primates against glanders with a gold nanoparticle glycoconjugate vaccine. Vaccine 33:686–692.

226. Chen W, Zhang B, Mahony T, Gu W, Rolfe B, Xu ZP. 2016. Efficient and Durable Vaccine against Intimin β of Diarrheagenic *E. coli* Induced by Clay Nanoparticles. Small 12:1627–1639.

227. Montero D, Orellana P, Gutiérrez D, Araya D, Salazar JC, Prado V, Oñate Á, del Canto F, Vidal R. 2014. Immunoproteomic Analysis To Identify Shiga Toxin-Producing *Escherichia coli* Outer Membrane Proteins Expressed during Human Infection. Infect Immun 82:4767–4777.

228. Perna NT, Plunkett G, Burland V, Mau B, Glasner JD, Rose DJ, Mayhew GF, Evans PS, Gregor J, Kirkpatrick HA, Posfai G, Hackett J, Klink S, Boutin A, Shao Y, Miller L, Grotbeck EJ, Davis WN, Lim A, Dimalanta ET, Potamousis K, Apodaca J, Anantharaman TS, Lin J, Yen G, Schwartz DC, Welch RA, Blattner FR. 2003. Genome sequence of enterohaemorrhagic *Escherichia coli* O157:H7. Nature 409:529–533.

229. Pallen MJ, Beatson SA, Bailey CM. 2005. Bioinformatics analysis of the locus for enterocyte effacement provides novel insights into type-III secretion. BMC Microbiol 5:9.

230. Martorelli L, Garimano N, Fiorentino GA, Vilte DA, Garbaccio SG, Barth SA, Menge C, Ibarra C, Palermo MS, Cataldi A. 2018. Efficacy of a recombinant Intimin, EspB and Shiga toxin 2B vaccine in calves experimentally challenged with *Escherichia coli* O157:H7. Vaccine 36:3949–3959.

231. Perez-Lopez A, Behnsen J, Nuccio SP, Raffatellu M. 2016. Mucosal immunity to pathogenic intestinal bacteria. Nat Rev Immunol 16:135–148.

232. Shekar A, Ramlal S, Jeyabalaji JK, Sripathy MH. 2019. Intranasal co-administration of recombinant active fragment of Zonula occludens toxin and truncated recombinant EspB triggers potent systemic, mucosal immune responses and reduces span of *E. coli* O157:H7 fecal shedding in BALB/c mice. Med Microbiol Immunol 208:89–100.

233. Ma Z, Zhang H, Shang W, Zhu F, Han W, Zhao X, Han D, Wang PG, Chen M. 2014. Glycoconjugate Vaccine Containing *Escherichia coli* O157:H7 O-Antigen Linked with Maltose-Binding Protein Elicits Humoral and Cellular Responses.

PLoS One 9:e105215.

CURRICULUM VITAE

Daniel Tapia Date: 03/25/2021

PRESENT POSITION AND ADDRESS:

Doctoral candidate, Graduate School of Biomedical Science (GSBS)
University of Texas Medical Branch at Galveston
Department of Microbiology and Immunology
301 University Blvd.
Galveston, TX 77555
Email: datapia@utmb.edu

BIOGRAPHICAL:

Date of Birth:	09/10/1994
Birthplace:	Michoacán, Mexico
Languages:	English, Spanish

EDUCATION:

08/2016 – Present	**Doctor of Philosophy,** Doctoral Candidate Biomedical Science Department of Microbiology and Immunology The University of Texas Medical Branch, Galveston, TX
06/2015 – 06/2016	**Post-baccalaureate Research Education Program (PREP)** Graduate Certificate Program Graduate School of Biomedical Sciences The University of Texas Medical Branch, Galveston, TX
08/2013 – 05/2015	**Bachelor of Science in Molecular and Cell Biology** Texas A&M University, College Station, TX

PROFESSIONAL AND TEACHING EXPERIENCE:

Professional Experience/Training:

10/2018 – Present	**Sealy Institute for Vaccine Sciences Predoctoral Fellow**, University of Texas Medical Branch, Galveston, TX.
05/2015 – Present	**Graduate Research Fellow**, Department of Microbiology and Immunology, University of Texas Medical Branch, Galveston, TX Mentor: Alfredo Torres, Ph.D. Project: Development of a nano-glycoconjugate subunit vaccine against *Burkholderia pseudomallei* and Enterohemorrhagic *E. coli*
04/2017	**Advanced Immunology Mini-Lecture Series**: Role of Autophagy in Immunity

Course Directors: Janice Endsley, Ph.D. and Gregg N. Milligan, Ph.D.

GRANT SUPPORT:

10/2019 – Present UTMB	Sealy Institute for Vaccine Sciences Pre-Doctoral Fellowship,
03/2017 – Present	3R01AI126601-02S1 (R01-RSUM) Supplement for Underrepresented Minorities Project Title: "Glycoconjugate Nanoparticle Vaccines against *Burkholderia* Infections" Agency: NIH/NIAID
06/2015 – 06/2016	GM069285**,** PREPing to a Biomedical PhD (R25)

ACADEMIC COMMITEES:

08/2018 – 08/2019	Microbiology & Immunology, Executive Program Committee
08/2018 – 08/2019	Academic Committee Member, Student Representative
08/2018 – 09/2019	Student Representative for M&I Admissions Committee
09/2018 – 09/2019	GSBS Curriculum Committee, Student Representative
07/2017 – Present	*Committee in Support of Science Education*, Reviewer for participants in the UTMB High School Summer Biomedical Research Program

HONORS AND AWARDS:

08/2020	*Mardelle Susman Scientific Writing Award*, UTMB
12/2019	*The Arthur V. Simmang Scholarship*, UTMB
12/2019	*Eva Yznaga Seger, MD Presidential Scholarship*, UTMB
12/2018	*The Arthur V. Simmang Scholarship Fund*, UTMB
09/2018	Vaccinology Course Travel Award, Global Challenge Research Fund Networks (GCRF), BactiVac Network, United Nations Food and Agriculture Organization (FAO)
03/2018	*James W. McLaughlin Travel Award*, Poster Presentation, UTMB
12/2017	*Arun Kumar Chopra, Nirmal Rani Chopra and Dharam Dev Chopra Memorial Scholarship in the GSBS,* UTMB
11/2016	*Curtis W. Lambert Scholarship, UTMB*
08/2014	*Barnes and Noble JCT Scholarship*, Texas A&M University
08/2013	National Society of Collegiate Scholars Transfer Scholarship
05/2013	*Cypress Rotary Club Scholarship*, Lone Star Community College

COMMUNITY SERVICE AND ACTIVITIES:

08/2018 – 08/2019	Microbiology & Immunology Student Organization (MISO), President
04/2017 – 08/2018	Microbiology & Immunology Student Organization (MISO), Vice – President
08/2012 – 05/2013	Phi Theta Kappa-International Honor Society - Vice President of Honors in Action/Lifetime Member – Lead researcher for Honors in Action Project
08/2012 – 05/2013	National Honor Society of Collegiate Scholars - Vice President - Liaison for campus administration in project development

PROFESSIONAL AFFILIATIONS:

02/2019 – Present	American Society of Microbiology, Member; Washington, D.C., US
10/2018 – Present	VALIDATE Network, Affiliate, Oxford University, United Kingdom
10/2018 – Present	BactiVac, Member; Birmingham University, United Kingdom

CERTIFICATIONS:

05/2016 – Present	Federal Select Agent (SRA) Specimen Manipulation, Center for Disease Control and Prevention (CDC)
05/2016	Animal Biosafety Level 3 (ABSL3), International Biosafety Training Center, UTMB, Galveston, TX.
05/2016	Biosafety Level 2/3 (BSL2/3), International Biosafety Training Center, UTMB, Galveston, TX.

PUBLICATIONS:

1. **Tapia D**, Sanchez-Villamil JI, Borlee GI, Borlee BR, Walker DH, Torres AG. *Burkholderia pseudomallei* as an Enteric Pathogen: Identification of Virulence Factors Mediating Gastrointestinal Infection. *Infect Immun*. 2020 Oct 26:IAI.00654-20. doi: 10.1128/IAI.00654-20.
2. **Tapia D**, Sanchez-Villamil JI, Torres AG. Multicomponent gold nano-glycoconjugate as a highly immunogenic and protective platform against *Burkholderia mallei*. *NPJ Vaccines*. 2020 Sep 10;5:82. doi: 10.1038/s41541-020-00229-9.
3. **Tapia D**, Sanchez-Villamil JI, Torres AG. Emerging role of biologics for the treatment of melioidosis and glanders. *Expert Opin Biol Ther.* 2019 Dec;19(12):1319-1332. doi:10.1080/14712598.2019.1677602
4. Sanchez-Villamil JI, Navarro-Garcia F, Castillo-Romero A, Gutierrez-Gutierrez F, **Tapia D**, Tapia-Pastrana G (2019) Curcumin Blocks Cytotoxicity of Enteroaggregative and Enteropathogenic *Escherichia coli* by Blocking Pet and EspC Proteolytic Release

from Bacterial Outer Membrane. *Front. Cell. Infect. Microbiol.* 9:334. doi: 10.3389/fcimb.2019.00334

5. **Tapia D**, Sanchez-Villamil JI, Torres AG. Development of a Gold Nanoparticle Vaccine Against Enterohemorrhagic *Escerichia coli* O157:H7. *MBio*, 2019 Aug 13;10(4) doi: 10.1128/mBio.01869-19
6. Khakhum N, Bharaj P, Myers JN, **Tapia D**, Walker DH, Endsley JJ, Torres AG. Evaluation of *Burkholderia mallei* Δ*tonB* Δ*hcp1* (CLH001) as a live attenuated vaccine in murine models of glanders and melioidosis. *PLoS Negl Trop Dis*. 2019 Jul 15;13(7):e0007578. doi: 10.1371/journal.pntd.0007578.
7. **Tapia D**, Khakhum N, Torres, A.G., *Burkholderia mallei,* and Glanders. Springer. Book Chapter; 2019
8. Khakhum N, Bharaj P, Myers JN, **Tapia D**, Kilgore PB, Ross BN, Walker DH, Endsley JJ, Torres AG. *Burkholderia pseudomallei* Δ*tonB* Δ*hcp1* Live Attenuated Vaccine Strain Elicits Full Protective Immunity against Aerosolized Melioidosis Infection. *mSphere*. 2019 Jan 2;4(1):e00570-18. doi: 10.1128/mSphere.00570-18.
9. Ross BN, Myers JN, Muruato LA, **Tapia D**, Torres AG. Evaluating New Compounds to Treat *Burkholderia pseudomallei* Infections. *Front Cell Infect Microbiol*. 2018 Jun 25; 8:210. doi: 10.3389/fcimb.2018.00210
10. Muruato LA, **Tapia D**, Hatcher CL, Kalita M, Brett PJ, Gregory AE, Samuel JE, Titball RW, Torres AG. The Use of Reverse Vaccinology in the Design and Construction of Nano-glycoconjugate Vaccines against *Burkholderia pseudomallei*. *Clin Vaccine Immunol*. 2017 Sep 13. pii: CVI.00206-17. doi: 10.1128/CVI.00206-17.
11. **Tapia D**, Ross BN, Kalita A, Kalita M, Hatcher CL, Muruato LA, Torres AG. From In silico Protein Epitope Density Prediction to Testing *Escherichia coli* O157:H7 Vaccine Candidates in a Murine Model of Colonization. *Front Cell Infect Microbiol*. 2016 Aug 30;6:94. doi: 10.3389/fcimb.2016.00094.

Submitted:

1. **Tapia D,** Sanchez-Villamil JI, Torres, AG, Gold nano-glyconjugate vaccines augments protective humoral and cellular response against *Burkholderia pseudomallei* infection. [Submitted to mBio].

ABSTRACTS:

1. **Daniel Tapia**, Javier I. Sanchez-Villamil, Alfredo G. Torres. Multicomponent Gold-nanoparticle Vaccines Enhance Immunogenicity and Protection Against Inhalational *Burkholderia* infections. Transforming Vaccinology Keystone Symposium, Florence, Italy, Cancelled due to COVID-19.
2. **Daniel Tapia**, Javier I. Sanchez-Villamil, Alfredo G. Torres. Nanovaccines as highly immunogenic and protective therapy against inhalational *Burkholderia pseudomallei* infection. 9th World Melioidosis Congress. October 2019. Hanoi, Viet Nam.
   ****Selected for Oral Presentation.**
3. **Daniel Tapia**, Javier I. Sanchez-Villamil, Alfredo G. Torres. Development of A Multivalent Gold Nano-Glycoconjugate Vaccine Against *Burkholderia pseudomallei*. McLaughlin Symposium. March 2019. Galveston, TX

4. **Daniel Tapia**, Javier I. Sanchez-Villamil, Alfredo G. Torres. Development of A Multivalent Gold Nano-Glycoconjugate Vaccine Against *Burkholderia pseudomallei*. ASM Biothreats. January 28, 2019. Arlington, VA
5. **Daniel Tapia**, Javier I. Sanchez-Villamil, PhD, Laura A. Muruato, PhD, Alfredo G. Torres, PhD. Gold nano-glycoconjugate vaccine against *Burkholderia pseudomallei* provides protection in an *in vivo* model of melioidosis. McLaughlin Symposium. March 30, 2016. Galveston, TX
6. **Daniel Tapia**, Alfredo G. Torres, PhD. LomW phage protein of *Escherichia coli* O157:H7 protects against gastrointestinal colonization. McLaughlin Symposium. April 30, 2016. Galveston, TX.
7. **Daniel Tapia**, Anjana Kalita, Ph.D; Mridul Kalita, Ph.D; Brittany N. Ross; Alfredo G. Torres, PhD. Bioinformatic approach identifies candidates that confer protection against *Escherichia coli* O157:H7 *in vivo*. McLaughlin Symposium. April 30, 2016. Galveston, TX.
8. **Daniel Tapia**; Anjana Kalita, Ph.D; Mridul Kalita, Ph.D; Brittany N. Ross; Alfredo Torres, PhD. Vaccine Candidates Identified by *in silico* Analysis Confer Protection against *Escherichia coli* O157:H7 Murine Intestinal Colonization. ABRCMS Convention. November 13, 2015. Seattle, WA.

Permanent address: 210 Post Office St. Apt #B303 Galveston, TX, 77550

This dissertation was typed by Daniel Tapia.